FUEL CELL MEMBRANE-ELECTRODE-ASSEMBLIES WITH PGM-FREE CATALYST NANOFIBER CATHODES

By

Xiaomin Xu

Dissertation

Submitted to the Faculty of the

Graduate School of Vanderbilt University

in partial fulfillment of the requirements

for the degree of

DOCTOR OF PHILOSOPHY

in

Chemical Engineering

August 11, 2023

Nashville, Tennessee

Approved:

Peter N. Pintauro, Ph.D

Paul Laibinis, Ph.D

Piran Kidambi, Ph.D

Janet Macdonald, Ph.D

DEDICATION

Dedicated to my parents, Shulin Xu (徐树林) and Jiangying Xue (薛江英), for supporting me during this endeavor.

ACKNOWLEDGEMENTS

I could not express my appreciation for the people who generously supported and guided me to complete this dissertation. First, I substantially appreciate Professor Peter N. Pintauro for accepting me into his research group, offering indispensable guidance, and inspiring me to dig into the fuel cell world. He was extensively involved in each step of this study, and he remained excited and curious about the development of fuel cell study, which inspired me to pursue it for the rest of my life. My gratitude goes to my committee members Professor Paul Laibinis, Piran Kidambi, and Janet Macdonald, for their helpful guidance and encouragement.

I also want to thank Professor Pinaturo's group members for their generous help. Professor Ryszard Wycisk and his advice, troubleshooting assistance, and expertise in polymer chemistry and electrospinning operation were invaluable to me. I also want to thank Dr. Narae Kang for her guidance during my first year at Vanderbilt. I especially want to thank Zezhou Yang, whose friendship and support were essential for me to pass this difficult time. I also want to thank Xiaozong Fan for his different views on my study.

Several collaborations made significant contributions to this project. Dr. Barr Zulevi, Dr. Alexey Serov, Dr. Kyle Ellis, and Dr. Sam McKinney at Pajarito Powder provided all the PGM-free catalysts I needed to finish this work. This group also helped tremendously in confirming baseline performance, sharing experience on cathode and MEA fabrication, and providing their insights.

I also want to thank several members of the Vanderbilt community for their diligent work. Professor Anthony Hmelo trained me on scanning electron microscopes. Professor James R. McBride assisted me with troubleshooting and supported me in finishing the characterization with energy-dispersive X-ray spectroscopy. Angie Pernell, Felisha Baquera, Jenni Chandler, and Brittany Hill provided friendly administrative assistance. Most importantly, I thank my family for their indispensable love and support. My parents, Shulin Xu, and Jiangying Xue gave me everything I needed to go through the ups and downs and finish this work.

This research is supported by the U.S. Department of Energy Fuel Cell Technologies Office through the Fuel Cell Performance and Durability (FC-PAD) Consortium (Fuel Cells Program Manager: David Peterson). The work at Vanderbilt University was funded under DOE contract No. EE-0008376.

TABLE OF CONTENTS

Chapter Page

LIST OF TABLES

Table Page

LIST OF FIGURES

Figure Page

CHAPTER I

INTRODUCTION AND BACKGROUND

Growing energy demand in recent years has drawn increasing attention to the use of H_2/air fuel cells, especially in motor vehicles.[1] Among the various types of fuel cell, the proton exchange membrane fuel cell (PEMFC) is a good engine candidate in motor vehicles due to its moderate operating temperature (typically 60 °C to 80 °C) and high power density.[2,3] Currently, most motor vehicles are powered by internal combustion engines, which produce mechanical output by burning fuel (gasoline or diesel), releasing heat, and then partially transforming the heat into output. This process is constrained by the laws of thermodynamics,[4] so gasoline and diesel engines' thermal efficiencies are only 20% and 40%, respectively. By contrast, a PEMFC is an electrochemical energy converter that directly converts the chemical energy in fuel (H_2) into direct current electricity,[3] yielding a high energy efficiency of over 50%.[5] Furthermore, PEMFC engines emit only water, so they avoid the environmental problems caused by internal combustion engines, including toxic emissions of nitrogen oxide, carbon monoxide, particulate matter, and greenhouse gases.

In addition to PEMFCs, battery-powered motors are a competitive candidate to replace internal combustion engines in vehicles, including those powered by lead-acid (Pb-A), nickel-metal hydride (NiMH), and lithium-ion (Li-ion) batteries. However, the specific energy (energy per unit weight) of a PEM fuel cell plus compressed hydrogen storage tanks is four times that of the batteries (600 Wh/kg vs. 150 Wh/kg).[6] To increase the range of electric cars from 100 to 150 miles, negligible extra weight is needed in a

fuel cell electric vehicle (FCEV), while a battery electric vehicle (BEV) requires significantly more weight. Also, substantial space is needed for batteries in BEVs, especially for Pb-A and NiMH batteries. To achieve a range of 250–300 miles, even Li-ion batteries require 400–600 liters of space, twice that required for fuel cells at the same range.[6] Furthermore, it typically takes hours to fully recharge BEVs, while refilling FCEVs with hydrogen takes only a few minutes.

Small vehicles powered by fuel cells have been released that offer all these advantages, such as the Toyota Mirai, Honda Clarity, and Hyundai Nexo, and fuel cell trucks have been developed by Cummins, General Motors, Toyota, Volvo, and Daimler, while Fuji Electric, Ballard, UTC, Hydrogenics, Nuvera, and Proton Motor Fuel Cell GmbH manufacture fuel cell buses. Thus, more and more vehicles on the road are powered by fuel cells.[7] Taking the United States as an instance, the number of FCEVs released/sold has increased from 4 in 2012 to ~15,000 in 2022.[8]

1.1 Principles of H_2/Air PEMFCs

1.1.1 Fuel Cell Components

Figure 1.1 shows a schematic diagram of a single-cell PEMFC. In the middle of a PEMFC is a proton exchange membrane. Perfluorosulfonic acid (PFSA) (such as Nafion, LIQUion, and Aquivion) is the most prevalent proton-conducting ionomer in PEMFCs, as a fully hydrated PFSA membrane's proton conductivity of 0.1 S/cm is remarkably high.[9] This is due to the high proton mobility of a fully hydrated membrane, which is only one order of magnitude lower than that of aqueous sulfuric acid solution.[3] The

membrane is fixed between two electrodes in a sandwich commonly known as a membrane electrode assembly (MEA). The two electrodes are anode and cathode, and each constitutes a thin catalyst layer containing catalyst and PFSA ionomer. The fuel cell reaction (Equation 1.1) comprises two half-cell electrochemical reactions, the anodic hydrogen oxidation reaction (HOR) (Equation 1.2), and the cathodic oxygen reduction reaction (ORR) (Equation 1.3).

$$H_2 + {}^1/_2\, O_2 \rightarrow H_2O \qquad \text{(Equation 1.1)}$$

$$H_2 \rightarrow 2H^+ + 2e^- \qquad \text{(Equation 1.2)}$$

$${}^1/_2\, O_2 + 2H^+ + 2e^- \rightarrow H_2O \qquad \text{(Equation 1.3)}$$

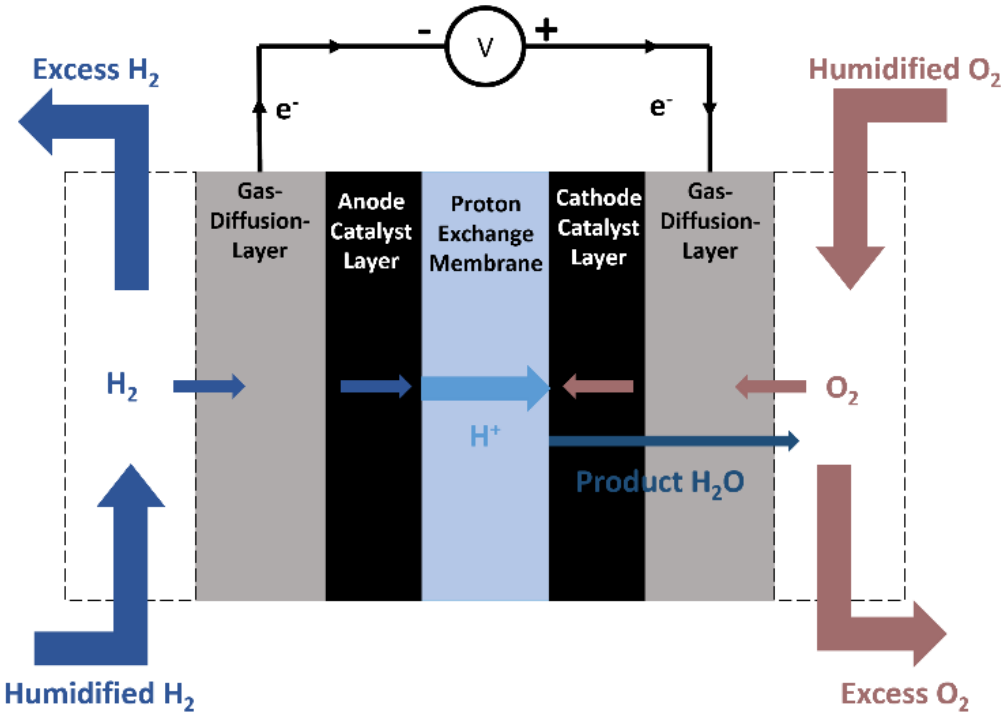

Figure 1.1. Schematic diagram of a typical single-cell PEMFC.

The MEA is sandwiched between two gas diffusion layers (GDLs), which have multiple functions in a PEMFC, including (i) providing a pathway for reactant gases to move into and electrogenerated water to move out of the catalyst layer, (ii) allowing electrons into the catalyst layer to complete the electrical circuit, (iii) providing mechanical support to the MEA, and (iv) removing the generated heat during operation. A multicell configuration will also have bipolar plates that electrically connect the anode of one cell to the cathode of the adjacent cell (not shown in Figure 1.1). The present study conducted tests only in a single-cell PEMFC.

1.1.2 Fuel Cell Operation Theory

A fuel cell's performance can be summarized in a graph of its voltage-current density characteristics as shown in Figure 1.2. This graph, called a fuel cell polarization curve (or V-i curve), shows the current density output of a fuel cell at a given voltage. Polarization curves are also an essential tool for evaluating MEA performance.

The thermodynamic (ideal) potential in Figure 1.2 is calculated from Gibbs free energy using Equation 1.4:

$$\mathrm{E_{thermo}} = \frac{-\Delta \mathrm{G}}{\mathrm{nF}} \qquad \text{(Equation 1.4)}$$

where E_{thermo} is thermodynamic (ideal) fuel cell potential, ΔG is Gibbs free energy, n is the number of electrons per molecule of H_2, and F is the Faraday constant.[3]

Under standard conditions (25 °C), the theoretical potential of hydrogen-oxygen fuel cell operation is 1.23 V, while the open circuit voltage (OCV) of an actual fuel cell is below 1.0 V, largely for the following reasons: (i) the operating temperature of a PEMFC

is 80 °C, and, according to the Nernst equation, increased temperature reduces potential (although, in an actual fuel cell, increasing the operating temperature would accelerate the reaction, as irreversible losses also decrease with temperature and thus compensate for the potential loss);[3] (ii) the reactant gases, O_2 and (mainly) H_2, permeate the proton exchange membrane, which results in the depolarization of the cathode (by H_2 permeation) and anode (by O_2 permeation); (iii) some electrons may cross over the proton exchange membrane; (iv) poisoning occurs in the ionomer and thus lower the proton conductivity in the catalyst layers and the proton exchange membrane. The combined effects result in an actual fuel cell's OCV being lower than the theoretical potential (1.23 V) and generally below 1.0 V.[3]

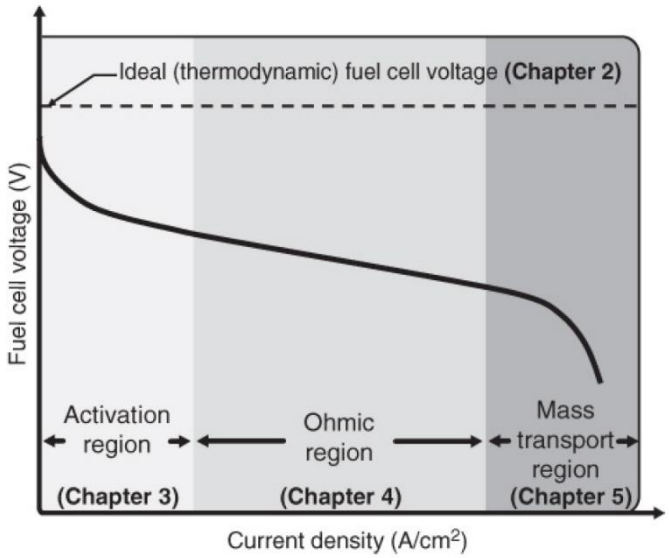

Figure 1.2. Schematic of a fuel cell's V-i curve. The actual voltage of a fuel cell (solid line) is lower than the thermodynamic (ideal) potential (dashed line) due to irreversible losses. Three major losses influence the shape of this V-i curve at different current density regions. Adapted from Ryan O'Hayre, Suk-Won Cha, Whitney Colella, and Fritz B.Prinz (**2016**) *Fuel Cell Fundamentals*.[2]

In Figure 1.2, the x-axis is current density rather than current, because large fuel cell area generates more electricity (current) than small fuel cell area. Consequently, it makes sense to normalize current by fuel cell area. Theoretically, an ideal fuel cell should have a constant voltage output at any current density (the dashed line). Because of the three irreversible losses during fuel cell operation, however, the polarization curve does not show constant voltage output. As seen in Figure 1.2, the three irreversible losses are activation loss, ohmic loss, and mass transport loss, each dominant at different current density regions.[2]

Activation loss (η_{act}) dominates in the low current density region and occurs at both electrodes, especially the cathode, as the rate of ORR is six times lower than the rate of HOR.[3] Activation loss occurs because the energy barrier (activation energy) hinders the conversion from reactant to product. The possibility of reactant species passing through the energy barrier determines the reaction rate. To reduce activation loss, one can increase the concentration of reactant gases, increase the reaction's operating temperature, or use catalysts to decrease the activation energy.[2]

The ohmic loss (η_{ohmic}) dominates in the intermediate current density region and occurs due to ionic and electronic transportation. Electronic transportation is achieved mainly by the external electrical circuit. By contrast, ionic transportation involves protons (ions) from the anode passing through the proton exchange membrane to the cathode. ORR may occur at the interfaces between the membrane and the cathode catalyst layer, or protons may be transferred deep into the cathode by the PFSA ionomer and react with gases and electrons on the catalytic sites. Ohmic loss is mainly the loss that occurs during proton transportation through the membrane and catalyst layer. To increase proton

transportation, one can minimize the proton exchange membrane's thickness (according to Ohm's law), improve the ionomer content in the catalyst layer, or decrease the ionomer equivalent weight (the ionomer weight per mole of sulfonic acid groups).[2]

Mass transport loss (or concentration loss) (η_{conc}) dominates in the high current density region, which consists of both the reactant gases' movement into and the product water's exit from the cell. Even though sufficient reactant gases are provided at the flow channel, gases still need to pass through the void phase in the GDL and catalyst layer to reach the active catalyst sites. Furthermore, if too much water remains in the cathode catalyst layer, water flooding will occur and reduce power generation. To limit concentration loss, one can increase the gas diffusion coefficient (by increasing the catalyst layer's porosity) or decrease the thickness of the catalyst layer to facilitate reactant and product transportation.[2]

In conclusion, Equation 1.5 represents actual fuel cell voltage output (V):[2]

$$\mathrm{V} = \mathrm{E}_{\mathrm{thermo}} - \eta_{\mathrm{act}} - \eta_{\mathrm{ohmic}} - \eta_{\mathrm{conc}} \qquad \text{(Equation 1.5)}$$

1.1.3 Challenges in PEMFC Commercialization

As discussed previously, the electrodes (anode and cathode) in a PEMFC are thin catalyst layers that provide a location for half-cell reactions (HOR and ORR). Half-cell reactions can occur only in environments to which gases, electrons, and protons all have access, so the reaction location should be (i) highly porous, allowing reactant gases to pass in and generated water to move out, which is achieved by void phases in the catalyst layer; (ii) electronically conductive, which is achieved by electrons travelling through electrically conductive solids (catalyst and substrate); and (iii) proton conductive to allow

protons to travel through; thus, the catalyst must be intimate contact with the ionomer. Reactions can occur in a location meeting all three requirements, called the triple-phase boundary.[2,3]

Pt/C (active platinum atoms dispersed on a carbon support) is the commonly used catalyst in both electrodes, but its high cost is an obstacle to widespread fuel cell application.[7] In 2018, the US Department of Energy (DOE) estimated fuel cell system manufacturing costs and found that, even with the highest volume predictions, the total system cost is still $50/KW$_{net}$ to manufacture 100,000 units per year and $45/KW$_{net}$ for 500,000 units per year.[10] To compete economically with other alternative technologies, however, fuel cell system manufacturing would have to reduce cost to $30/KW$_{net}$.[1] The high cost is due mainly to the Pt/C catalysts at the fuel cell stack and the stainless-steel bipolar plates. Research has focused on reducing the high catalyst cost by using substitutes for Pt/C catalysts at the electrodes, especially at the cathode. The proposed methods of decreasing catalyst costs include increasing the catalyst's electrochemical surface areas, such as by depositing Pt atoms on carbon nanotubes[11] or using Pt alloys with core-shell powders,[12] such as Pt/Ni,[13] PtAu/C,[14] and Pt/CO.[15] However, using these transition metals in Pt alloys may lead to cation leaching, which will contaminate the ionomer in the catalyst layer and membrane, thus reducing fuel cell power generation.[16] Furthermore, the activity target for this type of catalyst—a four-fold enhancement of mass activity—has yet to be achieved.[13]

Another, less expensive alternative is using only nonprecious metals as the cathode catalyst, i.e., creating platinum group metal (PGM)–free catalysts (i.e., catalysts that contain no Pt, Ru, Rh, Pd, Os, or Ir). This research used PGM-free catalysts to fabricate

MEAs and evaluate both short- and long-term fuel cell performance. Section 1.2 introduces the synthetic approach, actives sites, durability challenges, and proposed degradation mechanisms of PGM-free catalysts.

1.2 PGM-Free Catalysts

The development and use of PGM-free catalysts in PEMFCs has the potential to improve the economic viability of fuel cells in competition with alternative technologies. Thompson et al.[7] have estimated that the material and system manufacturing cost of using PGM-free catalysts (typically at 3–6 mg/cm^2) would be 200 times less than using Pt-based catalysts (at a loading of 0.142 mg_{Pt}/cm^2).[7] PGM-free catalysts that use a first-row transition metal (such as Fe, Co, Ni, and Mn) represent an attractive alternative, because (i) they exhibit moderately high intrinsic activity for ORR, (ii) there are a multitude of synthetic approaches for creating active site structures, (iii) they have been successfully incorporated into PEMFCs and achieved reasonably high initial power output results, and (iv) they can be manufactured inexpensively at scale.[17–19]

1.2.1 Synthetic Approaches for Fe-N-C PGM-Free Catalysts

Catalysts composed of transition metal, nitrogen, and carbon, called M-N-C catalysts (in which M=Fe, Co, Ni, or Mn), stand out as the best-performing PGM-free catalysts.[20,21] The transition metal affects catalyst morphology and electrocatalytic ORR activity in M-N-C catalysts. The results of a rotating disk electrode test show a clear ORR catalytic activity trend in alkaline and acidic media: Fe>Co>Ni>Mn.[22] Compared with

Fe-N-C, Co-N-C catalysts both produce less ORR activity and face a sourcing problem. Demand for cobalt is surging,[7] but its two primary sources are inadequate, because (i) cobalt is extracted as a by-product of copper mining, and cobalt production from copper mines will not increase unless copper prices rise; and (ii) extracting cobalt endangers miner health and pollutes the local environment. Mn-N-C catalysts are more durable but produce less catalytic activity than Fe-N-C catalysts. The low catalytic activity results from the low density of Mn-N-C catalysts' active sites, but previous studies have shown that simply increasing the amount of Mn precursor cannot improve active site density, as it only forms inactive and unstable metallic compounds, such as oxide or carbide.[23,24] No approach has yet synthesized Mn-N-C catalysts that are as active as Fe-N-C catalysts. Consequently, the present research fabricated MEAs and conducted fuel cell tests with Fe-N-C catalysts.

In recent decades, substantial efforts have been devoted to PGM-free ORR electrocatalyst synthesis. Various synthetic approaches have been developed to increase ORR activity by increasing turnover frequency and active site density.[25] In 2009, Dodelet et al.[26] synthesized carbon-supported iron-based catalysts with active sites within the micropores in the interstices of graphitic sheets.[26] They found that active site density can be improved considerably by ball-milling the mixture (carbon support, phenanthroline, and ferrous acetate) and pyrolyzing the mixture twice, first in argon and secondly in ammonia.

Subsequently, in 2013, Cheon et al.[27] employed a hard-templating approach to synthesize an ordered mesoporous porphyrinic carbon (M-OMPC) (in which the M=Fe, Co, or FeCo),[27] which exhibited high surface areas, tunable pore structures, and high

ORR activity. Based on this work, Serov et al. introduced a mechanochemical synthesis (hard-templating pore-former) approach,[28] which permits substantial amounts of Fe-N-C catalysts to be prepared. Pajarito Powder further developed this approach,[17,18,29] trademarked it as the VariPore method, and commercialized the catalyst. Using this method to synthesize catalysts can control the catalysts' morphology, chemical composition, and physical properties by the use of various pores and particle forms. The basic preparation steps of this approach comprise (i) infusing particle formers (such as silica and magnesia) with precursors of the final materials and (ii) transforming those precursors into catalysts (Figure 1.3).[30]

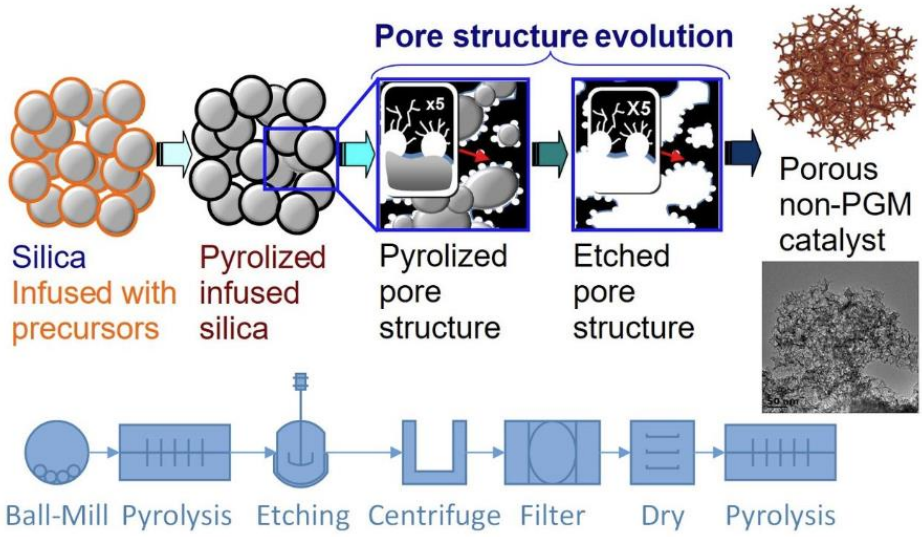

Figure 1.3. Schematics of catalyst manufacturing using the VariPore method. Adapted from Alexy Serov, Geoffrey McCool, Samuel McKinney, Henry Romero and Barr Zulevi (**2019**) *ECS Meeting Abstract*.[30]

Beyond the traditional synthetic approaches,[31] Proietti et al. in 2011 described an iron-acetate/phenanthroline/zeolitic imidazolate framework (ZIF)-derived electrocatalyst called a metal-organic framework (MOF) catalyst,[32] which showed improved volumetric activity and enhanced mass-transport properties. Subsequent work showed that even higher ORR activity could be achieved by optimizing the doped Fe content in the ZIF precursors[33], controlling the thermal activation temperature.[33,34]

1.2.2 The Active Site Conundrum of Fe-N-C PGM-Free Catalysts

In Pt/C catalysts, the active site structure comprises active Pt atoms dispersed on a carbon support,[35] but the active sites of Fe-N-C catalysts are more complicated. The nature of the active ORR sites in Fe-N-C PGM-free catalysts remains a topic of intense debate and requires further research for clarification.[36] For example, Varnell et al. identified the Fe particles encapsulated by graphitic C and N (CN_x) as active species.[37] Artyushkova et al. propose two distinct possible ORR pathways:

(i) four-electron reduction, which directly reduces O_2 to H_2O:

$$O_2 + 4e^- + 4H^+ \rightarrow 2H_2O \qquad \text{(Equation 1.6)}$$

(ii) a two-step, two-electron (2×2) pathway, which first reduces O_2 to H_2O_2 and then reduces H_2O_2 to H_2O:

$$O_2 + 2e^- + 2H^+ \rightarrow H_2O_2 \qquad \text{(Equation 1.7)}$$

$$H_2O_2 + 2e^- + 2H^+ \rightarrow 2H_2O \qquad \text{(Equation 1.8)}$$

Artyushkova et al. found that different active sites functioned through different ORR pathways. The Fe coordinated to N atoms (FeN_x) was identified as the active site

for the four-electron reduction. The metal-free electrocatalyst support acted as the active site from O_2 to H_2O_2, and the pyrrolic and pyridinic nitrogen appeared to be the active site from H_2O_2 to H_2O.[38]

Another commonly observed active site in Fe-N-C PGM-free catalysts is that of the FeN_4 moieties, which Chung et al. directly visualized on (CM+PANI)-Fe-C catalysts using aberration-corrected scanning transmission electron microscopy (STEM) as shown in Figure 1.4.[39] Figure 1.4a is a bright-field (BF) STEM image showing the overall morphology of the principal structures in (CM+PANI)-Fe-C catalysts, which comprise the primary fibrous carbon and secondary few-layer graphene sheet. Figures 1.4b and 1.4c are atomic-resolution high-angle annular dark-field STEM (HAADF-STEM) images. Figure 1.4b shows the dense fibrous carbon particles that consist of randomly oriented, intertwined, turbostratic graphitic domains. Figure 1.4c shows the single Fe atoms dispersed across the carbon surface (the few-layer graphene sheet phase). Figure 1.4d shows the electron energy loss (EEL) spectra, which confirm the presence of N atoms surrounding each Fe atom; the quantified Fe-to-N ratio from the EEL data is 1 to 4 (20.5% Fe and 79.5% N).

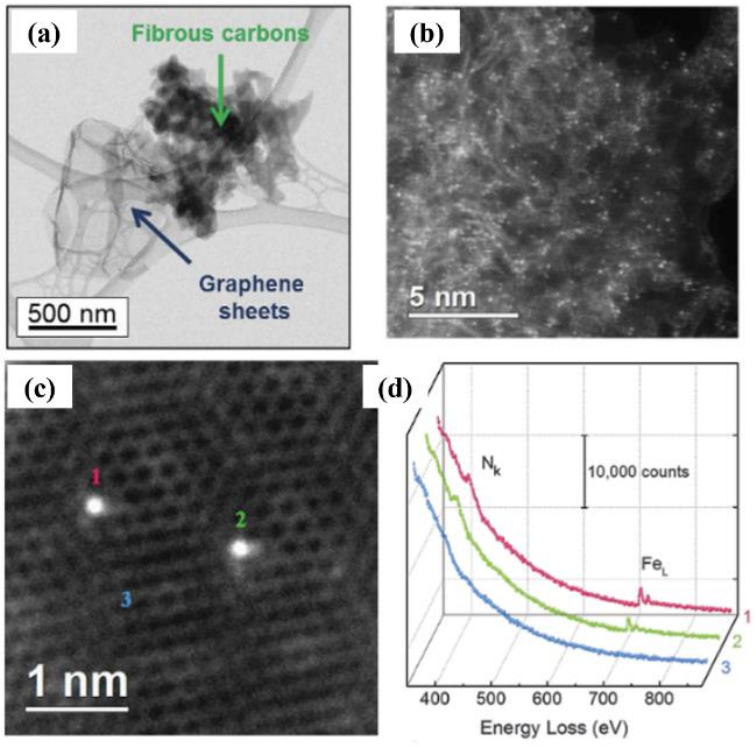

Figure 1.4. STEM images and EEL spectra of a (CM+PANI)-Fe-C catalyst. (a) BF-STEM image of a typical (CM+PANI)-Fe-C catalyst, showing primary fibrous carbons and secondary graphene sheets. (b) Atomic-resolution HAADF-STEM image of Fe atoms distributed across the surface of the fibrous carbon phase. (c) HAAD-STEM image of individual Fe atoms (labels 1, 2, and 3) in a few-layer graphene sheet. (d) The EEL spectra of the N and Fe atoms acquired from single Fe atoms (1 and 2) and few-layer graphene (3) demonstrate that N atoms are present around the Fe atoms. Adapted from Hoon T. Chung, David A. Cullen, Drew Higgins, Brian T. Sneed, Edward F. Holby, Karren L. More, and Piotr Zelenay (**2017**) *Science*.[39]

Some researchers believe that the active site structure is the Fe atom coordinated with the N atoms embedded in the carbon matrix.[39,40] For example, Nabae et al. developed a catalyst (synthesized through a carbon support + organic precursor) whose active site is Fe contained within a hexaaza macrocyclic ligand with a 14-membered ring (14MR) as shown in Figure 1.5a. This catalyst is more durable than the conventional Fe-N-C catalyst, whose active site is Fe contained within a porphyrinic 16-membered ring

(16MR) as shown in Figure 1.5b.[41] The 14MR active site is more durable due to the more compact ligand, which results in a strong Fe-N bond with an average bond distance of 1.90 Å, which is markedly shorter than the Fe-N bond distance in the 16MR (2.0 Å).[42] Similarly, Wu et al. propose that there are two active sites in Fe-N-C catalysts (synthesized through MOF) as shown in Figure 1.6: the defect-rich pyrrolic N-coordinated S1 site (FeN_4C_{12}) and the highly stable pyridinic N-coordinated S2 site (FeN_4C_{10}).[43] The S1 and S2 sites are ORR active for the direct four-electron reduction; S1 sites are more active but less stable than S2 sites.

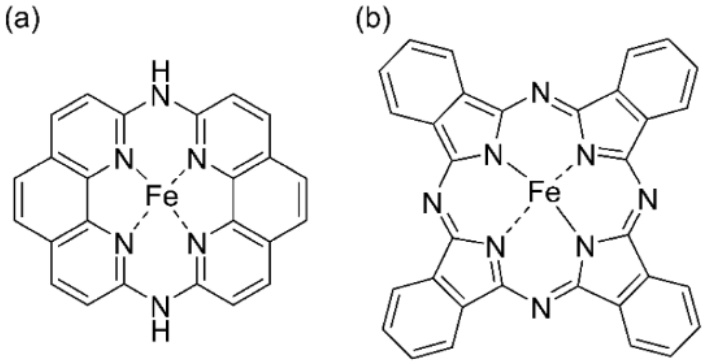

Figure 1.5. Atomistic structures of the ORR active sites: (a) Fe contained within a hexaaza macrocyclic ligand with a 14-membered ring (14MR); (b) Fe contained within a porphyrinic 16-membered ring (16MR). Adapted from Junya Ohyama, Makoto Moriya, Ryo Takahama, Kazuki Kamoi, Shin Kawashima, Ryoichi Kojima, Teruaki Hayakawa, and Yuta Nabae (**2021**) *JACS Au*.[41]

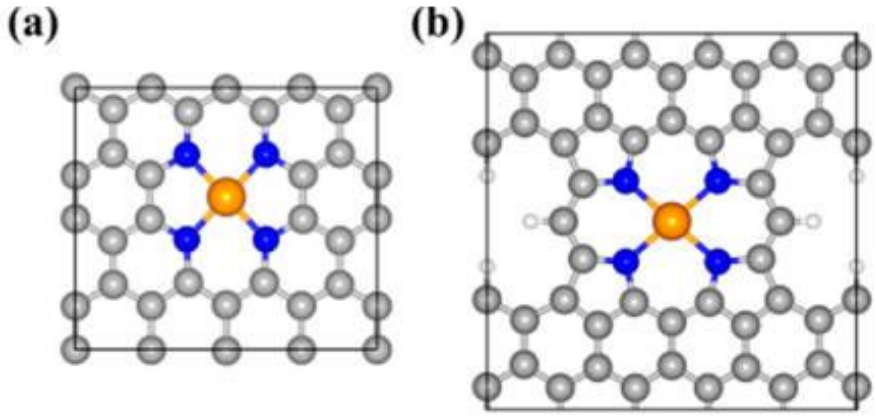

Figure 1.6. Atomistic structures of the ORR active site: (a) FeN_4C_{10} (S2 site); (b) FeN_4C_{12} (S1 site). Adapted from Kexi Liu, Gang Wu, and Guofeng Wang (**2017**) *Journal of Physical Chemistry C*.[44]

1.2.3 Degradation Challenges for Fe-N-C PGM-Free Catalysts

The estimated cost reduction achieved by replacing Pt-based catalysts with Fe-N-C PGM-free catalysts is substantial, encouraging, and exciting, but it was calculated on the assumption that Fe-N-C catalysts have a comparable durability to Pt-based catalysts. Fe-N-C catalysts' limited durability remains a formidable challenge that must be addressed before they can be used in commercialized fuel cell systems, however. Scant research has examined this catalyst's durability under fuel cell test conditions, and more work is needed to understand it fully. According to the published durability data, fuel cells with PGM-free catalyst cathodes typically degrade by 40% to 80% within the first 100 hours of fuel cell operation.[21,25,32,45–47] Currently, there are four proposed degradation mechanisms to explain the poor durability of the Fe-N-C PGM-free catalyst cathode's MEA: (i) water flooding at micropores, (ii) metal dissolution, (iii) H_2O_2 (or associated radicals) attacks, and (iv) the active sites' protonation or anion adsorption.

Degradation mechanism I: Water flooding at micropores

In 2016, Dodelet et al. [48] proposed that the degradation of Fe-N-C PGM-free catalysts originates in slow oxidation of the carbonaceous support, which in their study took around 15 hours to transform the cathode catalyst layer from hydrophobic to hydrophilic. Due to the increased hydrophilicity, water flooding occurred at the micropores, degrading the catalyst. Choi et al. [47] challenged that hypothesis and conducted cyclic voltammetry tests to monitor the specific capacitance change during durability tests at 100% and 60% relative humidity (RH). The specific capacitance revealed that the catalyst layer had been mostly hydrated at the beginning of life (BOL), and the performance loss was mainly at the kinetic (activation) loss region rather than at the mass transfer loss region (i.e., if water flooding had occurred in the catalyst layer, substantial mass transfer loss should have been detected). Dodelet et al. [49] then argued that water flooding at the micropores is not responsible for the degradation but is a trigger that causes the metal dissolution of FeN_4 sites (FeN_4 sites are located mainly in the micropores[50]). The authors suspect that, FeN_4 sites are unstable in an open system, such as one with hydrophilic micropores (pore size: >0.7 nm), through which water quickly passes (with protons and dissolved hydrogen peroxide). This would result in Fe atoms being dissolved, and the dissolved Fe ions would be quickly flushed out of the cell, a phenomenon detected and confirmed in their work by Fe Mössbauer spectroscopy and neutron activation analysis.

Degradation mechanism II: metal dissolution

Metal dissolution in Fe-N-C PGM-free catalysts has been well documented in the literature, but the challenge has been to determine whether the loss of Fe species affects ORR activity.[21,25]

In 2013, Ferrandon et al. used X-ray absorption near-edge structure to separately measure Fe loading in the cathode catalyst layer before and after 200 hours of potentiostatic hold at 0.4 V and 0.6 V, finding more catalyst kinetic performance loss at 0.6 V. The Fe specification results showed that 78% of the initial Fe was lost at 0.6 V and 84% at 0.4 V, but most of the lost Fe species were inactive for ORR, such as Fe sulfide.[51] Similarly, Choi et al. subsequently reported Fe demetallation from an Fe-based crystalline structure, but the demetallation had no adverse effect on ORR. [52]

Most Fe-N-C PGM-free catalysts have been acid-washed before fabrication into MEAs to remove inactive sites.[53] However, Mamtani et al. evaluated the impact of acid-washing at different stages during catalyst synthesis.[54] They reported a substantial performance loss when catalysts are acid-washed after the pyrolysis steps. Fe Mössbauer spectroscopy tests revealed that the detrimental ORR activity loss after acid-washing was the loss of FeN_4 sites.

Degradation mechanism III: H_2O_2 (or associated radicals) attacks

As mentioned, more H_2O_2 is generated in a PGM-free catalyst cathode than in a Pt-based catalyst cathode through an indirect two-electron transfer reaction (Equation 1.7).[38] Jaouen et al. [55,56] report that the disproportionation of H_2O_2 is minor during ORR in a PGM-free catalyst cathode. Goellner et al. conducted *ex situ* studies on M-N-C

(M=Cr, Fe, and Co) catalysts to evaluate the effect of H_2O_2 on M-N-C catalyst degradation.[57] The results suggest that degradation increases as the amount of H_2O_2 goes up and that H_2O_2 decreases the ORR activity at the high potential region and diminishes the transport property at the low potential region. Choi et al. found that active sites are electrochemically unstable to H_2O_2 in acidic media but not in alkaline ones.[58] This result reveals that, in the acidic media, the generated H_2O_2 cannot be quickly reduced to water but reacts with the Fe ions in the catalyst via Fenton reactions and induces reactive oxygen species, hydroxy radicals (·OH), and hydroperoxyl radicals (·OOH).[59] The generated reactive oxygen species attacked the carbon support in active sites rather than the H_2O_2 directly attacking the active sites. As discussed in Section 1.2.2, carbon support is vital for catalyst activity and durability.[44] The H_2O_2-induced reactive oxygen species attack (oxidize) active sites' carbon support has been regarded as the primary degradation mechanism in Fe-N-C catalyst cathode MEAs.[53] Studies also show that this attack on the carbon support further results in active site demetallation or structural disintegration of the catalyst layer.[52,60,61]

Degradation mechanism IV: active sites' protonation or anion adsorption

Whether the degradation mechanism of the protonation or anion adsorption of active sites occurs in the Fe-N-C catalyst cathode remains a matter of debate. On the one hand, Herranz et al. conducted *ex situ* tests on Fe-N-C catalysts and concluded that, when basic N-groups are protonated but not anion-bounded, the catalyst ORR activity is high; when the basic N-group is protonated and anion-bounded, however, ORR activity is low.[62]

On the other hand, Banham et al. assumed that, if this degradation occurs, there should be no differences in cathode catalyst layers of various loadings (thicknesses), as the ionomer content is the same, which is contrary to their results.[53] Some studies contend that the catalyst degradation is independent of anions.[63,64]

In conclusion, the extant experimental results cannot exclude any degradation mechanism. Still, it is commonly agreed that the H_2O_2 (and associated radicals) attack is the primary degradation mechanism in PGM-free catalyst cathode PEMFCs.[21,25,53,57,65] Furthermore, it is believed that the four degradation mechanisms could coexist in the cathode and even affect one another; in other words, one mechanism could initiate or accelerate the others.[21,25,36,66] Further and deeper study of the degradation mechanism is required to fully understand the degradation mechanisms of Fe-N-C catalysts.

1.2.4 Conclusion: Achievement in Fe-N-C PGM-Free Catalysts

In the past decades, substantial progress has been made in Fe-N-C PGM-free catalysts, especially in improving catalyst activity. Some Fe-N-C catalysts have already achieved comparable initial performance to that of Pt-based catalysts,[33,67–70] but limited catalyst durability remains the most significant challenge in Fe-N-C catalysts. Currently, more and more research seeks to improve Fe-N-C catalysts' durability by clarifying the degradation mechanism,[21,25,53,65] optimizing the catalyst synthesis procedure,[45,46,71,72] optimizing the cathode catalyst layer design,[67,73] etc. Despite the challenges, Ballard collaborated with Nisshinbo Holdings in 2017 to develop the first commercialized PGM-free catalyst-based PEMFC system.[74,75]

1.3 Objective and Rationale

This thesis focuses on the design, fabrication, characterization, and evaluation of nanofiber mat cathodes and hydrogen/air fuel cell MEAs with PGM-free catalysts, seeking to identify the best catalyst particle size and surface functionality for incorporation into submicron diameter electrospun fibers. The resulting MEAs employ a Pt/C spray powder anode (at a loading of 0.1 mg/cm^2) and a Nafion 211 membrane to overcome the shortcomings of traditional fuel cell structures. The PGM-free fiber cathode binder is a hydrophilic mixture of ionomer and polyethylene oxide (PEO) or a hydrophobic mixture of ionomer and polyvinylidene fluoride (PVDF), with the ionomer/PVDF weight ratio dictating the degree of hydrophobicity. The nanofiber mat cathode catalyst type, composition (binder type and ionomer/hydrophobic polymer weight ratio), and morphology (fiber diameter, fiber mat porosity, and mat thickness) are identified for MEAs that approach or meet the DOE's ElectroCat 2020 durability targets, e.g., a durability of 5,000 hours, which is estimated by extrapolating accelerated stress test (AST) results. Additionally, this thesis describes structure/performance correlations to clarify why nanofiber electrodes with PGM-free catalysts work well and to guide future nanofiber electrode research.

Slack et al. performed preliminary hydrogen/air fuel cell tests on electrospun fiber mat cathodes containing a MOF-derived Fe-N-C catalyst from Pajarito Powder, in which the cathode catalyst binder was a blend of Nafion and PVDF.[73] When incorporating fiber mats into an MEA, a fiber cathode (containing 70 wt% catalysts and 1:1 (w:w) Nafion:PVDF binder) performed well, with excellent long-term stable power output as

shown in Figure 1.7;[73] a power density of 80 mW/cm^2 at 0.5 V was durable for 300 hours of operation (for a H_2/air fuel cell operating at 80 °C, 100% RH, and 200 kPa_{abs} with a cathodic PGM-free catalyst loading of 3.0 mg/cm^2). The stable performance of the nanofiber MEA contrasts with the declining power of a conventional sprayed cathode MEA with a neat Nafion binder. The results in Figure 1.7 also show that the nanofiber cathode's power output depends on the binder's Nafion:PVDF weight ratio; as expected, higher power is attained with less non-conducting PVDF. The excellent performance of the fiber mat cathode MEAs is a consequence of (1) the highly desirable nanofiber electrode morphology, in which inter- and intra-fiber porosity, a uniform distribution of catalyst and binder, and a very thin binder coating on all the catalyst particles improves both water removal and oxygen access to catalyst sites; and (2) the presence of hydrophobic PVDF in the binder, which limits water access to the catalyst surface, thus eliminating or minimizing the degradation of catalyst performance during a constant voltage test. In a nanofiber mat configuration, the state-of-the-art PGM-free catalysts from Pajarito, with an ionomer/PVDF binder composition offering the optimum hydrophilicity/hydrophobicity for high power and minimal activity degradation, will make it possible to meet the MEA durability targets set by the DOE.

To overcome the shortcomings of traditional cathode designs with PGM-free electrodes (in terms of fuel cell power output and MEA durability), this dissertation research designed, fabricated, characterized, and evaluated fiber mat cathode MEAs with Fe-N-C–based PGM-free ORR cathode catalysts for H_2/air fuel cells. The research also generated functional correlations and insights regarding the electrospinning of particle/polymer mixtures into fiber mats as well as the relationship between fiber

electrode composition and structure, the hydrophobicity/hydrophilicity of the cathode binder, and both short- and long-term MEA performance.

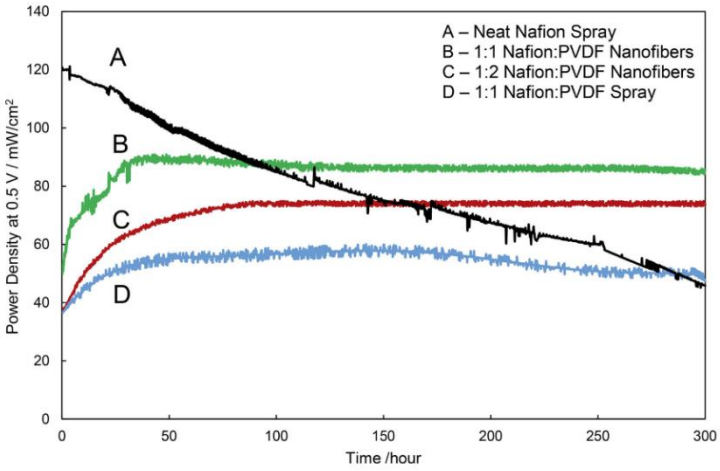

Figure 1.7. H_2/air fuel cell power density at 0.5 V over time for 300 hours with MEAs using a PGM-free catalyst at 3.0 mg/cm^2 and either a nanofiber cathode (with a 1:1 or 1:2 Nafion:PVDF binder) or a sprayed cathode (with neat Nafion or a 1:1 Nafion:PVDF binder). All the MEAs had a Nafion 211 membrane and a sprayed anode with Nafion binder and Johnson Matthey Pt/C HiSpec 4000 at 0.1 mg_{Pt}/cm^2. Fuel cell operating conditions: 80 °C, 100% RH, 200 kPa_{abs}, and 125/500 sccm H_2/air feed gas flow rates. Adapted from John Slack, Barr Halevi, Geoff McCool, Jingkun Li, Ryan Pavlicek, Ryszard Wycisk, Sanjeev Mukerjee, and Peter Pintauro (**2018**) ChemElectroChem.[73]

1.4 Background of Electrospinning and Its Application in PEMFC

Electrospinning is an economically sound strategy for fabricating nonwoven fibrous structures with fiber diameters in the submicron range for various applications, including filtration media, medical products, and sensors.[76–79] Pintauro and colleagues have shown that electrospinning can be used to fabricate membranes and electrodes for fuel cells and batteries, including (1) proton exchange membranes with high H^+ conductivity at low RH

for H_2/air fuel cells,[80] (2) species-selective membranes for H_2/Br_2 regenerative fuel cells,[81] (3) high conductivity anion exchange membranes,[82] (4) particle/polymer electrodes for Li-ion batteries (nanofibers with TiO_2, C, Si, or $LiCoO_2$ particles with poly[acrylic acid] or PVDF binders),[83] and (5) nanofiber Pt/C and Pt-alloy particle/polymer fiber mat electrodes for H_2/air fuel cells.[15,84–86]

Figure 1.8 shows a typical laboratory schematic of the electrospinning setup. Electrospinning is typically conducted at room temperature with controlled RH. The electrospinning solution is drawn into a syringe with a stainless needle spinneret. High voltage (6–15 KV) is applied to the needle, which constructs a strong electric field between the spinneret tip and the collector. The pump pushes the solution out of the syringe at a constant rate. The RH, voltage applied to the needle, flow rate of the syringe's electrospinning solution, and distance between the spinneret tip and collector are all controlled. The drum rotates and laterally oscillates to collect a fiber mat of uniform thickness.

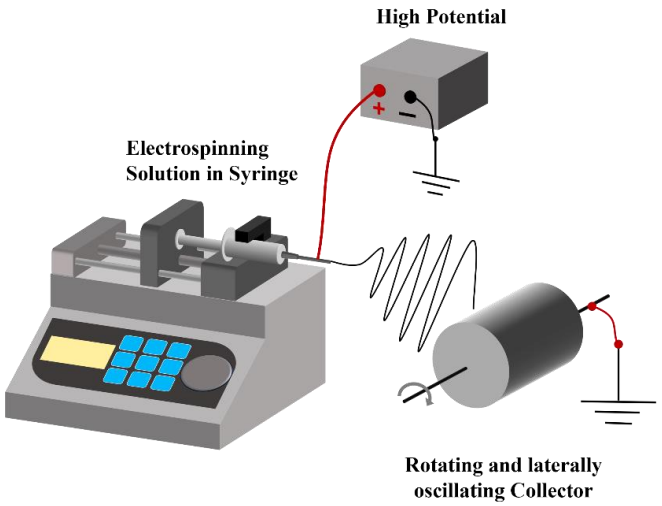

Figure 1.8. Schematic of a laboratory electrospinning setup.

During the electrospinning process, the polymer solution or melt is extruded through the spinneret under the influence of the strong electric field. Meanwhile, the high shear forces generated at the spinneret tip break up agglomerates, and solvent from the particle/binder jet quickly evaporates and minimizes particle re-agglomeration. Under these combined effects, fiber mats are formed with a uniform fiber diameter and less agglomeration.

Thompson et al. report that fiber morphology depends on the electrospinning solution's composition and the electrospinning conditions, such as the distance between tip and collector, electric potential, solution viscosity, solvent, solution density, and polymer concentration.[87] Previous attempts to electrospin fiber mats with Nafion as the only ionomer in the solution have failed, forming only electrospray droplets,[88] because Nafion in either alcohol or organic solvents produces only micellar dispersion.[89] To electrospin fiber mats, the solution requires sufficient entanglement chains,[90] which may be achieved by adding carrier polymer to the electrospinning solution, such as polyacrylic acid (PAA), PEO, or PVDF.

In 2010, Wenjing et al. successfully electrospun Pt/C catalyst with a Nafion/PAA blended binder and fabricated it into an MEA.[86] The mass activity of a fiber cathode MEA is almost twice that of a decal cathode MEA (mass activity: 0.23 A/mg_{Pt} vs. 0.11 A/mg_{Pt}, respectively). This result offers a promising method for decreasing catalyst and MEA fabrication costs in PEMFCs through the design of electrode morphologies. Later, Brodt et al. found that the carrier polymer (PAA) in fiber mats adversely affected fuel cell performance by diluting the Nafion binder and consequently decreasing proton conductivity in the catalyst layer, but attempts to remove the PAA failed.[91] Fortunately,

Waldrop et al. later successfully fabricated an electrospun fiber mat with a Pt/C catalyst, salt-form Nafion (with Na^+, Li^+, or Cs^+), and PEO carrier polymer, with the PEO being extracted before MEA testing by means of a hot-soaking step with no harm to the fiber morphology.[92] A fuel cell power improvement was observed after the carrier polymer's (PEO) removal. The MEA with a fiber electrode of Nafion/PEO binder (with the PEO extracted) generated 15% more power at 0.65 V than an MEA with a fiber electrode of Nafion/PAA binder (1,135 vs. 957 mW/cm^2, respectively) at 100% RH.[93]

Brodt et al. subsequently found that electrode morphology had no influence on Pt dissolution (after a 10,000-cycle AST using a square-wave cycle between 0.6 V and 0.95 V, with three seconds per step under H_2/N_2),[91] but this protected the catalysts from carbon corrosion (cycling from 1.0 V to 1.5 V at a scan rate of 500 mV/S under H_2/N_2 for 1,000 cycles). To further improve the durability of the Pt/C catalyst fiber cathode, Brodt et al. then used PVDF as a carrier polymer to fabricate fiber mats, with the PVDF functioning to (i) effectively enable electrospinning and (ii) provide a hydrophobic polymer to expel electrogenerated water from the cathode and protect the catalyst from degradation.[85] When the PVDF content in the cathode binder was over 50 wt%, the carbon corrosion rate as measured by a DOE-approved AST (a triangular wave between 1.0 V and 1.5 V at a scan rate of 500 mV/s for 1,000 cycles under H_2/N_2) was effectively reduced to near zero, accompanied by an overall decrease in MEA power output.[1] The authors attribute the power output decrease (as PVDF content increased) to the binder's substantial decrease in proton conductivity (due to the dilution of Nafion with an uncharged PVDF).[94] Subsequent work by Slack et al. revealed that PVDF in fiber mats had profound effects on both the structural and electrochemical properties of fuel cell cathodes.

PVDF's robust mechanical properties increased the cathode's mechanical strength and thus prevented the cathode pores from collapsing, and its hydrophobic properties increased the cathode's hydrophobicity and consequently decreased the carbon corrosion rate.[95] Next, Slack et al. electrospun PGM-free catalyst fiber mats with a Nafion:PVDF (w:w) 50:50 blended binder and fabricated it into an H_2/air fuel cell MEA,[73] which generated stable power output at 0.5 V for 300 hours at 80 mW/cm^2. This work is shown in Figure 1.7 and discussed in Section 1.3.

1.5 Outline of Remaining Chapters

The present research used three types of Fe-N-C PGM-free catalysts provided by Pajarito Powder. The Gen-1 and Gen-2 PMF catalysts were synthesized through the hard-templating pore-former approach and the MOF-based PGM-free catalysts were synthesized through the metal-organic-framework approach. The catalysts were used to fabricate MEAs with Nafion 211 and a Pt/C powder anode (0.1 mg_{Pt}/cm^2) and were evaluated in H_2/air fuel cells at 80 °C, 200 kPa_{abs}, and 100% RH.

Chapter II of this dissertation describes fiber cathode MEAs with Nafion/PVDF binder using Gen-1 PMF catalysts. The cathode catalyst loading was between 0.75 and 3.0 mg/cm^2, and the total binder content was constant relative to the amount of catalyst at 50 wt%. The fiber mat cathodes were made with either Nafion/PEO binder (from which the PEO was extracted before testing) or a Nafion/PVDF blended binder in which the Nafion/PVDF weight ratio was 50:50, 67:33, 75:25, or 80:20. For comparison, two types of conventional powder cathode were also fabricated with either a neat Nafion binder or a

50:50 (w:w) Nafion:PVDF binder. The experiments examined how cathode binder composition (the amount of PVDF added to the Nafion), cathode morphology (powder vs. fiber), and cathode catalyst loading (0.75–3.0 mg/cm^2) affect the power output and durability of MEAs.

Chapter III discusses the use of MOF-based PGM-free catalysts in slurry/powder and nanofiber cathode MEAs. Fiber mats with Nafion/PVDF binder and a MOF-based Fe-N-C catalyst were successfully electrospun with Nafion:PVDF weight ratios of 50:50, 67:33, 75:25, 80:20, and 83:17. The fiber mats were incorporated into a fuel cell MEA with a Nafion 211 membrane and a Pt/C anode. The effect of cathode binder composition on initial power and MEA durability was assessed, and the results are compared with those of a Gen-1 PMF fiber mat cathode MEA.

Chapter IV describes a new generation of PMF catalysts, termed Gen-2 PMF catalyst, that differ from the Gen-1 PMF catalyst described in Chapter II. The two generations of PMF catalyst were used to fabricate Nafion powder, Nafion fiber, and 75:25 (w:w) Nafion:PVDF fiber cathodes. The experiments examined the effect of the catalysts on cathode morphology, initial fuel cell power output, and MEA durability.

In Chapter V, a new type of hybrid fiber/particle cathode with Gen-2 PMF catalysts is described. The MEAs were evaluated in terms of initial power output (power density at BOL) and the power generated after a 30K voltage-cycling AST (square-wave cycles between 0.6 V and 0.95 V with three seconds at each step). Three types of hybrid cathodes (containing both catalyst particles and fiber mats in the catalyst layer) were designed, fabricated, and evaluated: (1) the hybrid type I cathode, in which catalyst particles are interspersed between fibers; (2) the hybrid type II cathode, in which catalyst

particles and Nafion are interspersed between fibers; and (3) the hybrid type III cathode, in which catalyst particles, Nafion, and fluorinated ethylene propylene (FEP) are interspersed. In all the hybrid cathodes, redispersed fibers were used, and the binder for the PMF catalyst particles was Nafion; that is, the fibers were electrospun with a mixture of Nafion and PEO, and the PEO was removed after the fiber electrospinning. The hybrid cathode MEAs were compared to (1) an MEA with a conventional powder cathode with Nafion binder; (2) an MEA in which the cathode was composed of only redispersed fibers; (3) a fiber mat cathode MEA with a neat Nafion binder; (4) the best fiber mat cathode MEA with a cathode composed of Nafion and PVDF binder and Gen-1 PMF catalyst; and (5) the best fiber mat cathode MEA with Nafion and PVDF binder and a MOF-based PGM-free catalyst.

1.6 References

1. Cells, T. F. *et al.* Fuel Cell 2016 Multi-Year Research, Development, and Demonstration Plan. *Department of Energy, Multi-Year Research, Development, and Demonstration Plan* **2015**, 1–58 (2016).
2. O'Hayre, R., Cha, S.-W. & Prinz, F. B. *Fuel Cell Fundamentals*. (John Wiley & Sons, 2016).
3. Frano Barbir. *PEM Fuel Cell Theory and Practice*. (Academic Press; 2nd edition (October 9, 2012), 2012).
4. M. Scott Shell. *Thermodynamics and Statistical Mechanics*. (Cambridge University Press; 1st edition (August 5, 2015), 2015).
5. Xie, F. *et al.* Recent progresses in H2-PEMFC at DICP. *Journal of Energy Chemistry* **36**, 129–140 (2019).
6. Thomas, S. Fuel Cell and Battery Electric Vehicles as power plants. *National Hydrogen Assocation Conference and Hydrogen Expo* 1–12 (2009).

7. Thompson, S. T. & Papageorgopoulos, D. Platinum group metal-free catalysts boost cost competitiveness of fuel cell vehicles. *Nat Catal* **2**, 558–561 (2019).

8. FCEV Cumulative Sales Data (California Fuel Cell Partnership,2022). *https://h2fcp.org/sites/default/files/FCEV-Sales-Tracking.pdf*.

9. Peron, J. *et al.* Properties of Nafion® NR-211 membranes for PEMFCs. *J Memb Sci* **356**, 44–51 (2010).

10. Thompson, S. T. *et al.* Direct hydrogen fuel cell electric vehicle cost analysis: System and high-volume manufacturing description, validation, and outlook. *J Power Sources* **399**, 304–313 (2018).

11. Lv, H., Cheng, N., Mu, S. & Pan, M. Heat-treated multi-walled carbon nanotubes as durable supports for PEM fuel cell catalysts. *Electrochim Acta* **58**, 736–742 (2011).

12. Long, N. V. *et al.* The development of mixture, alloy, and core-shell nanocatalysts with nanomaterial supports for energy conversion in low-temperature fuel cells. *Nano Energy* **2**, 636–676 (2013).

13. Gasteiger, H. A., Kocha, S. S., Sompalli, B. & Wagner, F. T. Activity benchmarks and requirements for Pt, Pt-alloy, and non-Pt oxygen reduction catalysts for PEMFCs. *Appl Catal B* **56**, 9–35 (2005).

14. Ma, Y. *et al.* High active PtAu/C catalyst with core-shell structure for oxygen reduction reaction. *Catal Commun* **11**, 434–437 (2010).

15. Slack, J. J. *et al.* Nanofiber Fuel Cell MEAs with a PtCo/C Cathode. *J Electrochem Soc* **166**, F3202–F3209 (2019).

16. Braaten, J. P., Xu, X., Cai, Y., Kongkanand, A. & Litster, S. Contaminant Cation Effect on Oxygen Transport through the Ionomers of Polymer Electrolyte Membrane Fuel Cells. *J Electrochem Soc* **166**, F1337–F1343 (2019).

17. Serov, A., Kovnir, K., Shatruk, M. & Kolen'ko, Y. v. Critical Review of Platinum Group Metal-Free Materials for Water Electrolysis: Transition from the Laboratory to the Market : Earth-abundant borides and phosphides as catalysts for sustainable hydrogen production. *Johnson Matthey Technology Review* **65**, 207–226 (2021).

18. Serov, A. *et al.* Highly stable precious metal-free cathode catalyst for fuel cell application. *J Power Sources* **327**, 557–564 (2016).

19. Kishi, H. *et al.* Structure of active sites of Fe-N-C nano-catalysts for alkaline exchange membrane fuel cells. *Nanomaterials* **8**, 1–14 (2018).

20. Shao, M., Chang, Q., Dodelet, J. P. & Chenitz, R. Recent Advances in Electrocatalysts for Oxygen Reduction Reaction. *Chem Rev* **116**, 3594–3657 (2016).

21. Shao, Y., Dodelet, J., Wu, G. & Zelenay, P. PGM-Free Cathode Catalysts for PEM Fuel Cells: A Mini-Review on Stability Challenges. *Advanced Materials* **31**, 1807615 (2019).

22. Wang, X. *et al.* Size-controlled large-diameter and few-walled carbon nanotube catalysts for oxygen reduction. *Nanoscale* **7**, 20290–20298 (2015).

23. Zhang, H., Osgood, H., Xie, X., Shao, Y. & Wu, G. Engineering nanostructures of PGM-free oxygen-reduction catalysts using metal-organic frameworks. *Nano Energy* **31**, 331–350 (2017).

24. Wu, G. *et al.* Carbon nanocomposite catalysts for oxygen reduction and evolution reactions: From nitrogen doping to transition-metal addition. *Nano Energy* **29**, 83–110 (2016).

25. Osmieri, L. *et al.* Status and challenges for the application of platinum group metal-free catalysts in proton-exchange membrane fuel cells. *Curr Opin Electrochem* **25**, 100627 (2021).

26. Lefèvre, M., Proietti, E., Jaouen, F. & Dodelet, J. P. Iron-Based catalysts with improved oxygen reduction activity in polymer electrolyte fuel cells. *Science (1979)* **324**, 71–74 (2009).

27. Cheon, J. Y. *et al.* Ordered mesoporous porphyrinic carbons with very high electrocatalytic activity for the oxygen reduction reaction. *Sci Rep* **3**, (2013).

28. Serov, A., Artyushkova, K., Andersen, N. I., Stariha, S. & Atanassov, P. Original Mechanochemical Synthesis of Non-Platinum Group Metals Oxygen Reduction Reaction Catalysts Assisted by Sacrificial Support Method. *Electrochim Acta* **179**, 154–160 (2015).

29. Workman, M. J. *et al.* Platinum group metal-free electrocatalysts: Effects of synthesis on structure and performance in proton-exchange membrane fuel cell cathodes. *J Power Sources* **348**, 30–39 (2017).

30. Serov, A. *et al.* Varipore^{TM}: A Powerful Manufacturing Platform for Fuel Cell and Electrolyzer Applications. *ECS Meeting Abstracts* **MA2019-02**, 1734–1734 (2019).

31. Barkholtz, H. M. & Liu, D. J. Advancements in rationally designed PGM-free fuel cell catalysts derived from metal-organic frameworks. *Materials Horizons* vol. 4 20–37 Preprint at https://doi.org/10.1039/c6mh00344c (2017).

32. Proietti, E. *et al.* Iron-based cathode catalyst with enhanced power density in polymer electrolyte membrane fuel cells. *Nat Commun* **2**, (2011).

33. Zhang, H. *et al.* High-performance fuel cell cathodes exclusively containing atomically dispersed iron active sites. *Energy Environ Sci* **12**, 2548–2558 (2019).

34. Zhang, H. *et al.* Single Atomic Iron Catalysts for Oxygen Reduction in Acidic Media: Particle Size Control and Thermal Activation. *J Am Chem Soc* **139**, 14143–14149 (2017).

35. Borup, R. *et al.* Scientific aspects of polymer electrolyte fuel cell durability and degradation. *Chem Rev* **107**, 3904–3951 (2007).

36. Martinez, U. *et al.* Progress in the Development of Fe-Based PGM-Free Electrocatalysts for the Oxygen Reduction Reaction. *Advanced Materials* **31**, 1–20 (2019).

37. Varnell, J. A. *et al.* Identification of carbon-encapsulated iron nanoparticles as active species in non-precious metal oxygen reduction catalysts. *Nat Commun* **7**, (2016).

38. Artyushkova, K., Serov, A., Rojas-Carbonell, S. & Atanassov, P. Chemistry of Multitudinous Active Sites for Oxygen Reduction Reaction in Transition Metal-Nitrogen-Carbon Electrocatalysts. *Journal of Physical Chemistry C* **119**, 25917–25928 (2015).

39. Chung, H. T. *et al.* Direct atomic-level insight into the active sites of a high-performance PGM-free ORR catalyst. *Science (1979)* **357**, 479–484 (2017).

40. Thompson, S. T. *et al.* ElectroCat: DOE's approach to PGM-free catalyst and electrode R&D. *Solid State Ion* **319**, 68–76 (2018).

41. Ohyama, J. *et al.* High Durability of a 14-Membered Hexaaza Macrocyclic Fe Complex for an Acidic Oxygen Reduction Reaction Revealed by In Situ XAS Analysis. *JACS Au* **1**, 1798–1804 (2021).

42. Moriya, M. *et al.* Fourteen-membered macrocyclic Fe complexes inspired by Fen4-center-embedded graphene for oxygen reduction catalysis. *Journal of Physical Chemistry C* **124**, 20730–20735 (2020).

43. Li, J. *et al.* Identification of durable and non-durable FeNx sites in Fe–N–C materials for proton exchange membrane fuel cells. *Nat Catal* **4**, 10–19 (2021).

44. Liu, K., Wu, G. & Wang, G. Role of Local Carbon Structure Surrounding FeN4 Sites in Boosting the Catalytic Activity for Oxygen Reduction. *Journal of Physical Chemistry C* **121**, 11319–11324 (2017).

45. Larouche, N., Chenitz, R., Lefèvre, M., Proietti, E. & Dodelet, J. P. Activity and stability in proton exchange membrane fuel cells of iron-based cathode catalysts synthesized with addition of carbon fibers. *Electrochim Acta* **115**, 170–182 (2014).

46. Yang, L. *et al.* Activity, Performance, and Durability for the Reduction of Oxygen in PEM Fuel Cells, of Fe/N/C Electrocatalysts Obtained from the Pyrolysis of Metal-Organic-Framework and Iron Porphyrin Precursors. *Electrochim Acta* **159**, 184–197 (2015).

47. Choi, J. Y. *et al.* Is the rapid initial performance loss of Fe/N/C non precious metal catalysts due to micropore flooding? *Energy Environ Sci* **10**, 296–305 (2017).

48. Zhang, G., Chenitz, R., Lefèvre, M., Sun, S. & Dodelet, J. P. Is iron involved in the lack of stability of Fe/N/C electrocatalysts used to reduce oxygen at the cathode of PEM fuel cells? *Nano Energy* **29**, 111–125 (2016).

49. Chenitz, R. *et al.* A specific demetalation of Fe-N4 catalytic sites in the micropores of NC-Ar + NH3 is at the origin of the initial activity loss of the highly active Fe/N/C catalyst used for the reduction of oxygen in PEM fuel cells. *Energy Environ Sci* **11**, 365–382 (2018).

50. Jaouen, F., Lefèvre, M., Dodelet, J. P. & Cai, M. Heat-treated Fe/N/C catalysts for O2 electroreduction: Are active sites hosted in micropores? *Journal of Physical Chemistry B* **110**, 5553–5558 (2006).

51. Ferrandon, M. *et al.* Stability of iron species in heat-treated polyaniline-iron-carbon polymer electrolyte fuel cell cathode catalysts. *Electrochim Acta* **110**, 282–291 (2013).

52. Choi, C. H. *et al.* Stability of Fe-N-C catalysts in acidic medium studied by operando spectroscopy. *Angewandte Chemie - International Edition* **54**, 12753–12757 (2015).

53. Banham, D. *et al.* Critical advancements in achieving high power and stable nonprecious metal catalyst-based MEAs for real-world proton exchange membrane fuel cell applications. *Sci Adv* **4**, 1–8 (2018).

54. Mamtani, K. *et al.* Evolution of N-Coordinated Iron–Carbon (FeNC) Catalysts and Their Oxygen Reduction (ORR) Performance in Acidic Media at Various Stages of Catalyst Synthesis: An Attempt at Benchmarking. *Catal Letters* **146**, 1749–1770 (2016).

55. Choi, C. H. *et al.* Unraveling the Nature of Sites Active toward Hydrogen Peroxide Reduction in Fe-N-C Catalysts. *Angewandte Chemie - International Edition* **56**, 8809–8812 (2017).

56. Jaouen, F. & Dodelet, J. P. O2 reduction mechanism on non-noble metal catalysts for PEM fuel cells. Part I: experimental rates of O2 electroreduction, H 2O2 electroreduction, and H2O2 disproportionation. *Journal of Physical Chemistry C* **113**, 15422–15432 (2009).

57. Goellner, V., Armel, V., Zitolo, A., Fonda, E. & Jaouen, F. Degradation by Hydrogen Peroxide of Metal-Nitrogen-Carbon Catalysts for Oxygen Reduction. *J Electrochem Soc* **162**, H403–H414 (2015).

58. Choi, C. H. *et al.* The Achilles' heel of iron-based catalysts during oxygen reduction in an acidic medium. *Energy Environ Sci* **11**, 3176–3182 (2018).

59. Kumar, K. *et al.* On the Influence of Oxygen on the Degradation of Fe-N-C Catalysts. *Angewandte Chemie* **132**, 3261–3269 (2020).

60. Martinaiou, I. *et al.* Effect of metal species on the stability of Me-N-C catalysts during accelerated stress tests mimicking the start-up and shut-down conditions. *Electrochim Acta* **243**, 183–196 (2017).

61. Stariha, S. *et al.* PGM-free Fe-N-C catalysts for oxygen reduction reaction: Catalyst layer design. *J Power Sources* **326**, 43–49 (2016).

62. Herranz, J. *et al.* Unveiling N-Protonation and Anion-Binding Effects on Fe / N / C Catalysts for O 2 Reduction in Proton-Exchange-Membrane Fuel Cells. *Journal of Physical Chemistry C* **115**, 16087–16097 (2011).

63. Strickland, K. *et al.* Anion Resistant Oxygen Reduction Electrocatalyst in Phosphoric Acid Fuel Cell. *ACS Catal* **8**, 3833–3843 (2018).

64. Tylus, U. *et al.* Engendering anion immunity in oxygen consuming cathodes based on Fe-Nx electrocatalysts: Spectroscopic and electrochemical advanced characterizations. *Appl Catal B* **198**, 318–324 (2016).

65. Banham, D. *et al.* A review of the stability and durability of non-precious metal catalysts for the oxygen reduction reaction in proton exchange membrane fuel cells. *J Power Sources* **285**, 334–348 (2015).

66. Martinez, U., Komini Babu, S., Holby, E. F. & Zelenay, P. Durability challenges and perspective in the development of PGM-free electrocatalysts for the oxygen reduction reaction. *Curr Opin Electrochem* **9**, 224–232 (2018).

67. Uddin, A. *et al.* High Power Density Platinum Group Metal-free Cathodes for Polymer Electrolyte Fuel Cells. *ACS Appl Mater Interfaces* **12**, 2216–2224 (2020).

68. He, Y., Liu, S., Priest, C., Shi, Q. & Wu, G. Atomically dispersed metal-nitrogen-carbon catalysts for fuel cells: Advances in catalyst design, electrode performance, and durability improvement. *Chem Soc Rev* **49**, 3484–3524 (2020).

69. Wang, X. X. *et al.* Nitrogen-Coordinated Single Cobalt Atom Catalysts for Oxygen Reduction in Proton Exchange Membrane Fuel Cells. *Advanced Materials* **30**, 1–11 (2018).

70. Wang, Y.-C. *et al.* S-Doping of an Fe/N/C ORR Catalyst for Polymer Electrolyte Membrane Fuel Cells with High Power Density. *Angewandte Chemie* **127**, 10045–10048 (2015).

71. Li, J. *et al.* Atomically dispersed manganese catalysts for oxygen reduction in proton-exchange membrane fuel cells. *Nat Catal* **1**, 935–945 (2018).

72. Liu, S. *et al.* Atomically dispersed iron sites with a nitrogen–carbon coating as highly active and durable oxygen reduction catalysts for fuel cells. *Nat Energy* **7**, 652–663 (2022).

73. Slack, J. *et al.* Electrospun Fiber Mat Cathode with Platinum-Group-Metal-Free Catalyst Powder and Nafion/PVDF Binder. *ChemElectroChem* **5**, 1537–1542 (2018).

74. Banham, D., Choi, J., Kishimoto, T. & Ye, S. Integrating PGM-Free Catalysts into Catalyst Layers and Proton Exchange Membrane Fuel Cell Devices. *Advanced Materials* **31**, 1804846 (2019).

75. Ballard & Nisshinbo Holding. Ballard to Offer World's First PEM Fuel Cell Product Using Non Precious Metal Catalyst. *https://www.ballard.com/about-ballard/newsroom/news-releases/2017/09/13/ballard-to-offer-world-s-first-pem-fuel-cell-product-using-non-precious-metal-catalyst* (2017).

76. Gopal, R. *et al.* Electrospun nanofibrous filtration membrane. *J Memb Sci* **281**, 581–586 (2006).

77. Zhang, Y., Chwee, T. L., Ramakrishna, S. & Huang, Z. M. Recent development of polymer nanofibers for biomedical and biotechnological applications. *J Mater Sci Mater Med* **16**, 933–946 (2005).

78. Luoh, R. & Hahn, H. T. Electrospun nanocomposite fiber mats as gas sensors. *Compos Sci Technol* **66**, 2436–2441 (2006).

79. Sawicka, K., Gouma, P. & Simon, S. Electrospun biocomposite nanofibers for urea biosensing. in *Sensors and Actuators, B: Chemical* vol. 108 585–588 (2005).

80. Ballengee, J. B., Haugen, G. M., Hamrock, S. J. & Pintauro, P. N. Properties and Fuel Cell Performance of a Nanofiber Composite Membrane with 660 Equivalent Weight Perfluorosulfonic Acid. *J Electrochem Soc* **160**, F429–F435 (2013).

81. Park, J. W., Wycisk, R. & Pintauro, P. N. Nafion/PVDF nanofiber composite membranes for regenerative hydrogen/bromine fuel cells. *J Memb Sci* **490**, 103–112 (2015).

82. Park, A. M., Wycisk, R. J., Ren, X., Turley, F. E. & Pintauro, P. N. Crosslinked poly(phenylene oxide)-based nanofiber composite membranes for alkaline fuel cells. *J Mater Chem A Mater* **4**, 132–141 (2015).

83. Self, E. C. *et al.* High Areal Capacity Si/LiCoO2 Batteries from Electrospun Composite Fiber Mats. *ChemSusChem* **10**, 1823–1831 (2017).

84. Brodt, M., Wycisk, R. & Pintauro, P. N. Nanofiber Electrodes with Low Platinum Loading for High Power Hydrogen/Air PEM Fuel Cells. *J Electrochem Soc* **160**, F744–F749 (2013).

85. Brodt, M., Wycisk, R., Dale, N. & Pintauro, P. Power Output and Durability of Electrospun Fuel Cell Fiber Cathodes with PVDF and Nafion/PVDF Binders. *J Electrochem Soc* **163**, F401–F410 (2016).

86. Zhang, W. & Pintauro, P. N. High-Performance Nanofiber Fuel Cell Electrodes. *ChemSusChem* **4**, 1753–1757 (2011).

87. Thompson, C. J., Chase, G. G., Yarin, A. L. & Reneker, D. H. Effects of parameters on nanofiber diameter determined from electrospinning model. *Polymer (Guildf)* **48**, 6913–6922 (2007).

88. Chen, H., Snyder, J. D. & Elabd, Y. A. Electrospinning and solution properties of Nafion and poly(acrylic acid). *Macromolecules* **41**, 128–135 (2008).

89. Ballengee, J. B. & Pintauro, P. N. Morphological Control of Electrospun Nafion Nanofiber Mats. *J Electrochem Soc* **158**, B568 (2011).

90. Loppinet, B., Gebel, G. & Williams, C. E. Small-angle scattering study of perfluorosulfonated ionomer solutions. *Journal of Physical Chemistry B* **101**, 1884–1892 (1997).

91. Brodt, M. *et al.* Fabrication, In-Situ Performance, and Durability of Nanofiber Fuel Cell Electrodes. *J Electrochem Soc* **162**, F84–F91 (2015).

92. Waldrop, K. *et al.* Electrospun Nanofiber Electrodes for High and Low Humidity PEMFC Operation. *J Electrochem Soc* **170**, 024507 (2023).

93. Waldrop, K. *et al.* Electrospun Particle/Polymer Fiber Electrodes with a Neat Nafion Binder for Hydrogen/Air Fuel Cells. *ECS Trans* **92**, 595–602 (2019).

94. Woo Park, J. *et al.* Electrospun Nafion/PVDF single-fiber blended membranes for regenerative H2/Br2 fuel cells. *J Memb Sci* **541**, 85–92 (2017).

95. Slack, J. J. *et al.* Impact of Polyvinylidene Fluoride on Nanofiber Cathode Structure and Durability in Proton Exchange Membrane Fuel Cells. *J Electrochem Soc* **167**, 054517 (2020).

CHAPTER II

HIGH DURABILITY PLATINUM GROUP METAL-FREE CATALYST FIBER CATHODE MEAS FOR PROTON EXCHANGE MEMBRANE FUEL CELLS

2.1 Introduction

The H_2/air proton exchange membrane (PEM) fuel cell is a promising candidate for electric vehicle power plants due to its high hydrogen conversion efficiency, fast start-up time, response to load variations, and zero emissions.[1] It is competitive with internal combustion engines regarding drive distance, such as in municipal transportation (buses), autos, and long-haul and light-duty trucks. However, the high cost of the Pt used as the electrode catalysts in such a fuel cell is an obstacle to widespread commercialization.[2] One way to reduce the overall cost of a PEM fuel cell is to use a Pt-based cathode catalyst with an ultra-high oxygen reduction activity so that less Pt material is used in a fuel cell stack. Studies in the literature focused on synthesizing new cathode catalysts since the cathodic oxygen reduction reaction is six times slower than the anodic hydrogen oxidation reaction and, thus, is the reaction that limits power generation in a PEM fuel cell. Examples of this approach include carbon-supported Pt-alloys,[3] core-shell powders,[4] and shape-controlled catalysts.[5] Another approach is to use a low-cost and low-activity platinum-group-metal-free (PGM-free) catalyst at a high catalyst loading for the cathode.[6,7] Recent research[8–12] in the field of PGM-free oxygen reduction reaction (ORR) electrocatalysts has resulted in the discovery of several families of moderately high

activity compounds on carbon particles, where a transition metal forms a surface-active complex with nitrogen of the form M-N-C (where M denotes a metal species, such as Fe, Co, Ni, or Mn). M-N-C catalysts are an attractive alternative to conventional precious metal (e.g., Pt) catalysts because (i) they exhibit moderately high intrinsic activity for oxygen reduction, (ii) there is a multitude of synthetic approaches to create M-N-C structures, (iii) they have been successfully incorporated into PEM fuel cells, with reasonably high initial power output results, and (iv) such catalysts can be manufactured inexpensively at scale.[13–16] Unfortunately, fuel cells with PGM-free catalyst cathodes still do not meet the U.S. DOE targets for MEA performance and durability.[17] Thus, there is a need to redesign the catalyst material and the cathode morphology to better exploit the inherent advantages of PGM-free catalysts. In particular, there is a need to improve the durability of such catalysts, which means that one must minimize electro-generated hydrogen peroxide (produced via the 2-electron transfer reduction of O_2 with H^+) or expel this chemical species from the cathode before it attacks (oxidizes) the catalyst's carbon substrate.[18–20]

In the present study, PGM-free catalysts from Pajarito Powder were electrospun into particle/binder fiber mat cathodes and then tested in a fuel cell MEA. Electrospinning is an economically viable method to fabricate non-woven fiber mats whose fiber diameter is typically in the sub-micron range. Electrospun fibers have been used in several widely differing applications, including sensors,[21] filtration media,[22,23] and medical products.[24] For energy and electrochemical applications, studies from the laboratories of X. Zhang and P. N. Pintauro have shown that electrospinning can be utilized to fabricate cation, anion, or bipolar membranes, particle/polymer electrodes for fuel cells and batteries, and

pyrolyzed carbon fiber mat electrodes for capacitors, batteries, and sensors.[25–37] Fuel cell cathodes composed of Pt-based catalyst particle/polymer electrospun fiber mats were found to work remarkably well in MEAs. Fiber cathode MEAs showed high power output and excellent metal dissolution durability, as determined by a voltage cycling accelerated stress test.[38–40] In these studies, fiber mat electrodes were electrospun with catalyst powder, perfluorosulfonic acid ionomer (Nafion), and a carrier polymer (e.g., polyacrylic acid). The carrier polymer was necessary to create well-formed fibers from a micellar dispersion of Nafion. Another study[41] used polyvinylidene fluoride (PVDF) as both a carrier polymer to electrospun fiber mats and a hydrophobic additive, which expelled electro-generated water from the cathode and decreased or eliminated carbon corrosion in a Pt/C catalyst cathode, where carbon is lost via the following reaction:

$$C + 2H_2O \rightarrow CO_2 + 4H^+ + 4e^- \qquad (1)$$

In a conventional Pt/C fuel cell, this reaction can occur during fuel cell start-up and shutdown. However, in a Pt/C catalyst Nafion/PVDF fiber cathode, when the PVDF content in the binder is greater than 50 wt%, the carbon corrosion rate, as measured by a DOE-approved voltage cycling accelerated stress test[42], was reduced to near zero. Unfortunately, the addition of PVDF to Nafion resulted in a substantial decrease in the binder's proton conductivity (due to the dilution of Nafion with PVDF and specific molecular-level interactions between Nafion and PVDF, which trapped/deactivated water[43]). Hence, eliminating carbon corrosion was accompanied by an overall decrease in MEA power output. A similar power versus durability trade-off with Nafion/PVDF binders was observed by Slack et al.[44] with a PGM-free catalyst (from Pajarito Powder, LLC). A powder cathode MEA with a neat Nafion binder initially outperformed fiber and

powder cathode MEAs with a Nafion/PVDF binder. However, the power output for the neat Nafion powder cathode MEA decreased by 63% after 300 hours of constant voltage operation (the power density at 0.5 V decreased from 120 mW/cm^2 to 45 mW/cm^2). In contrast, the fiber cathode MEA with a 50:50 (w:w) Nafion:PVDF binder generated a constant power density of 80 mW/cm^2 at 0.5 V for 300 hours.

Herein, a more in-depth examination of a Fe-based PGM-free catalyst in fiber cathode MEAs with Nafion/PVDF binder is presented. The cathode catalyst material for all experiments was a PMF Fe-N-C catalyst (from Pajarito Powder, LLC.) synthesized through a hard-templating pore-former approach. The cathode catalyst loading was between 0.75 and 3.0 mg/cm^2, and the total binder content was constant relative to the amount of catalyst at 50 wt%. Fiber mat cathodes were made with either Nafion/PEO binder, where PEO was extracted before the test, or with a Nafion/PVDF blended binder, where the Nafion:PVDF weight ratio was 50:50, 67:33, 75:25, or 80:20. As a comparison, two conventional powder cathodes were also fabricated, with either a neat Nafion binder or a 50:50 (w:w) Nafion:PVDF binder. Experiments focused on how the cathode binder composition (amount of PVDF added to Nafion), cathode morphology (powder versus fiber), and cathode catalyst loading (0.75-3.0 mg/cm^2) affect MEA power output and durability in an H_2/air fuel cell, operating at 80 °C, 100% RH, and 200 kPa (absolute pressure).

2.2 Experimental

2.2.1 Electrospinning Catalyst/Nafion/PVDF Fiber Mats

Electrospinning solutions consisted of the following components in a solvent of 50:28:22 (w:w:w) dimethylformamide (DMF):Acetone:tetrahydrofuran (THF): (a) Fe-based PGM-free catalyst powder (from Pajarito Powder, synthesized by a hard-templating-pore-former approach, denoted as PMF catalyst), (b) Nafion as a solvent dispersion (20 wt% 1100 EW Nafion resin, obtained by drying an Ion Power Liquion 1115 solution and then redispersing the dry powder in a 70:30 (w:w) DMF:acetone solvent mixture), and (c) a PVDF solution composed of 10 wt% Kynar HSV 900 PVDF (Arkema, Inc.) in a 70:30 (w:w) DMF:acetone solvent. An electrospinning solution was prepared using the following procedure: (i) dispersing the PGM-free catalyst powder in DMF/acetone/THF solvent, (ii) adding the Nafion dispersion to the catalyst solution followed by 60 minutes of high energy ultrasonic agitation using a sonic horn (Sonic & Materials Inc. VibraCell Ultrasonicator) and an additional 30 minutes of low energy mixing in a sonication bath (Fisher Scientific Inc. FS20D Ultrasonic Cleaner), and (iii) adding the PVDF solution followed by mechanically stirring for 12 hours.

Electrospinning was performed at room temperature inside a custom-built plexiglass chamber with relative humidity control as described in previous studies.[38,39] The catalyst powder/polymer solution was drawn into a 3-mL syringe with a 22-gauge stainless needle spinneret. The electrospun fiber mat was collected on a rotating and laterally oscillating cylindrical drum.

2.2.2 Electrospinning Catalyst/Nafion/PEO Fiber Mats

The Nafion/PEO electrospinning solution comprised the following components in a 50:50 (w:w) water:isopropanol solvent: (i) Fe-N-C PMF catalyst powder, (ii) Nafion dispersion (20 wt% 1100 Nafion resin, obtained by drying an Ion Power Liquion 1115 solution and then redispersing the resin in 50:50 (w:w) water:isopropanol solvent), and (iii) a PEO solution (5 wt% PEO form Sigma Aldrich in a water:isopropanol 50:50 (w:w) mixture). The solution was made using the following procedure: (i) dispersing PMF catalyst powder in water/isopropanol solvent, (ii) adding the Nafion dispersion to the catalyst solution followed by 60 minutes of high energy ultrasonic agitation using the sonic horn and an additional 30 minutes of low energy mixing in a sonication bath, and (iii) adding the PEO solution followed by mechanically stirring for 12 hours. Electrospinning was performed using the same apparatus as Nafion/PVDF fiber mats.

Table 2.1 lists the electrospinning conditions for a Nafion/PVDF and Nafion/PEO fiber mats. Table 2.2 lists the electrospinning solution and final dry fiber cathode compositions for all Nafion/PVDF and Nafion/PEO fiber mat cathodes.

Table 2.1. Electrospinning Conditions for Fiber Mats with Nafion/PVDF or Nafion/PEO Binder

	Nafion/PVDF fiber	Nafion/PEO fiber
Potential [KV]	10.8-12	6.0-7.5
Relative Humidity [%]	50-55	20
Flow Rate [mL/hr]	0.5	0.75
Needle Tips to Collector Distance [cm]	8	15-20

Table 2.2. Electrospinning Solution and Final Dry Fiber Cathode Composition

Solution	Electrospinning Solution [g]	Dry Fiber Cathode Composition [wt%]
1	0.33 g catalyst, 0.015 g DMF, 0.020 g acetone, 0.65 g THF, 1.32 g stock solution A, 0.66 g stock solution B	50 catalyst, 40 Nafion, 10 PVDF
2	0.32 g catalyst, 0.027 g DMF, 0.025 g acetone, 0.66 g THF, 1.18 g stock solution A, 0.79 g stock solution B	50 catalyst, 37.5 Nafion, 12.5 PVDF
3	0.30 g catalyst, 0.009 g DMF, 0.018 g acetone, 0.68 g THF, 0.99 g stock solution A, 1.02 g stock solution B	50 catalyst, 33.3 Nafion, 16.7 PVDF
4	0.27 g catalyst, 0.0015 g DMF, 0.015 g acetone, 0.69 g THF, 0.68 g stock solution A, 1.35 g stock solution B	50 catalyst, 25 Nafion, 25 PVDF
5	0.20 g catalyst, 0.37 g water, 0.37 g isopropanol, 0.99 g stock solution C[3], 1.08 g stock solution D[4]	50 catalyst, 50 Nafion

[1]Stock Solution A: 20 wt% Nafion, in 70:30 DMF:acetone w:w

[2]Stock Solution B: 10 wt% PVDF in 70:30 DMF:acetone w:w

[3]Stock Solution C: 20 wt% Nafion, in 50:50 water:isopropanol w:w

[4]Stock Solution D: 5 wt% PEO in 50:50 water:isopropanol w:w

2.2.3 PGM-Free Powder Cathode Preparation

Conventional PGM-free catalyst powder cathodes contained a cathode binder of neat Nafion binder or a 50:50 (w:w) mixture of Nafion:PVDF. The ink for the cathodes with Nafion/PVDF was made using the same procedure as the corresponding electrospinning solution but at lower solids (catalyst + Nafion + PVDF) content (2.5 wt%) to facilitate airbrush spraying. A neat Nafion binder ink (2.5 wt% solids) contained 50 wt% PMF catalyst powder and 50 wt% Nafion dispersion (20 wt% 1100 Nafion resin, obtained by drying an Ion Power Liquion 1115 solution in 50:50 (w:w) water:isopropanol solvent). The neat Nafion binder ink was prepared by: (i) dispersing the PMF catalyst powder in a 50:50 (w:w) water:isopropanol mixed solvent, (ii) adding Nafion dispersion to the catalyst solution followed by 60 minutes of high energy ultrasonic agitation (Sonic & Materials Inc. VibraCell Ultrasonicator) and an additional 30 minutes of low energy

sonication bath mixing (Fisher Scientific Inc. FS20D Ultrasonic Cleaner), and (iii) mechanically stirring the ink for 12 hours.

2.2.4 Pt/C Powder Anode Preparation

All PGM-free catalyst cathode MEAs (powder or fiber mat cathode) employed a Pt/C powder anode composed of Pt/C catalyst (Johnson Matthey, HiSPEC 4000 with 40% Platinum on carbon) and Nafion dispersed in a 50:50 (w:w) water:isopropanol solvent. Nafion was added as a 20 wt% dispersion of 1100 Nafion resin in 50:50 (w:w) water/isopropanol solvent, where the Nafion was obtained by drying an Ion Power Liquion 1115 solution. The ink preparation was identical to the PGM-free neat Nafion powder cathode ink. The Pt/C catalyst ink was airbrush sprayed onto a Sigracet 29BC gas-diffusion-layer (GDL) at a Pt loading of 0.1 mg_{Pt}/cm^2, with a dry catalyst/Nafion weight ratio of 65/35.

2.2.5 Membrane-Electrode-Assembly (MEA) Preparation

All Nafion/PVDF fiber cathode MEAs contained a Nafion 211 membrane and a Pt/C anode. Electrospun fiber mats (each mat provided 0.75 mg/cm^2 of catalysts) were cut into 5 cm^2 squares. Four mats were stacked to achieve a catalyst loading of 3.0 mg/cm^2, two mats were stacked to reach 1.5 mg/cm^2, and one mat for loading of 0.75 mg/cm^2. A Sigracet 29BC gas-diffusion-layer (GDL), the stacked PGM-free catalyst fiber mats, a Nafion 211 membrane, and a Pt/C anode (which was a Pt/C catalyst ink sprayed onto GDL) were then hot pressed together at 35 MPa pressure and 140 °C for 10 minutes to create a membrane-electrode-assembly (MEA).

Fiber mats with Nafion/PEO binder were first hot-pressed onto a Nafion 211 membrane at 140 °C and 35 MPa for 10 minutes, followed by a two-hour hot water (80 °C) soaking step to remove PEO carrier polymer. Then the fiber mats and membrane were hot pressed with a Pt/C anode and cathode Sigracet 29BC GDLs at 35 MPa pressure and 140 °C for 10 minutes.

Powder cathode inks (with either neat Nafion or Nafion/PVDF binder) were manually airbrush sprayed onto Sigracet 29BC carbon paper GDLs until the dry cathode catalyst loading was 3.0 mg/cm^2. The cathode was then hot pressed with a Pt/C powder anode and a Nafion 211 membrane at 35 MPa and 140 °C for 10 minutes.

2.2.6 Fuel Cell Tests

Fuel cell tests were conducted using a Scribner Series 850e test station with temperature, back pressure, and mass flow rate control. The fuel cell test fixture accommodated a 5 cm^2 MEA and contained single serpentine flow channels for anode and cathode feed gases. Fuel cell performance data were collected at 80 °C, 100% relative humidity (RH), and 200 kPa$_{abs}$, with feed gases of H_2/air at 0.125/0.5 SLPM (standard liters per minute). An initial fuel cell polarization curve was collected after loading the MEA in the fuel cell test fixture, allowing the system to reach the fuel cell operating temperature of 80 °C and then waiting for the open circuit voltage (OCV) to stabilize, which took approximately one hour. Immediately thereafter, a fuel cell durability test (a long-time potentiostatic hold at 0.5 V) was carried out, followed by the collection of another polarization curve.

2.2.7 Scanning Electron Microscopy

Top-down scanning electron microscope (SEM) images of PMF catalyst powder and fiber cathodes were obtained with a MERLIN Microscope. The images were used to assess the overall quality of the fiber mat, e.g., the presence of bead-on-fiber defects. Prior to imaging, a catalyst powder or fiber mat electrode was slightly pressed onto double-sided conductive tape and placed on a flat specimen holder. Then, the sample was sputter coated with a thin layer of gold to improve imaging contrast. ImageJ software (made available by the National Institute of Health (NIH): https://imagej.nih.gov/ij/index.html) was used for digitizing collected SEM images to determine the average particle size and the average fiber diameter.

2.3 Results and Discussions

2.3.1 PMF Catalyst Cathode Morphology

Top-down SEM images of a conventional PMF catalyst powder cathode with either a neat Nafion binder or a 50:50 (w:w) Nafion:PVDF binder are shown in Figures 2.1a and 2.1b. Large catalyst particles and agglomerates of multiple particles were present, even after sonicating the catalyst/binder ink for several hours. The largest particle/agglomerate is ~4 μm for the powder cathode with a Nafion binder and ~5 μm for the powder cathode with a 50:50 (w:w) Nafion:PVDF binder. As expected, adding PVDF to a catalyst/Nafion ink had no apparent effect on dispersing the catalyst particles

or breaking up agglomerates in a conventional powder ink used to make a powder cathode.

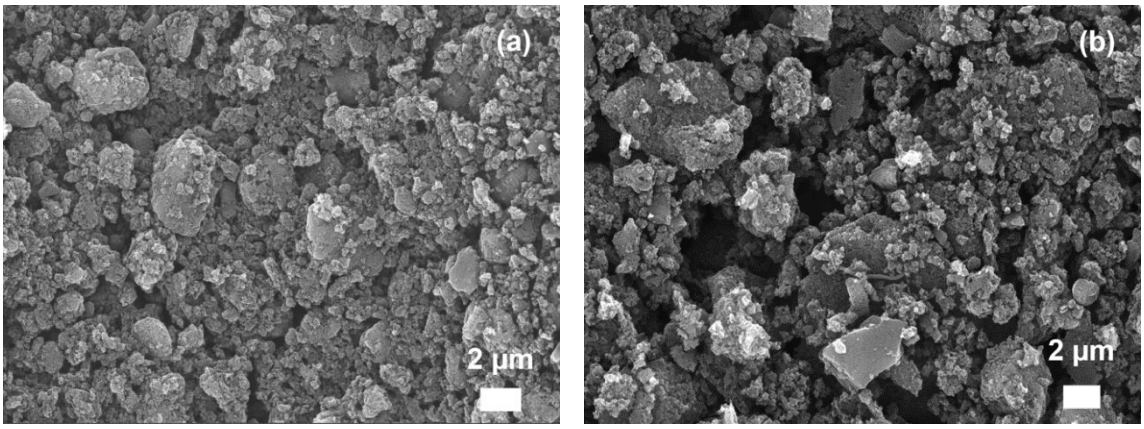

Figure 2.1. Top-down SEM images of PMF catalyst (a) powder cathode with a neat Nafion binder, (b) powder cathode with a 50:50 (w:w) Nafion:PVDF binder.

A dispersion of catalyst particles with Nafion in either a water/alcohol mixture or an organic solvent mixture could not be electrospun due to a lack of polymer chain entanglements. The resulting solutions only formed electrospray droplets and thus required the addition of a suitable carrier polymer.[45] The present study used polyethylene oxide (PEO) or polyvinylidene fluoride (PVDF) as the carrier polymer to fabricate fiber mats. An SEM image of an electrospun PMF catalyst fiber mat with Nafion/PEO binder is shown in Figure 2.2a (before PEO extraction). PEO was extracted by soaking the fiber mats in hot water (80 °C) for two hours, a method that has been used in Pt/C catalysts fiber mats. A recently published paper confirmed that the hot water soaking step could remove PEO with the fiber morphology retained.[46] A similar study was not conducted in this work; nonetheless, it can be assumed that PEO was extracted from PMF catalyst

fibers with no substantial change in the fiber morphology. Henceforth, such fiber mats are denoted as a Nafion fiber cathode since there is no PEO when the electrodes are evaluated in a fuel cell.

Figures 2.2 b-e show fiber mats with Nafion:PVDF binders of weight ratios 50:50, 67:33, 75:25, and 80:20, respectively. It should be noted here that electrospun fibers could not be made when the PVDF content in ink was < 20 wt%. That is to say, when the PVDF concentration was lower than 20 wt%, the solution only produced sprayed droplets, for a flow rate between 0.3 mL/hr to 1.5 mL/hr, an applied voltage between 1 kV to 12 kV, and a distance between the spinneret tip and the collector of 8 to 18 cm.

Electrospun fibers with either Nafion/PEO or Nafion/PVDF binder appear porous with a highly roughened surface. The average fiber diameter for PMF catalyst fiber mats ranged from 0.9-1.7 μm (see Table 2.3). There were some bead-on-fiber defects in all of the fiber mats due to the large particle size of the PMF catalyst (an average particle size of ~500 nm, with some particles or multi-particle agglomerates > 500 nm). As expected, more droplets and bead-on-fiber defects were formed as the Nafion/PVDF binder weight ratio increased, i.e., as the concentration of PVDF carrier polymer in the electrospinning solution decreased. Overall, the SEM results in Figures 2.1 and 2.2 show smaller catalyst particles in electrospun mats, which is ascribable to the high shear forces at the spinneret tip during electrospinning which breaks up agglomerates, and the rapid evaporation of solvent from the particle/binder jet, which minimizes particle re-agglomeration.

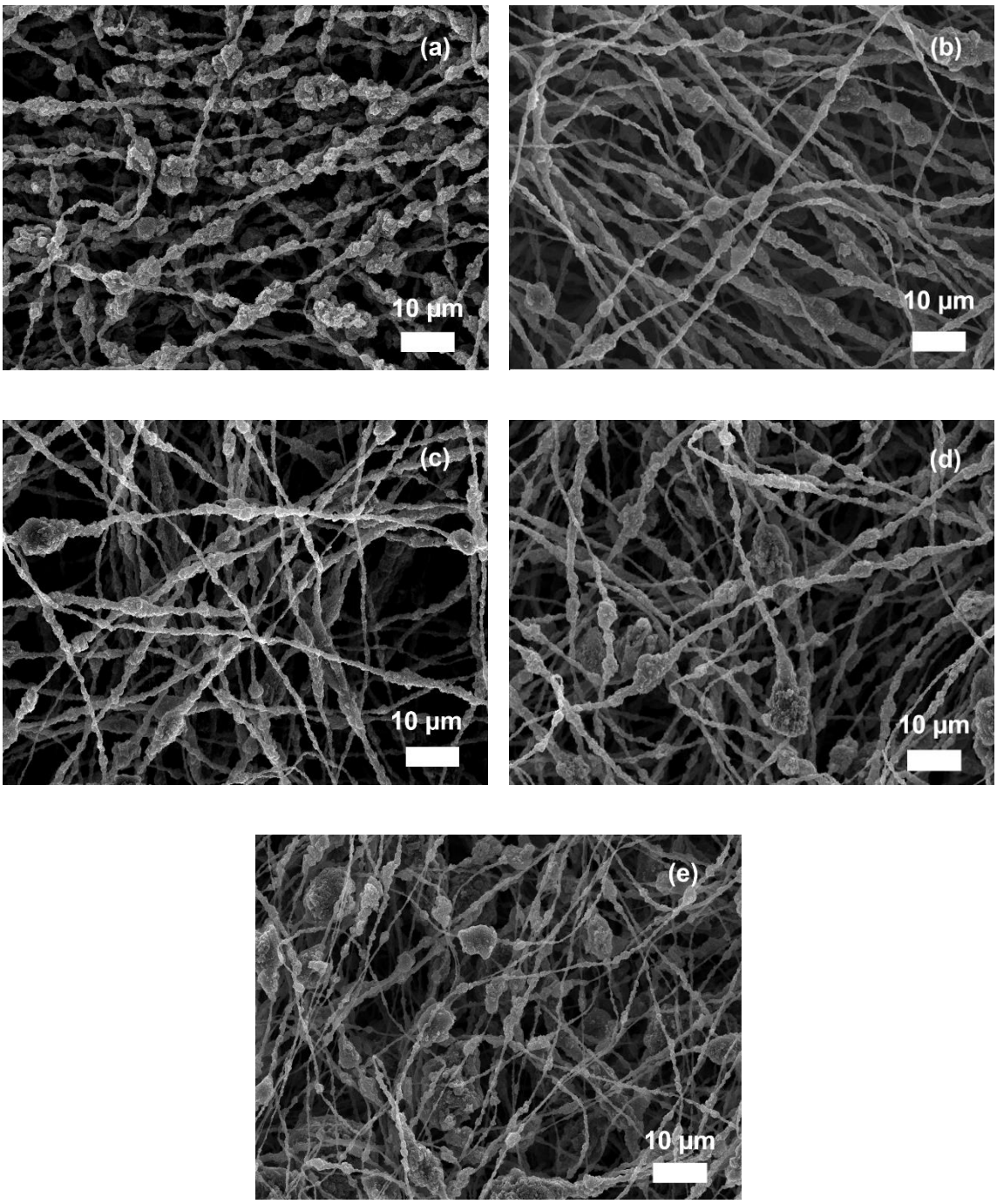

Figure 2.2. Top-down SEM images of PMF catalyst (a) fiber mat with Nafion/PEO binder (before PEO extraction), (b) fiber mat with a 50:50 (w:w) Nafion:PVDF binder, (c) fiber mat with a 67:33 (w:w) Nafion:PVDF binder, (d) fiber mat with a 75:25 (w:w) Nafion:PVDF binder, and (e) fiber mat with an 80:20 (w:w) Nafion:PVDF binder.

Table 2.3. Average Fiber Diameter for all PMF Catalyst Fiber Mats.

Fiber Mat	Average Fiber Diameter [μm]
Nafion/PEO fiber	1.7
50:50 (w:w) Nafion:PVDF Fiber	1.2
67:33 (w:w) Nafion:PVDF Fiber	1.1
75:25 (w:w) Nafion:PVDF Fiber	1.1
80:20 (w:w) Nafion:PVDF Fiber	0.9

2.3.2 Fuel Cell Tests of Powder and Fiber Cathodes with Nafion Binder

Hydrogen/air polarization curves for MEAs with a PMF catalyst Nafion powder cathode and a Nafion fiber cathode (PEO extracted) are shown in Figure 2.3 for a cathode PMF catalyst loading of 3.0 mg/cm^2. The polarization curves were collected at the start of the experiment (identified as beginning-of-life, BOL). The catalyst:Nafion weight ratio of the fiber mat cathode after PEO extraction was 50:50, i.e., the same as that for a neat Nafion powder cathode (when no PEO was present in the ink), so meaningful comparisons of the two MEA can be made. V-i data were collected at 80 °C with air and hydrogen at 200 kPa$_{abs}$ pressure and 100% relative humidity (RH).

As shown in Figure 2.3, the polarization curves of the PMF powder cathode and fiber cathode MEAs are the same in the high potential region but not at low potentials (high current densities). At voltages < 0.55V, the powder cathode MEA encountered a water-flooding issue, as indicated by the rapid drop in power density; consequently, the maximum power density of the powder cathode MEA was only 186 mW/cm^2. On the other hand, electro-generated water can be quickly removed in the fiber cathode MEA, and thus its maximum power density was 240 mW/cm^2 (30% higher than the powder

cathode MEA). This higher power density for the fiber cathode MEA is consistent with prior studies with Pt-based catalyst cathode MEAs.[37,38] Additionally, Chintam et al.[37] conducted neutron radiography tests on Pt-based catalyst fiber and powder cathode MEAs which showed that water was more effectively expelled from fiber cathode MEAs during H_2/air fuel cell operation.

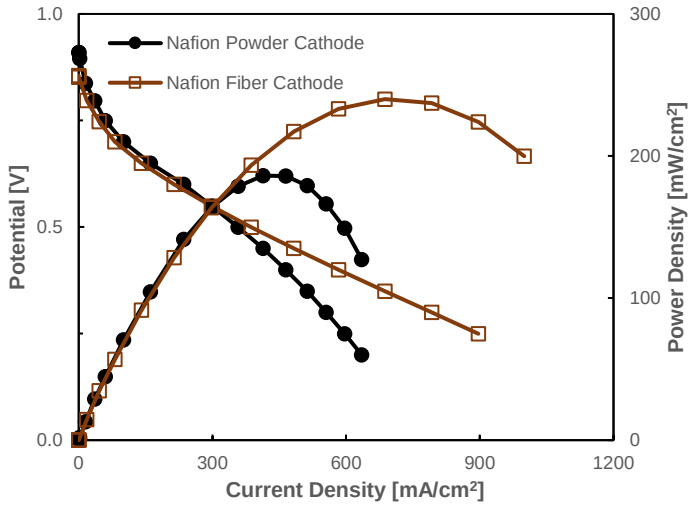

Figure 2.3. H_2/air polarization curves of PMF-catalyst powder cathode MEA with a neat Nafion binder (circle symbol) and a fiber mat cathode MEA made with a Nafion/PEO (PEO extracted) binder (square symbol). Fuel cell operating conditions: 80 °C, 100% relative humidity, 200 kPa_{abs} pressure, and 0.125/0.5 SLPM (standard liters per minute) H_2/air feed gas flow rate. All MEAs have a Nafion 211 membrane and a Pt/C catalyst powder anode (0.1 mg_{Pt}/cm^2). PGM-free catalyst cathode loading was 3.0 mg/cm^2.

The long-term stability of the MEAs in Figure 2.3 was evaluated by a potentiostatic hold experiment at 0.5 V with H_2/air gas feeds. Figure 2.4a shows a plot of power density at 0.5 V vs. time for a 50-hour test; Figure 2.4b shows the polarization curves collected at the end-of-test (EOT) after 50-hour operation; Figure 2.4c shows the EOT/BOL power density ratio at 0.7 V, 0.5 V, and 0.3 V (the BOL and EOT data were

obtained from Figures 2.3 and 2.4b). As was seen in previous studies with PGM-free catalysts and Nafion binder cathodes,[47–49] a power loss (cathode degradation) began immediately. The power drop was fast during the first 10 hours of the test, and then the degradation slowed with a near-line power loss versus time, where the decay rate was 1.0 mW/cm^2/hr for the Nafion powder cathode MEA and 0.7 mW/cm^2/hr for the Nafion fiber cathode MEA. Thus, after 50 hours of operation, the power output of the Nafion fiber cathode MEA was higher than that of the Nafion powder cathode MEA for all potentials, as shown in Figure 2.4b. For both MEAs, the power loss was attributed to the combined effects of metal dissolution due to the highly acidic sulfonic acid moieties in the Nafion binder[50] and peroxide attack (oxidation) on the carbon-based cathode catalyst active sites, where H_2O_2 is produced via the 2-electron reduction of O_2 with H^+[51–53]:

$$2H^+ + 2e^- + O_2 \rightarrow H_2O_2 \qquad (2)$$

The transient behavior in Figure 2.4a and the EOT/BOL power density ratio in Figure 2.4c indicate that the degradation of the fiber cathode MEA was less severe than the powder cathode MEA during the catalyst degradation test. The better durability of the fiber cathode MEA was attributed to the unique fiber cathode morphology, where there is a low ionomer/catalyst ratio in the interior portion of the fiber (less acidic groups near metal catalyst sites[54]). Meanwhile, the intra- and inter-fiber porosity facilitates the rapid removal of water and peroxide species. There was no evidence that less peroxide was generated in the fiber cathode, but further studies are needed to prove/verify this conclusion.

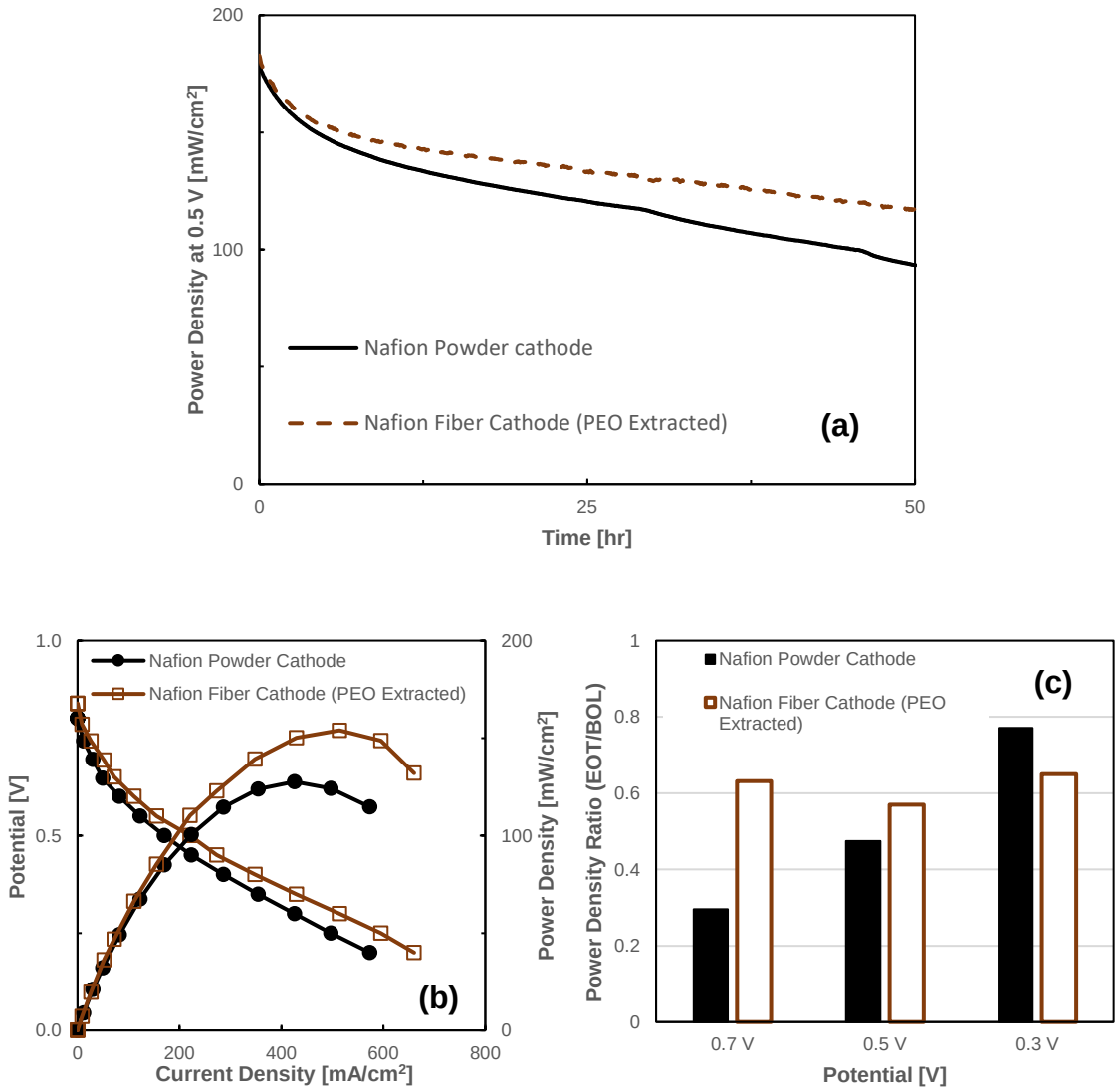

Figure 2.4. (a) H_2/air power density at 0.5 V vs. time, (b) H_2/air polarization curve at EOT (after 50-hours constant voltage operation), and (c) power density ratio of EOT to BOL at 0.7 V, 0.5 V, and 0.3 V for PMF-catalyst Nafion powder and Nafion fiber (PEO extracted) cathode MEAs. Fuel cell operating conditions: 80 °C, 100% relative humidity, 200 kPa_{abs} pressure, and 0.125/0.5 SLPM (standard liters per minute) H_2/air feed gas flow rate. All MEAs have a Nafion 211 membrane and a Pt/C catalyst powder anode (0.1 mg_{Pt}/cm^2). PGM-free catalyst cathode loading was 3.0 mg/cm^2.

2.3.3 Fuel Cell Performance of MEAs with a Nafion/PVDF Cathode Binder

In the present study, polyvinylidene fluoride (PVDF) has two functions as a cathode binder component. First, PVDF is a carrier polymer for electrospinning fibers (an alternative to PEO). Second, PVDF is a hydrophobic additive that drives water away from PGM-free catalyst particles during fuel cell operation, thus protecting catalytic sites from electro-generated hydrogen peroxide attack. Hydrogen/air polarization curves for a PMF catalyst powder cathode MEA and a fiber cathode MEA with a 50:50 (w:w) Nafion:PVDF binder are shown in Figure 2.5. The cathode catalyst loading was 3.0 mg/cm^2, and the cathode's catalyst:binder weight ratio was 50:50.

The initial (BOL) fuel cell polarization plots for a PMF catalyst cathode MEA with 50:50 (w:w) Nafion:PVDF binder in either a powder or a fiber cathode morphology are shown in Figure 2.5. The power output of the fiber cathode MEA was approximately 2X that of the powder cathode MEA (e.g., maximum power density: 32 mW/cm^2 vs. 17 mW/cm^2). Still, these power densities are far below those in Figure 2.3 for powder and fiber cathode MEAs with a neat Nafion binder. This could be attributed to a combination of factors: (1) the hydrophobicity of PVDF dramatically decreased the water concentration[55] near the catalyst surface, thus slowing the oxygen reduction reaction rate (ORR) (it is known that fast ORR kinetics requires the presence of water[56,57]), (2) the carrier polymer (PVDF) diluted Nafion binder and lowered the proton mobility/conductivity[43] of the binder, and (3) PVDF lowered the oxygen transport rate in the binder (the oxygen permeability in wet Nafion[58] is three orders of magnitude greater than that in PVDF[59]).

Initial fuel cell experiments used a 50:50 (w:w) Nafion:PVDF binder in powder and fiber cathode MEAs because a prior study by Slack et al.[44] utilized this binder. The polarization curves from that study are also plotted in Figure 2.5, which differ from the present research MEAs because a different catalyst and a different catalyst/binder composition were used; a metal-organic-framework (MOF)-type PGM-free catalyst was employed in that study and the catalyst to binder (Nafion + PVDF) weight ratio in Slack's study was 70:30, versus 50:50 for the catalyst to binder (Nafion + PVDF) weight ratio in the present study. In the present study, only electrospray droplets were produced for the PMF catalyst when Slack's 70:30 catalyst/binder ratio was examined (a 50:50 catalyst:binder ratio was needed with PMF powder to make fibers). The higher PVDF content in the 50:50 PMF:binder fibers suppressed power generation. The MOF catalyst that Slack used in his fibers may have been more active than the PMF catalyst used here. Nonetheless, Slack did no ORR catalytic activity studies, nor were any kinetic studies carried out as part of the present study. There are no established methods in the literature to calculate ORR kinetic parameters with PGM-free catalysts because the catalysts are continuously degrading with time, as per Figure 2.4a.

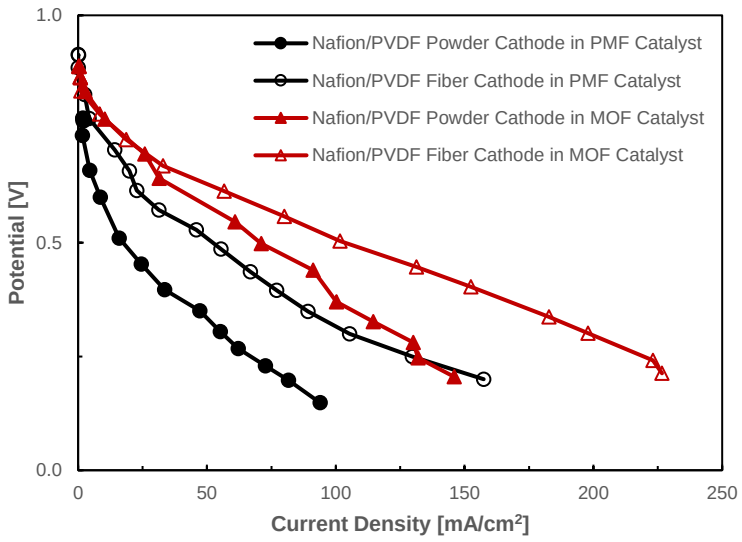

Figure 2.5. H_2/air polarization curves of PMF-catalyst (circle symbol) and MOF-catalyst cathode MEA with cathode binder of 50:50 (w:w) Nafion:PVDF in either a powder (solid symbol) or fiber (open symbol) morphology. Fuel cell operating conditions: 80 °C, 100% relative humidity, 200 kPa_{abs} pressure, and 0.125/0.5 SLPM (standard liters per minute) H_2/air feed gas flow rate. All MEAs have a Nafion 211 membrane and a Pt/C catalyst powder anode at a loading of 0.1 mg_{Pt}/cm^2. PGM-free catalyst cathode loading is 3.0 mg/cm^2. The MOF-catalyst cathode MEA data was adapted from John Slack, Barr Halevi, Geoff McCool, Jingkun Li, Ryan Pavlicek, Ryszard Wycisk, Sanjeev Mukerjee, and Peter Pintauro (**2018**) *ChemElectroChem*.[44]

Long-term (50-hour) H_2/air fuel cell durability tests at 0.5 V were conducted on powder and fiber cathode MEAs with a 50:50 Nafion:PVDF binder. The results of these tests are shown in Figure 2.6a as the measured power density at 0.5 V versus time and in Figure 2.6b as the high frequency resistance (HFR) versus time, where the HFR is a measure of the sum of the contact resistance between the cathode and Nafion membrane and the resistance of the cathode binder. Hydrogen/air polarization curves at EOT were also collected after 50 hours of constant voltage hold (at 0.5 V). These data are shown in Figure 2.6c. The measured BOL and EOT power densities at 0.7 V, 0.5 V, and 0.3 V,

obtained from the polarization curves in Figure 2.5 (BOL) and Figure 2.6c (EOT), are compared in Figure 2.6d.

As shown in Figure 2.6a, the powder and fiber cathode MEAs' power density increased after start-up and stabilized at 25 mW/cm^2 (powder) and 41 mW/cm^2 (fiber). A similar trend in power density versus time was reported by Slack et al.[44] for a cathode MEA with a MOF-type PGM-free catalyst and Nafion/PVDF binder (both powder and fibers). They explained the increase in power during the first few hours of constant voltage operation as an acceleration in oxygen reduction reaction due to water generation near the catalyst surface, increasing the proton conductivity of the binder, which was evidenced by a decrease in the high frequency resistance (HFR). Figures 2.6a and 2.6b show that the power density and HFR changed during the initial stages of the constant voltage hold experiment. HFR first decreased after start-up (the power density increased simultaneously) and then stabilized at the same point when the power density also stabilized. The slow activation of the catalyst and hydration of the Nafion/PVDF binder affected the power output at 0.3 V, 0.5 V, and 0.7 V, as shown in Figure 2.6d.

The Nafion/PVDF fiber cathode was more durable than a neat Nafion fiber MEA due to the increased binder hydrophobicity, which expelled water and minimized electro-generated peroxide contact with catalyst particles. A similar explanation was presented by Slack et al. [44] in their paper with a MOF-based PGM-free catalyst fiber cathode.

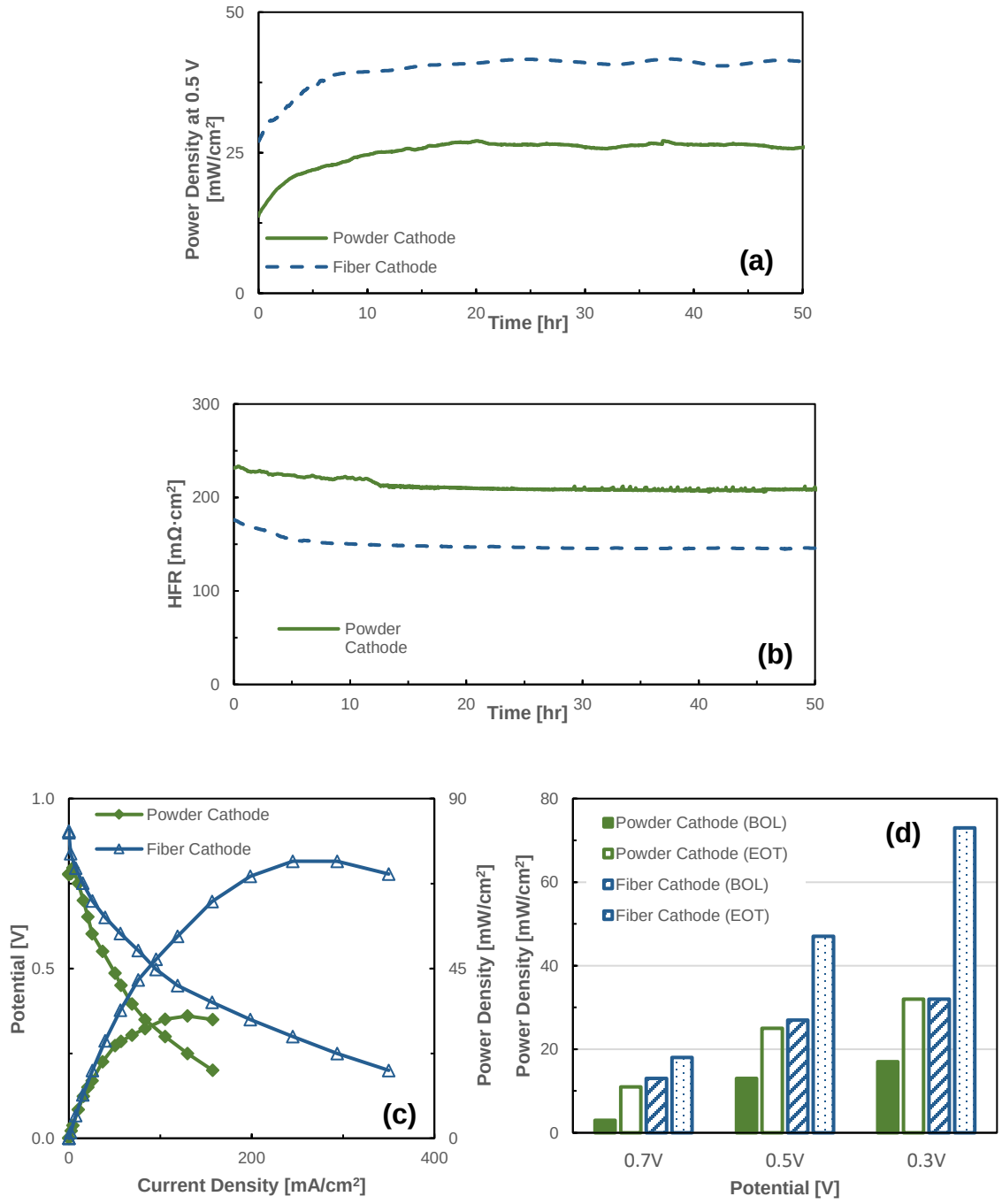

Figure 2.6. H_2/air fuel cell (a) power density at 0.5 V vs. time and (b) HFR vs. time, (c) H_2/air polarization curve after 50-hours constant voltage operation (EOT), and (d) power densities at 0.7 V, 0.5 V, and 0.3 V at BOL and EOT for PMF-catalyst powder and fiber mat cathode MEA with cathode binder of 50:50 (w:w) Nafion:PVDF. Fuel cell operating conditions: 80 °C, 100% relative humidity, 200 kPa_{abs} pressure, and 0.125/0.5 SLPM (standard liters per minute) H_2/air feed gas flow rate. All MEAs have a Nafion 211 membrane and a Pt/C catalyst powder anode at a loading of 0.1 mg_{Pt}/cm^2. PGM-free catalyst cathode loading is 3.0 mg/cm^2.

In the present study and the work of Slack et al.[44], the long-term power output of the fiber cathode MEA was almost twice that of a powder cathode MEA with a 50:50 (w:w) Nafion:PVDF binder. The higher power was associated with the robust fiber mat morphology. The fiber cathode has a lower gas transport resistance (which is a consequence of the high inter- and intra- fiber porosity of the fiber cathode, a thinner coating of binder on catalyst particles, and less agglomeration of catalyst particles), as was the case for MEAs with Pt/C and PtCo/C fiber mat cathodes.[31,36,38]

Figures 2.7a and 2.7b contrast the differences in polarization curves for MEAs with Nafion/PVDF fiber mat cathodes at different cathode binder weight ratios (Nafion:PVDF binders of 50:50, 67:33, 75:25, 80:20). The polarization curves are also compared to an MEA with Nafion fibers cathode (PEO extracted) which is the same as that shown in Figure 2.3. For all cathodes, the catalyst loading was 3.0 mg/cm^2, and the total binder content was constant relative to the amount of catalyst at 50 wt%. As the PVDF content in the fiber cathode binder increased from 20 wt% to 50 wt%, less power was generated for all potentials. This was attributed to the hydrophobicity of PVDF, which decreased the rate of the oxygen reduction reaction[56,57] (this effect dominates in the high potential (low current density) region of a polarization curve). At the same time, increasing the PVDF content decreased the binder proton conductivity[43] (this effect dominates at the moderate current density region of the polarization curves). The decrease in binder conductivity with increasing PVDF content is manifested in the measured increase in HFR, as shown in Figure 2.7c. The polarization curve of the 75:25 Nafion:PVDF fiber cathode MEA was reproduced three times as shown in Appendix A of this dissertation.

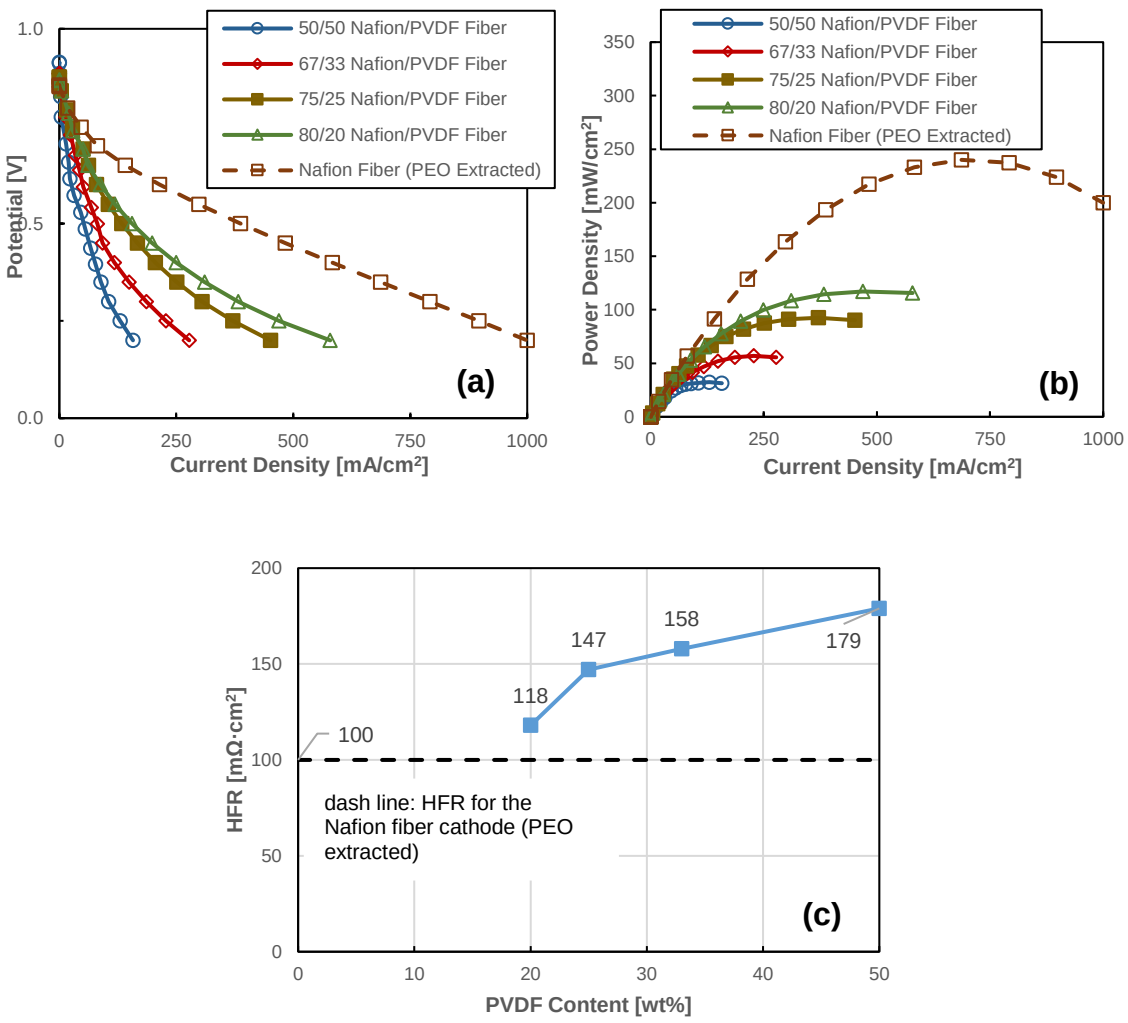

Figure 2.7. (a) H_2/air polarization curves (b) power density vs. current density of PMF-catalyst fiber cathode MEA at cathode Nafion:PVDF binder weight ratio of 50:50, 67:33, 75:25, and 80:20, and a Nafion fiber (PEO extracted) cathode MEA. (c) High frequency resistance vs. PVDF content. For all the cathodes, the total binder content was constant relative to the amount of catalyst at 50 wt%, and the PGM-free catalyst cathode loading was 3.0 mg/cm^2. Fuel cell operating conditions: 80 °C, 100% relative humidity, 200 kPa$_{abs}$ pressure, and 0.125/0.5 SLPM (standard liters per minute) H_2/air feed gas flow rate. All MEAs have a Nafion 211 membrane and a Pt/C catalyst powder anode at a loading of 0.1 mg$_{Pt}$/cm^2.

The effect of Nafion/PVDF weight ratio on MEA durability during constant potential operation at 0.5 V was also examined using the same MEAs as those in Figure

2.7. Figure 2.8a shows power density plots vs. time plots at 0.5 V, and Figure 2.8b shows the polarization curves collected at the end-of-test (EOT, i.e., after 50 hours of operation). Figure 2.9 shows the power density ratio of EOT to BOL at 0.7 V, 0.5 V, and 0.3 V, obtained from the polarization curves at BOL (Figure 2.7a) and EOT (Figure 2.8b). For all MEAs, the cathode catalyst loading was 3.0 mg/cm^2, and the total binder content was constant relative to the amount of catalyst at 50 wt%. As was the case in Figure 2.6 for a 50:50 Nafion:PVDF binder, the power output for all Nafion/PVDF fiber cathode MEAs increased initially after start-up and then stabilized after ca. 15 hours. Table 2.4 summarizes the stabilized power densities at 0.5 V.

The power output of the 80:20 Nafion:PVDF fiber cathode MEA did not stabilize after the initial rise but instead reached a maximum power density of 103 mW/cm^2 after ca. 15 hours and then slowly decreased for the remainder of the test at a decay rate of 0.2 mW/cm^2/hr. The slow decline in power over time for the 80:20 Nafion:PVDF fiber cathode MEA was due to insufficient PVDF (hydrophobicity) in the cathode binder to expel water and stop catalyst degradation. Although there was some cathode degradation, the 80:20 Nafion:PVDF fiber cathode MEA generated the highest power density ever recorded with a Nafion:PVDF binder (103 mW/cm^2 after 15 hours of constant voltage hold). As discussed above with regards to Figure 2.2, the electrospun fibers with an 80:20 Nafion:PVDF binder had more agglomerates than those with higher PVDF contents. Such agglomerates are unwanted and should decrease power output and durability due to clustering of catalyst particles, which will increase the mass transfer resistance for O_2 to reach an active site within a catalyst cluster and the mass transfer resistance for product water to exit the cluster interior. The poor fiber morphology, however, is compensated to

some extent by the improved proton conductivity of fibers with the lowest PVDF content (the drop in conductivity with increasing PVDF content is highly nonlinear, as indicated by Park et al.[43]). The best fiber cathode binder for both high and stable power at 0.5 V is 75:25 (w:w) Nafion:PVDF, which surpassed the power output of a neat Nafion fiber cathode after 86 hours of constant voltage operation. As shown in Figure 2.9, the EOT:BOL power density ratio is over 1.0 for all cathodes with Nafion/PVDF binder, while it is less than 1.0 for Nafion fiber cathodes. It should be noted that the power density ratio of EOT:BOL is less dependent on cathode binder composition at 0.7 V (the current density at this voltage is low, there is little water generated, and the hydrophobicity of the cathode has little effect on durability). In contrast, the power density ratio at 0.5 V and 0.3 V show the same binder composition dependence, where increasing the PVDF content increases the EOT:BOL ratio.

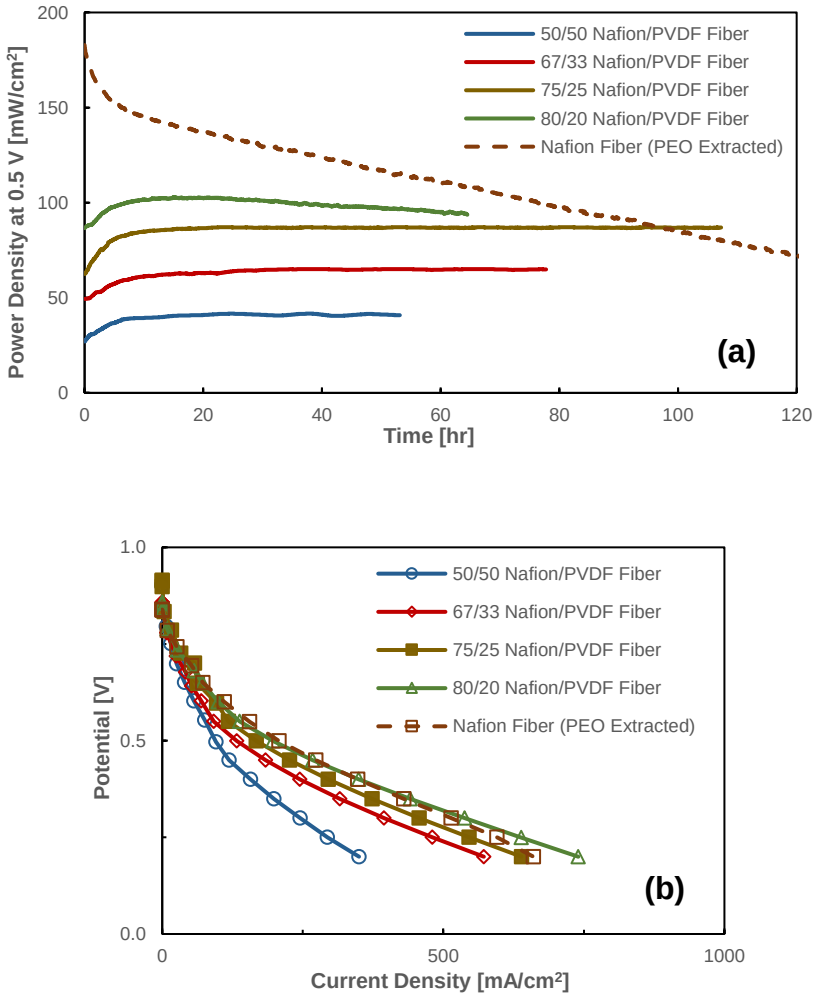

Figure 2.8. (a) H_2/air fuel cell power density at 0.5 V vs. time, and (b) H_2/air polarization curve after 50-hours operation of PMF-catalyst fiber mat cathode MEA at cathode Nafion:PVDF binder weight ratio of 50:50, 67:33, 75:25, and 80:20 and a Nafion fiber (PEO extracted) cathode MEA. For all the cathodes, total binder content was constant relative to the amount of catalyst at 50 wt%, and cathode loading was fixed at 3.0 mg/cm^2. Fuel cell operating conditions: 80 °C, 100% relative humidity, 200 kPa_{abs} pressure, and 0.125/0.5 SLPM (standard liters per minute) H_2/air feed gas flow rate. All MEAs have a Nafion 211 membrane and a Pt/C catalyst powder anode at a loading of 0.1 mg_{Pt}/cm^2.

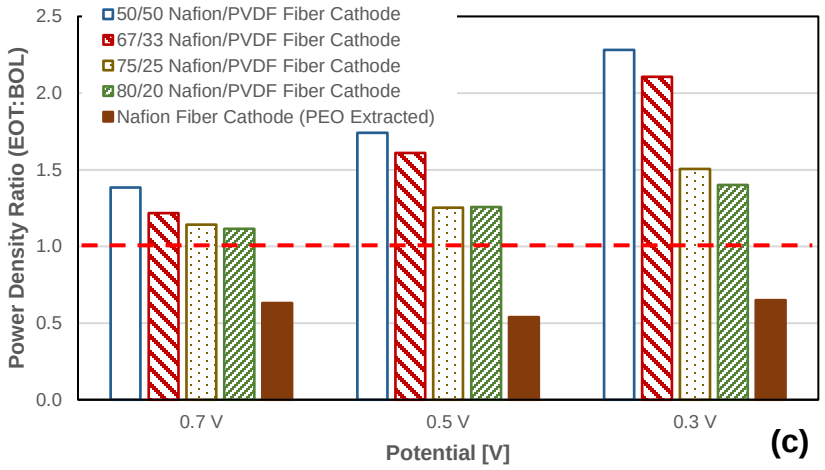

Figure 2.9. Power density ratio of EOT to BOL at 0.7 V, 0.5 V, and 0.3 V of PMF-catalyst fiber mat cathode MEA at cathode Nafion:PVDF binder weight ratio of 50:50, 67:33, 75:25, and 80:20 and a Nafion fiber (PEO extracted) cathode MEA (the power density values are obtained from Figure 2.7 and Figure 2.8).

Table 2.4. Stable Power Density (0.5 V) after 50 hours of a 0.5 V constant voltage operation for PMF Catalyst Cathode MEAs.

Cathode	stable power density (0.5 V) after 50 hours of a 0.5 V constant voltage hold [mW/cm^2]
Nafion Powder	93 (power density is degrading at a rate of 1.0 mW/cm^2/hr)
50:50 Nafion:PVDF Powder	25
Nafion Fiber (PEO extracted)	117 (power density is degrading at a rate of 0.7 mW/cm^2/hr)
50:50 Nafion:PVDF Fiber	41
67:33 Nafion:PVDF Fiber	65
75:25 Nafion:PVDF Fiber	88
80:20 Nafion:PVDF Fiber	96 (power density is degrading at a rate of 0.2 mW/cm^2/hr)

2.3.4 Effect of Catalyst Fiber Cathode Loading on Power Output and Durability

The effect of fiber cathode catalyst loading on fuel cell power output and cathode catalyst degradation was investigated with PMF catalyst loadings of 0.75 mg/cm^2, 1.5 mg/cm^2, and 3.0 mg/cm^2, where the fiber cathode binder was fixed at 75:25 (w:w) Nafion:PVDF. V-i fuel cell polarization data were collected at 80 °C with fully humidified air and hydrogen at a pressure of 200 kPa$_{abs}$. As shown in Figure 2.10, a substantial (80%) power gain was achieved when the cathode catalyst loading was increased from 0.75 mg/cm^2 to 1.5 mg/cm^2, i.e., the maximum power density was 45 mW/cm^2 at 0.75 mg/cm^2 and 81 mW/cm^2 at 1.5 mg/cm^2. In contrast, only a moderate (16%) power gain was observed when the cathode loading was further increased to 3.0 mg/cm^2 (the maximum power density was 94 mW/cm^2) due to cathode thickness effects. From SEM freeze fractured MEA cross sections, the PMF fiber cathode thickness at catalyst loadings of 0.75 mg/cm^2, 1.5 mg/cm^2, and 3.0 mg/cm^2 was 27, 53, and 99 μm, respectively. These thicknesses are substantially greater than the ~5-10 μm thickness observed in low catalyst loading Pt-based fuel cell cathodes [60]. It is more difficult to utilize all available catalyst material in the back of a thick electrode due to longer transport pathways and higher transport resistances for protons.[61,62] Also, PGM-free catalyst cathodes have higher oxygen transport resistance (longer O_2 transport pathways) because oxygen molecules must diffuse through the entire cathode thickness, from the gas feed channel to the front of the cathode. Thus, in a thick cathode, oxygen may not reach catalyst sites at the cathode/membrane interface and protons might not reach the back of the cathode, as the electrode/GDL interface.[61,63]

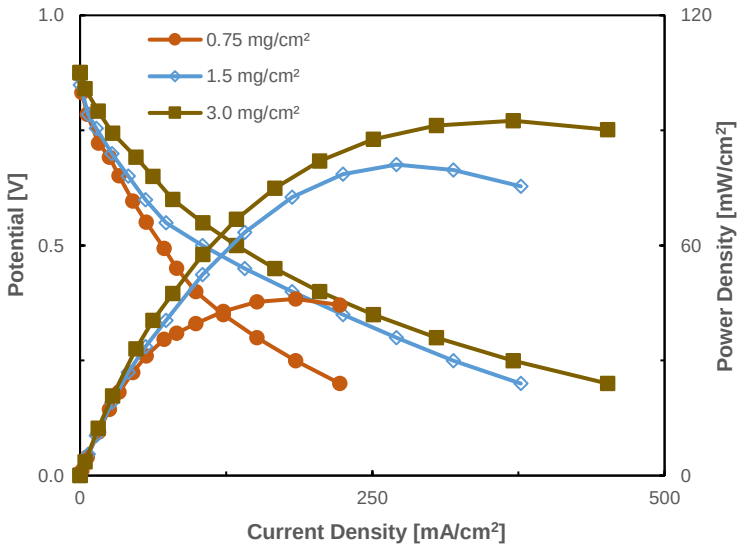

Figure 2.10. H_2/air polarization curves of PMF-catalyst fiber mat cathode MEA at a cathode catalyst loading of 0.75 mg/cm^2, 1.5 mg/cm^2, and 3.0 mg/cm^2 and cathode biner of 75:25 (w:w) Nafion:PVDF. Fuel cell operating conditions: 80 °C, 100% relative humidity, 200 kPa_{abs} pressure, and 0.125/0.5 SLPM (standard liters per minute) H_2/air feed gas flow rate. All MEAs have a Nafion 211 membrane and a Pt/C catalyst powder anode at a loading of 0.1 mg_{Pt}/cm^2.

The effect of fiber cathode catalyst loading on MEA (cathode) durability was evaluated in a constant voltage hold experiment with the same MEAs as those shown in Figure 2.10. The results of these tests are plotted in Figure 2.11 as the power density at 0.5 V vs. time. A plateau, i.e., power stabilization, was achieved in all fiber cathode MEAs, which indicated that the cathode catalyst loading did not affect the catalyst durability. The results suggest that there was no significant shift in the cathode region/location where oxygen was being reduced, i.e., ORR was not shifting from degraded catalyst to unused catalyst over the course of the constant voltage hold experiment. Thus, it can be concluded that PVDF hydrophobic effects dominate/control the durability of thin and thick cathodes.

For the MEAs with cathode loadings of 1.5 and 3.0 mg/cm^2, there was an increase in power output with time during the first ca. 15 hours of the experiment, followed by a plateauing/stabilizing of the power density. However, for the MEA with a cathode loading of 0.75 mg/cm^2, the power density is stable from the moment the constant voltage hold experiment begins. As discussed above regarding Figure 2.6, the power rise during the first few hours of a voltage hold experiment was attributed to an acceleration in the oxygen reduction reaction rate as a consequence of water generation near the catalyst surface, which improved the ORR kinetics and increased in the proton conductivity of the binder. The cathode at 0.75 mg/cm^2 was the thinnest. It produced the lowest initial current density (80 mA/cm^2 at 0.5 V), but this current was high enough to generate a sufficient amount of water so that any transient behavior in power output concluded during the break-in period for this MEA (during the first 30-60 minutes of MEA operation).

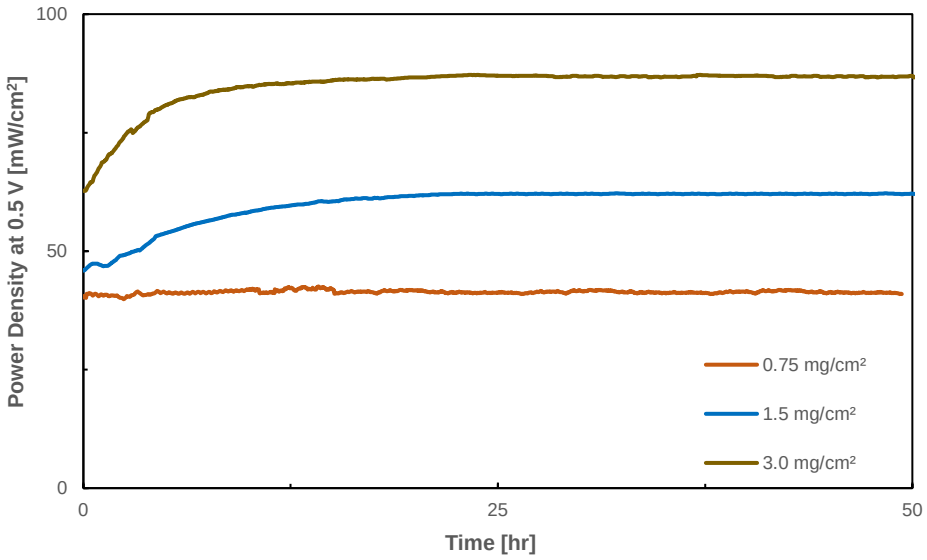

Figure 2.11. H_2/air power density at 0.5 V vs. time of PMF-catalyst fiber mat cathode MEA at a cathode catalyst loading of 0.75 mg/cm^2, 1.5 mg/cm^2, and 3.0 mg/cm^2, and the fiber cathode biner was 75:25 (w:w) Nafion:PVDF. Fuel cell operating conditions: 80 °C, 100% relative humidity, 200 kPa_{abs} pressure, 0.125/0.5 SLPM H_2/air feed gas flow rate. All MEAs have a Nafion 211 membrane and a Pt/C catalyst powder anode at a loading of 0.1 mg_{Pt}/cm^2.

2.4 Conclusions

A comprehensive experimental examination of fiber and powder fuel cell cathodes with one type of Fe-based PGM-free catalyst was carried out. Nanofiber mat cathodes were electrospun with a PMF catalyst and a binder of either neat Nafion or a blend of Nafion and PVDF. Fuel cell MEAs were evaluated in terms of their initial power output and their durability after a long-time constant voltage hold experiment. Fiber mat cathode MEAs with Nafion (after PEO carrier polymer extraction) or Nafion/PVDF binder at a cathode catalyst loading of 3.0 mg/cm^2 generated more power than the

corresponding powder cathode MEA. This is attributed to the unique fiber morphology, which facilitated O_2 transport in and water out of the MEA.

Degradation occurs in powder and fiber cathode MEA with neat Nafion binder due to attack of the carbon substrate of the cathode catalyst by hydrogen peroxide (which is generated by the 2-electron transfer reduction of O_2). Degradation was reduced or eliminated in powder and fiber cathode MEAs when a Nafion/PVDF cathode binder (with a sufficient amount of PVDF) was employed. The lower degradation rates were due to the PVDF hydrophobicity, which rapidly expelled water and dissolved H_2O_2. While PVDF addition to the cathode binder improved MEA durability, it also decreased MEA power output since the presence of PVDF slowed ORR kinetics (reduced the water content near catalyst particles) and decreased both the proton conductivity and oxygen permeability in the cathode binder. In the present study, MEA with a 75:25 (w:w) Nafion:PVDF fiber cathode binder achieved the highest long-term-stable power at 0.5 V (88 mW/cm^2), where there was a balance between the necessary hydrophobicity to expel peroxide and the requisite Nafion binder content for good proton conductivity and oxygen transport. The effect of fiber cathode catalyst loading on MEA fuel cell power and durability was conducted on MEAs whose cathode binder was 75:25 (w:w) Nafion:PVDF. Experimental results showed that power increased with increasing cathode loading up to 3.0 mg/cm^2. However, the impact of loading on power was more pronounced at lower catalyst contents due to the cathode fiber mat thickness. When the loading was too high, the cathode became too thick, limiting proton access in portions of the cathode far from the membrane and limiting oxygen access to regions of the cathode close to the membrane.

2.5 Reference

1. O'Hayre, R., Cha, S.-W. & Prinz, F. B. *Fuel Cell Fundamentals*. (John Wiley & Sons, 2016).
2. Papageorgopoulos, D. Fuel Cell R&D Overview Fuel Cells. *Annual Merit Review and Peer Evaluation Meeting* 33 (2019).
3. Ma, Y. *et al.* High active PtAu/C catalyst with core-shell structure for oxygen reduction reaction. *Catal Commun* **11**, 434–437 (2010).
4. Long, N. V. *et al.* The development of mixture, alloy, and core-shell nanocatalysts with nanomaterial supports for energy conversion in low-temperature fuel cells. *Nano Energy* **2**, 636–676 (2013).
5. Lv, H., Cheng, N., Mu, S. & Pan, M. Heat-treated multi-walled carbon nanotubes as durable supports for PEM fuel cell catalysts. *Electrochim Acta* **58**, 736–742 (2011).
6. Banham, D. *et al.* New insights into non-precious metal catalyst layer designs for proton exchange membrane fuel cells: Improving performance and stability. *J Power Sources* **344**, 39–45 (2017).
7. Banham, D., Choi, J., Kishimoto, T. & Ye, S. Integrating PGM-Free Catalysts into Catalyst Layers and Proton Exchange Membrane Fuel Cell Devices. *Advanced Materials* **31**, 1804846 (2019).
8. Wang, X. *et al.* Size-controlled large-diameter and few-walled carbon nanotube catalysts for oxygen reduction. *Nanoscale* **7**, 20290–20298 (2015).
9. Reshetenko, T. *et al.* The Effect of Proton Conductivity of Fe–N–C–Based Cathode on PEM Fuel cell Performance. *J Electrochem Soc* **167**, 084501 (2020).
10. Shao, Y., Dodelet, J., Wu, G. & Zelenay, P. PGM-Free Cathode Catalysts for PEM Fuel Cells: A Mini-Review on Stability Challenges. *Advanced Materials* **31**, 1807615 (2019).
11. Zhang, H. *et al.* High-performance fuel cell cathodes exclusively containing atomically dispersed iron active sites. *Energy Environ Sci* **12**, 2548–2558 (2019).
12. Martinez, U., Komini Babu, S., Holby, E. F. & Zelenay, P. Durability challenges and perspective in the development of PGM-free electrocatalysts for the oxygen reduction reaction. *Curr Opin Electrochem* **9**, 224–232 (2018).

13. Serov, A., Kovnir, K., Shatruk, M. & Kolen'ko, Y. v. Critical Review of Platinum Group Metal-Free Materials for Water Electrolysis: Transition from the Laboratory to the Market : Earth-abundant borides and phosphides as catalysts for sustainable hydrogen production. *Johnson Matthey Technology Review* **65**, 207–226 (2021).

14. Serov, A. *et al.* Highly stable precious metal-free cathode catalyst for fuel cell application. *J Power Sources* **327**, 557–564 (2016).

15. Reshetenko, T. *et al.* Electron and proton conductivity of Fe-N-C cathodes for PEM fuel cells: A model-based electrochemical impedance spectroscopy measurement. *Electrochem commun* **118**, 106795 (2020).

16. Kishi, H. *et al.* Structure of active sites of Fe-N-C nano-catalysts for alkaline exchange membrane fuel cells. *Nanomaterials* **8**, 1–14 (2018).

17. Cells, T. F. *et al.* Fuel Cell 2016 Multi-Year Research, Development, and Demonstration Plan. *Department of Energy, Multi-Year Research, Development, and Demonstration Plan* **2015**, 1–58 (2016).

18. Goellner, V., Armel, V., Zitolo, A., Fonda, E. & Jaouen, F. Degradation by Hydrogen Peroxide of Metal-Nitrogen-Carbon Catalysts for Oxygen Reduction. *J Electrochem Soc* **162**, H403–H414 (2015).

19. Choi, C. H. *et al.* Unraveling the Nature of Sites Active toward Hydrogen Peroxide Reduction in Fe-N-C Catalysts. *Angewandte Chemie - International Edition* **56**, 8809–8812 (2017).

20. Choi, C. H. *et al.* The Achilles' heel of iron-based catalysts during oxygen reduction in an acidic medium. *Energy Environ Sci* **11**, 3176–3182 (2018).

21. Luoh, R. & Hahn, H. T. Electrospun nanocomposite fiber mats as gas sensors. *Compos Sci Technol* **66**, 2436–2441 (2006).

22. Hwang, K., Kwon, B. & Byun, H. Preparation of PVdF nanofiber membranes by electrospinning and their use as secondary battery separators. *J Memb Sci* **378**, 111–116 (2011).

23. Gopal, R. *et al.* Electrospun nanofibrous filtration membrane. *J Memb Sci* **281**, 581–586 (2006).

24. Zhang, Y., Chwee, T. L., Ramakrishna, S. & Huang, Z. M. Recent development of polymer nanofibers for biomedical and biotechnological applications. *J Mater Sci Mater Med* **16**, 933–946 (2005).

25. Padbury, R. & Zhang, X. Lithium-oxygen batteries - Limiting factors that affect performance. *J Power Sources* **196**, 4436–4444 (2011).

26. Ji, L., Lin, Z., Alcoutlabi, M. & Zhang, X. Recent developments in nanostructured anode materials for rechargeable lithium-ion batteries. *Energy Environ Sci* **4**, 2682–2689 (2011).

27. Lee, H., Yanilmaz, M., Toprakci, O., Fu, K. & Zhang, X. A review of recent developments in membrane separators for rechargeable lithium-ion batteries. *Energy Environ Sci* **7**, 3857–3886 (2014).

28. Ballengee, J. B. & Pintauro, P. N. Morphological Control of Electrospun Nafion Nanofiber Mats. *J Electrochem Soc* **158**, B568 (2011).

29. Park, A. M. & Pintauro, P. N. Alkaline Fuel Cell Membranes from Electrospun Fiber Mats. *Electrochemical and Solid-State Letters* **15**, B27 (2012).

30. Waldrop, K., Wycisk, R. & Pintauro, P. N. Application of electrospinning for the fabrication of proton-exchange membrane fuel cell electrodes. *Curr Opin Electrochem* **21**, 257–264 (2020).

31. Brodt, M., Wycisk, R. & Pintauro, P. N. Nanofiber Electrodes with Low Platinum Loading for High Power Hydrogen/Air PEM Fuel Cells. *J Electrochem Soc* **160**, F744–F749 (2013).

32. Ballengee, J. B., Haugen, G. M., Hamrock, S. J. & Pintauro, P. N. Properties and Fuel Cell Performance of a Nanofiber Composite Membrane with 660 Equivalent Weight Perfluorosulfonic Acid. *J Electrochem Soc* **160**, F429–F435 (2013).

33. Fischer, R., Pintauro, P. N. & Jennings, G. K. Properties of stretched 830EW Aquivion. (2012).

34. Self, E. C. *et al.* High Areal Capacity Si/LiCoO2 Batteries from Electrospun Composite Fiber Mats. *ChemSusChem* **10**, 1823–1831 (2017).

35. Waldrop, K. *et al.* Electrospun Particle/Polymer Fiber Electrodes with a Neat Nafion Binder for Hydrogen/Air Fuel Cells. *ECS Trans* **92**, 595–602 (2019).

36. Slack, J. J. *et al.* Nanofiber Fuel Cell MEAs with a PtCo/C Cathode. *J Electrochem Soc* **166**, F3202–F3209 (2019).

37. Chintam, K. *et al.* Improved Water Management of Electrospun Nanofiber Membrane Electrode Assemblies at High Current Densities Measured in Operando Using Neutron Radiography. *ECS Meeting Abstracts* **MA2019-02**, 1403–1403 (2019).

38. Zhang, W. & Pintauro, P. N. High-Performance Nanofiber Fuel Cell Electrodes. *ChemSusChem* **4**, 1753–1757 (2011).

39. Brodt, M. *et al.* Fabrication, In-Situ Performance, and Durability of Nanofiber Fuel Cell Electrodes. *J Electrochem Soc* **162**, F84–F91 (2015).

40. Waldrop, K. Preparation and Characterization of Polymer/Particle Electrospun Fiber Electrodes for Hydrogen/air Fuel Cells. (2021).

41. Brodt, M., Wycisk, R., Dale, N. & Pintauro, P. Power Output and Durability of Electrospun Fuel Cell Fiber Cathodes with PVDF and Nafion/PVDF Binders. *J Electrochem Soc* **163**, F401–F410 (2016).

42. Abdel-Baset, T. *et al.* The. US Deparment of Energy (DOE). Energy Efficiency and Renewable Energy https://energy.gov/eere/fuelcells/doe-technical-targets-polymer-electrolyte-membrane-fuel-cell-components. 30 (2017) doi:10.2172/1220127.

43. Woo Park, J. *et al.* Electrospun Nafion/PVDF single-fiber blended membranes for regenerative H2/Br2 fuel cells. *J Memb Sci* **541**, 85–92 (2017).

44. Slack, J. *et al.* Electrospun Fiber Mat Cathode with Platinum-Group-Metal-Free Catalyst Powder and Nafion/PVDF Binder. *ChemElectroChem* **5**, 1537–1542 (2018).

45. Chen, H., Snyder, J. D. & Elabd, Y. A. Electrospinning and solution properties of Nafion and poly(acrylic acid). *Macromolecules* **41**, 128–135 (2008).

46. Waldrop, K. *et al.* Electrospun Nanofiber Electrodes for High and Low Humidity PEMFC Operation. *J Electrochem Soc* **170**, 024507 (2023).

47. Zhang, G., Chenitz, R., Lefèvre, M., Sun, S. & Dodelet, J. P. Is iron involved in the lack of stability of Fe/N/C electrocatalysts used to reduce oxygen at the cathode of PEM fuel cells? *Nano Energy* **29**, 111–125 (2016).

48. Chenitz, R. *et al.* A specific demetalation of Fe-N4 catalytic sites in the micropores of NC-Ar + NH3 is at the origin of the initial activity loss of the highly active Fe/N/C catalyst used for the reduction of oxygen in PEM fuel cells. *Energy Environ Sci* **11**, 365–382 (2018).

49. Uddin, A. *et al.* High Power Density Platinum Group Metal-free Cathodes for Polymer Electrolyte Fuel Cells. *ACS Appl Mater Interfaces* **12**, 2216–2224 (2020).

50. Herranz, J. *et al.* Unveiling N-Protonation and Anion-Binding Effects on Fe / N / C Catalysts for O 2 Reduction in Proton-Exchange-Membrane Fuel Cells. *Journal of Physical Chemistry C* **115**, 16087–16097 (2011).

51. Kumar, K. *et al.* On the Influence of Oxygen on the Degradation of Fe-N-C Catalysts. *Angewandte Chemie* **132**, 3261–3269 (2020).

52. Kumar, K. *et al.* Physical and Chemical Considerations for Improving Catalytic Activity and Stability of Non-Precious-Metal Oxygen Reduction Reaction Catalysts. *ACS Catal* **8**, 11264–11276 (2018).

53. Jaouen, F. O_2 Reduction Mechanism on Non-Noble Metal Catalysts for PEM Fuel Cells. Part II: A Porous-Electrode Model To Predict the Quantity of H_2O_2 Detected by Rotating Ring-Disk Electrode. *The Journal of Physical Chemistry C* **113**, 15433–15443 (2009).

54. Kabir, S. *et al.* Improving the bulk gas transport of Fe-N-C platinum group metal-free nanofiber electrodes via electrospinning for fuel cell applications. *Nano Energy* **73**, 1–3 (2020).

55. Nawn, G. *et al.* Structural analyses of blended Nafion/PVDF electrospun nanofibers. *Physical Chemistry Chemical Physics* **21**, 10357–10369 (2019).

56. Ramaker, D. E., Korovina, A., Croze, V., Melke, J. & Roth, C. Following ORR intermediates adsorbed on a Pt cathode catalyst during break-in of a PEM fuel cell by in operando X-ray absorption spectroscopy. *Physical Chemistry Chemical Physics* **16**, 13645–13653 (2014).

57. Wang, J. X., Markovic, N. M. & Adzic, R. R. Kinetic Analysis of Oxygen Reduction on Pt(111) in Acid Solutions: Intrinsic Kinetic Parameters and Anion Adsorption Effects. *Journal of Physical Chemistry B* **108**, 4127–4133 (2004).

58. Mohamed, H. F. M. *et al.* Free volume and permeabilities of O2 and H2 in Nafion membranes for polymer electrolyte fuel cells. *Polymer (Guildf)* **49**, 3091–3097 (2008).

59. Oliveira, F. *et al.* Process influences on the structure, piezoelectric, and gas-barrier properties of PVDF-TrFE copolymer. *J Polym Sci B Polym Phys* **52**, 496–506 (2014).

60. Gasteiger, H. A., Kocha, S. S., Sompalli, B. & Wagner, F. T. Activity benchmarks and requirements for Pt, Pt-alloy, and non-Pt oxygen reduction catalysts for PEMFCs. *Appl Catal B* **56**, 9–35 (2005).

61. Osmieri, L., Wang, H. & Neyerlin, K. C. Impact of Fabrication and Testing Parameters on the Performance of a Polymer Electrolyte Fuel Cell with Platinum Group Metal (PGM)-Free Cathode Catalyst. *J Electrochem Soc* **168**, 014503 (2021).

62. Landesfeind, J., Ebner, M., Eldiven, A., Wood, V. & Gasteiger, H. A. Tortuosity of Battery Electrodes: Validation of Impedance-Derived Values and Critical Comparison with 3D Tomography. *J Electrochem Soc* **165**, A469–A476 (2018).

63. Leonard, N. D. *et al.* Modeling of Low-Temperature Fuel Cell Electrodes Using Non-Precious Metal Catalysts. *J Electrochem Soc* **162**, F1253–F1261 (2015).

CHAPTER III

FABRICATION, MORPHOLOGY, AND PERFORMANCE OF FIBER MAT CATHODE MEAS WITH MOF PGM-FREE CATALYST

3.1 Introduction

Recent research[1–5] in the field of PGM-free oxygen reduction reaction (ORR) electrocatalysts has resulted in the discovery of several families of moderately high catalytic activity compounds that combine a transition metal with nitrogen and carbon to form M-N-C surface-active complexes (where M denotes a metal species, such as Fe, Co, Ni, or Mn). There are a variety of approaches to synthesizing M-N-C PGM-free catalysts, such as the hard-templating pore-former (PMF) method and the use of metal-organic-framework (MOF) precursors. In Chapter II of this dissertation, PMF catalysts provided by Pajarito Powder, LLC. were utilized to fabricate PGM-free catalyst cathode MEAs. This chapter investigated MOF-based PGM-free catalysts, which were also supplied by Pajarito Powder.

Electrospinning is an economically viable method of fabricating non-woven fiber mats, which can be used in numerous applications such as filtration media [6], lithium-ion batteries,[7,8] fuel cell electrodes,[9,10] and membranes.[11,12] Electrospinning has also been used to prepare PGM-free catalyst cathodes. For example, Li et al.[13] fabricated a PGM-free catalyst cathode with a three-dimensional carbon nanofiber web and an abundance of intra-fiber macropores and mesopores. Shui et al.[14] prepared a carbon-based nanofibrous catalyst mat, which had a high volumetric activity with moderate durability when tested

in a fuel cell membrane-electrode-assembly (MEA). Kabir et al.[15] electrospun a fiber mat cathode composed of a mixture of commercial PGM-free catalyst powder, Nafion® ionomer, and polyacrylic acid (PAA), where the resulting MEA produced 50% more power in a fuel cell than a conventional powder/Nafion cathode MEA. Slack et al.[16] prepared a fiber cathode using PGM-free catalysts, Nafion, and PVDF and showed a stable fuel cell power output of 80 mW/cm^2 at 0.5 V for 300 hours. In Chapter II of this dissertation, a nanofiber cathode MEA with PMF catalysts and a Nafion/PVDF binder generated 50 hours of stable power operation at 0.5 V. That study also showed that: (i) adding PVDF to the cathode binder (as low as 20 wt%) resulted in a decrease in power output, (ii) increasing the Nafion/PVDF weight ratio in the cathode binder increased power, but the long-term power output stability of an MEA suffered, and (iii) a fiber cathode with PMF catalyst and a binder of 75:25 (w:w) Nafion:PVDF was the best compromise in terms of power output and stable power production, where a measured power density of 88 mW/cm^2 at 0.5 V was maintained for 80 hours.

The present study used MOF-based PGM-free catalysts (provided by Pajarito Powder) in slurry/powder and nanofiber cathode MEAs. Fiber mats with Nafion/PVDF binder and a MOF-based Fe-N-C catalyst were successfully electrospun with Nafion:PVDF weight ratio of 50:50, 67:33, 75:25, 80:20, and 83:17. The fiber mats were incorporated into a fuel cell MEA with a Nafion 211 membrane and a Pt/C anode. The effect of cathode binder composition on initial power and MEA durability was assessed, and the results were compared with a PMF fiber mat cathode MEA.

3.2 Experimental

3.2.1 Electrospinning Catalyst/Nafion/PVDF Fiber Mats

Electrospinning solutions of MOF, Nafion, and PVDF for fiber cathode MEAs were made following the same procedure as in Chapter II for the PMF catalyst. First, an electrospinning solution was prepared with the following components in a solvent of 50:28:22 (w:w:w) dimethylformamide (DMF):Acetone:tetrahydrofuran (THF): (a) Fe-based MOF catalyst powder (where MOF denotes metal-organic framework, which was the precursor for this catalyst; where the catalyst was provided by Pajarito Powder, LLC), (b) Nafion dispersion (20 wt% 1100 EW Nafion in a 70:30 (w:w) DMF:acetone solvent, the Nafion resin which was obtained by drying an Ion Power Liquion 1115 solution and then redispersing the dry powder in the solvent mixture), and (c) a PVDF solution; 10 wt% Kynar HSV 900 KDa PVDF (Arkema, Inc.) in a 70:30 (w:w) DMF:acetone solvent. The electrospinning solution components were mixed as follows: (i) dispersing the MOF catalyst powders in DMF/acetone/THF solvent, (ii) adding the Nafion dispersion to the catalyst solution followed by 60 minutes of high energy ultrasonic agitation using a sonic horn (Sonic & Materials Inc. VibraCell Ultrasonicator) and an additional 30 minutes of low energy mixing in a sonication bath (Fisher Scientific Inc. FS20D Ultrasonic Cleaner), and (iii) adding the PVDF solution followed by mechanically stirring for 12 hours.

The same fiber electrospinning procedure was used as in Chapter II and previous studies [17,18]. Electrospinning was performed at room temperature in a custom-built plexiglass chamber with relative humidity control. The electrospinning solution was drawn into a 3-mL syringe with a 22-gauge stainless needle spinneret, and the

electrospun fiber mat was collected on a rotating and laterally oscillating cylindrical drum. Although the electrospinning solution composition and mixing procedure was the same for MOF and PMF catalysts, the electrospinning conditions (relative humidity, flow rate, and needle tip to collector distance) were different, as indicated in Table 3.1. The electrospinning solution and final dry fiber cathode compositions are listed in Table 3.2.

Table 3.1. Electrospinning Conditions for PMF and MOF Catalyst Fiber Mat with Nafion/PVDF Binder

	PMF Catalyst	MOF Catalyst
Potential [KV]	10.8-12	10.8-13.5
Relative Humidity [%]	50-55%	65-70%
Flow Rate [mL/hr]	0.5	0.75
Needle Tips to Collector Distance [cm]	8	17

Table 3.2. Electrospinning Solution and Final Dry Fiber Cathode Composition

Solution	Electrospinning Solution [g]	Dry Fiber Cathode Composition [wt%]
1	0.33 g catalyst, 0.053 g DMF, 0.036 g acetone, 0.65 g THF, 1.38 g stock solutionA[1], 0.55 g stock solution B[2]	50 catalyst, 41.7 Nafion, 8.3 PVDF
2	0.33 g catalyst, 0.015 g DMF, 0.020 g acetone, 0.65 g THF, 1.32 g stock solution A, 0.66 g stock solution B	50 catalyst, 40 Nafion, 10 PVDF
3	0.32 g catalyst, 0.027 g DMF, 0.025 g acetone, 0.66 g THF, 1.18 g stock solution A, 0.79 g stock solution B	50 catalyst, 37.5 Nafion, 12.5 PVDF
4	0.30 g catalyst, 0.009 g DMF, 0.018 g acetone, 0.68 g THF, 0.99 g stock solution A, 1.02 g stock solution B	50 catalyst, 33.3 Nafion, 16.7 PVDF
5	0.27 g catalyst, 0.0015 g DMF, 0.015 g acetone, 0.69 g THF, 0.68 g stock solution A, 1.35 g stock solution B	50 catalyst, 25 Nafion, 25 PVDF

[1]Stock Solution A: 20 wt% Nafion, in 70:30 (w:w) DMF:acetone

[2]Stock Solution B: 10 wt% PVDF in 70:30 (w:w) DMF:acetone

3.2.2 Conventional Powder Cathode Preparation

MOF/binder cathodes with a conventional powder electrode morphology with either a neat Nafion binder or a Nafion/PVDF binder were also prepared (using the same procedure as in Chapter II). The ink for the powder cathodes with Nafion/PVDF binder was prepared using the same procedure as the corresponding electrospinning solution but at lower solids (catalyst + Nafion + PVDF) content (2.5 wt%) to facilitate airbrush spraying.

The neat Nafion binder ink (at 2.5 wt% solids and a catalyst content of 50 wt%) was composed of MOF catalyst powder, Nafion dispersion (20 wt% 1100 Nafion resin, obtained by drying an Ion Power Liquion 1115 solution, in 50:50 (w:w) water:isopropanol solvent), and a mixed solvent of 50:50 (w:w) water:isopropanol. The ink was prepared using the following procedure: (i) dispersing the MOF catalyst powder in water/isopropanol solvent, (ii) adding Nafion dispersion to the catalyst solution followed by 60 minutes of high energy ultrasonic agitation and an additional 30 minutes of low energy sonication bath mixing, and (iii) mechanically stirring the ink for 12 hours. Powder cathode inks (with either neat Nafion or Nafion/PVDF binder) were manually airbrush sprayed onto Sigracet 29BC carbon paper GDLs until the dry cathode catalyst loading was 3.0 mg/cm^2.

3.2.3 Pt/C Powder Anode Preparation

All PGM-free catalyst cathode MEAs (either powder or fiber mat cathode) employed a Pt/C powder anode (same as in Chapter II) that was made with ink composed of 65 wt% Pt/C catalyst (Johnson Matthey, HiSPEC 4000 with 40% Platinum on carbon)

and 35 wt% Nafion (a dispersion of 20 wt% 1100 Nafion resin, obtained by drying an Ion Power Liquion 1115 solution and redispersing in a 50:50 [w:w] water:isopropanol) in a 50:50 (w:w) water:isopropanol mixed solvent. The Pt/C catalyst ink was prepared following the same procedure as the MOF catalyst cathodes with a neat Nafion binder. The ink was airbrush sprayed onto a Sigracet 29BC gas-diffusion-layer (GDL) at a Pt loading of 0.1 mg_{Pt}/cm^2.

3.2.4 Membrane-Electrode-Assembly (MEA) Preparation

All Nafion/PVDF fiber cathode MEAs contained a Nafion 211 membrane and a Pt/C anode. Electrospun fiber mats were cut into 5 cm^2 squares, and three mats were stacked to achieve a catalyst loading of ~3.0 mg/cm^2 (each stack had a loading of ~1.0 mg/cm^2). A Sigracet 29BC cathode gas diffusion layer (GDL), the stacked PGM-free catalyst fiber mats, a Nafion 211 membrane, and a Pt/C powder anode (Pt/C catalyst layer on 29BC GDL) were then hot pressed together at 35 MPa pressure and 140 °C for 10 minutes to create a membrane-electrode-assembly (MEA).

The powder cathode MEA comprised a powder cathode (PGM-free catalyst layer on 29BC GDL), Nafion 211 membrane, and a Pt/C powder anode (Pt/C catalyst layer on 29BC GDL). The Nafion 211 membrane was sandwiched by the MOF catalyst powder cathode and the Pt/C powder anode and then hot pressed together at 35MPa and 140 °C for 10 minutes.

3.2.5 Fuel cell Tests

Fuel cell tests were conducted using a Scribner Series 850e test station with temperature, back pressure, and mass flow rate under control. The fuel cell test fixture accommodated a 5 cm^2 MEA and contained single serpentine flow channels for anode and cathode feed gases. Fuel cell current-voltage data were collected at 80 °C, 200 kPa_{abs}, and 100% relative humidity (RH) with feed gases of H_2/air at 0.125/0.5 SLPM (standard liters per minute). An initial fuel cell polarization curve was collected after loading the MEA in the fuel cell test fixture, allowing the system to reach the fuel cell operating temperature of 80 °C, and then waiting for the open circuit voltage (OCV) to stabilize, which took approximately one hour. After that, fuel cell durability tests (a long-time potentiostatic hold at 0.3 V, 0.5 V, or 0.7 V) were carried out.

3.2.6 Scanning Electron Microscopy

Top-down scanning electron microscope (SEM) images of PGM-free catalyst powder and fiber mat cathodes were obtained with a MERLIN Microscope. Prior to imaging, a catalyst powder or fiber mat electrode was slightly pressed onto double-sided conductive tape and placed onto a flat specimen holder. The sample was then sputter coated with a thin layer of gold to improve imaging contrast. ImageJ software (made available by the National Institute of Health (NIH): https://imagej.nih.gov/ij/index.html) was used for digitizing collected SEM images to determine the overall quality of the fiber mat (the presence of bead-on giber or droplet defects, catalyst particle size, and the average fiber diameter).

3.3 Results and Discussion

3.3.1 MOF Catalyst Morphology

A top-down SEM image of a MOF catalyst powder cathode with neat Nafion binder is shown in Figure 3.1a. The largest agglomerate/particle size was ~2 μm, considerably smaller than the 4 μm size of PMF catalyst particles in a powder cathode at the same catalyst/binder composition (see Figure 2.1a in Chapter II). The SEM images of a powder cathode with a 75:25 (w:w) Nafion:PVDF binder are shown in Figure 3.1b, where the largest agglomerate/particle size was also ~2 μm. As was the case for PMF catalysts in Chapter II, adding PVDF to a catalyst/Nafion ink had no apparent effect on dispersing the catalyst or breaking up agglomerates during the conventional powder cathode fabrication.

A representative SEM image of an electrospun fiber mat with MOF catalyst is shown in Figure 3.1c, where the binder was a 75:25 weight ratio Nafion:PVDF mixture (the same composition as Figure 3.1b and the PMF fibers in Figure 2.2d in Chapter II). A highly porous and roughened fiber surface is visible from the image, with a smaller average fiber diameter (0.90 μm) compared to the PMF fibers in Figure 2.2d (1.1 μm) and fewer bead-on-fiber defects. The better quality of MOF fibers (fewer bead-on-fiber defects) was attributed to the smaller MOF catalyst particle size.

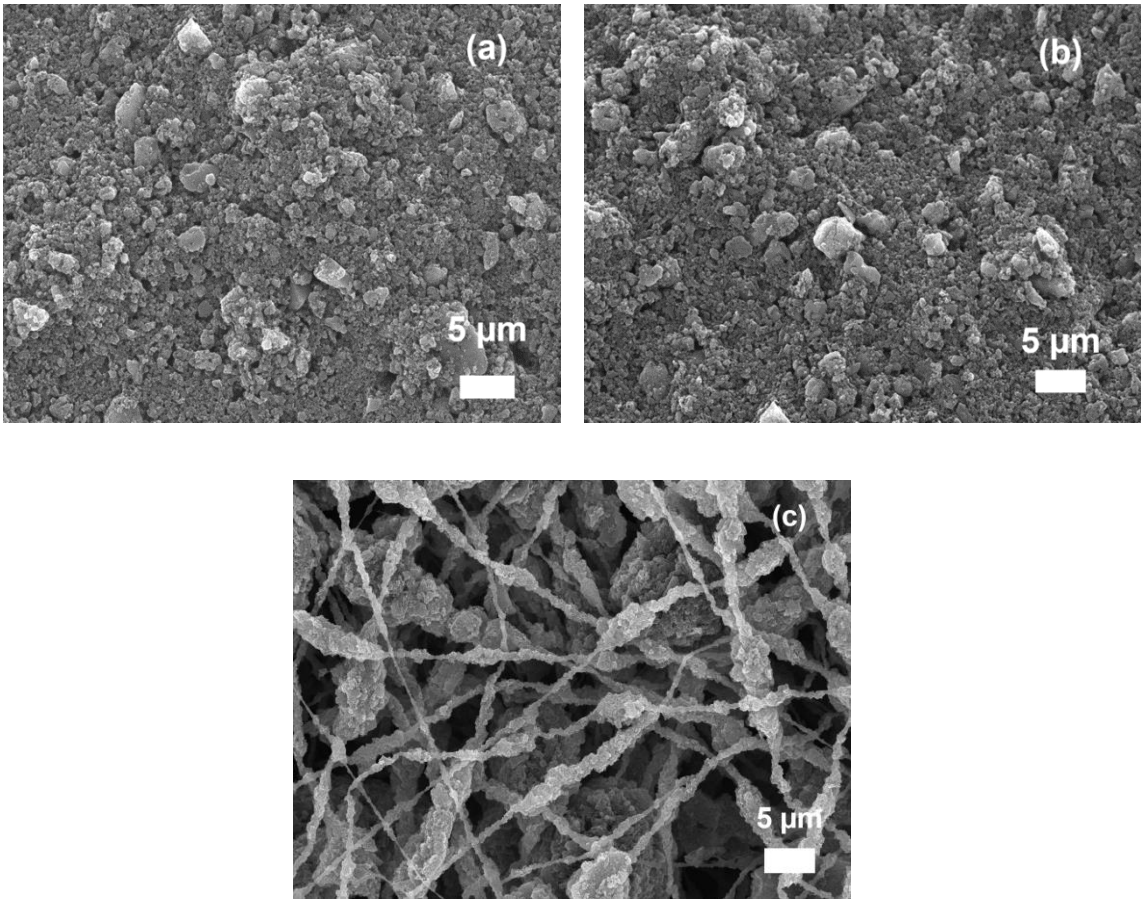

Figure 3.1. Top-down SEM images of MOF catalyst cathodes: (a) a powder cathode with a neat Nafion binder, (b) a powder cathode with a 75:25 (w:w) Nafion:PVDF binder, and (c) a fiber mat cathode with a 75:25 (w:w) Nafion:PVDF binder.

3.3.2 Fuel Cell Performance of Powder Cathode MEA with Different Cathode Binder

Hydrogen/air fuel cell polarization curves for MEAs with a MOF powder cathode and cathode binders of Nafion:PVDF at weight ratios of 50:50, 75:25, 80:20, and 83:17 are shown in Figure 3.2. Also shown in Figure 3.2 is a polarization curve for a powder cathode MEA with MOF catalyst and neat Nafion binder. For all cathodes, the cathode catalyst loading was 3.0 mg/cm^2, and the catalyst:binder (Nafion + PVDF) weight ratio was fixed at 50:50 (i.e., the cathode MOF content was set at 50 wt%). As can be seen, a

higher power was generated (over the entire potential range of 0.2-1.0 V) as the PVDF content in the powder cathode binder decreased from 50 wt% to 17 wt%. Also, the powder cathode MEA with neat Nafion binder initially outperformed the Nafion/PVDF powder cathode MEAs. Thus, as was the case with PMF cathode MEAs, even a small amount of PVDF in the cathode binder (17 wt%) with MOF catalyst particles had a profound effect on the initial power output of an MEA. As discussed for PMF cathode MEAs, the lower power was attributed to combined factors:

(i) Increased binder hydrophobicity, as evidenced by Nawn et al. [19] who showed that there was significantly less water in Nafion/PVDF polymer blends with as little as 10 wt% PVDF, where less water in the binder lowered/inhibited the oxygen reduction reaction kinetics.[20,21]

(ii) Lower proton conductivity, which was a consequence of PVDF driving water out of the binder (a more hydrophobic binder with lower water content) and Nafion binder being diluted by uncharged PVDF polymer (it should also be noted that the binder:catalyst ratio in fiber cathodes was maintained constant at 50:50, so an increase in PVDF content meant that there was less Nafion in the binder); Park et al.[22] found a precipitous drop in conductivity when only a small amount of PVDF was added to Nafion.

(iii) Decrease in oxygen permeability since the oxygen permeability in PVDF[23] is three orders of magnitude lower than in wet Nafion.[24]

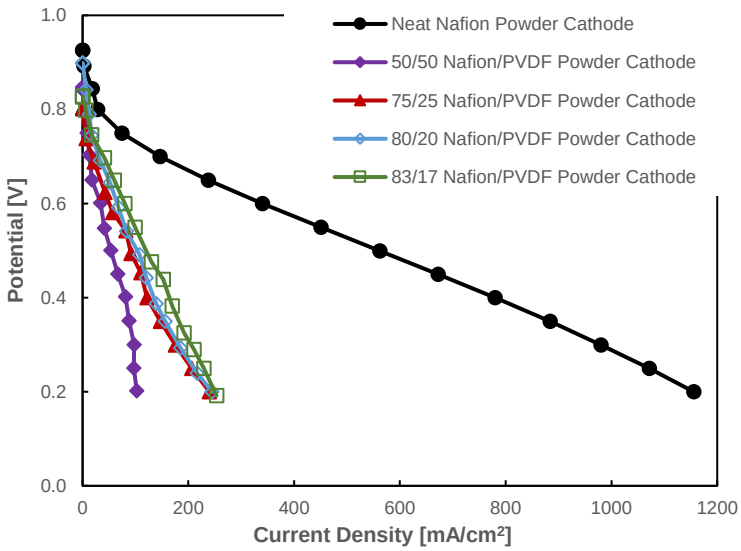

Figure 3.2. H_2/air fuel cell polarization curves of MOF catalyst powder cathode MEAs at cathode Nafion:PVDF binder weight ratio of 50:50, 75:25, 80:20, and 83:17, and a powder cathode MEA with a neat Nafion binder. For all the cathodes, total binder content was constant relative to the amount of catalyst at 50 wt% and PGM-free catalyst cathodes at the loading of 3.0 mg/cm^2. Fuel cell operating conditions: 80 °C, 100% relative humidity, 200 kPa$_{abs}$, and 0.125/0.5 SLPM H_2/air feed gas flow rate. All MEAs have a Nafion 211 membrane and a Pt/C catalyst powder anode at a loading of 0.1 mg$_{Pt}$/cm^2.

A long-term H_2/air fuel cell durability test at 0.5 V was also conducted on all the MEAs shown in Figure 3.2. The results of these tests are plotted in Figure 3.3, where the measured power density is plotted versus time. As was the case with PMF catalysts (Chapter II), the conventional powder cathode MEA with a neat Nafion binder and MOF catalyst underwent significant degradation over time with a monotonic power density decay that can be split into two distinct degradation phases: a rapid short-time decay (at a rate of 6.9 mW/cm^2/hr) during the first 10 hours of constant voltage operation followed by a slower and almost linear decline in power at 1.2 mW/cm^2/hr. The initial power loss may be due to metal (Fe) dissolution from MOF catalyst sites due to the highly acidic sulfonic acid moieties in the Nafion binder.[25] The slower power loss was attributed to

peroxide attack (oxidation) on the carbon-based cathode catalyst ORR sites, where H_2O_2 was produced via the 2-electron reduction of O_2 with H^+[26–28]:

$$2H^+ + 2e^- + O_2 \rightarrow H_2O_2 \qquad (1)$$

The long-term stability in power density of cathodes with Nafion/PVDF binder was attributed to the hydrophobicity of the binder, which expelled water and minimized electrogenerated peroxide contact with catalyst particles. Thus, less chemical attack (oxidation) of the PMF catalysts occurred with a Nafion/PVDF cathode binder, as was first observed by Slack et al.[16] with MOF catalysts. Although the neat Nafion powder electrode MEA generated a very high initial power density, its power density versus time decay curve will eventually intersect and drop below the curve for the Nafion/PVDF binder MEAs.

A power rise after start-up and then power stabilization can be seen in Figure 3.3 for a powder cathode MEA with a cathode Nafion:PVDF binder weight ratio of 50:50. A similar trend was reported by Slack et al.[16] and was observed with PMF catalyst, as discussed in Chapter II. The increase in power during the first few hours of constant voltage operation was attributed to an acceleration in oxygen reduction reaction over time, as a consequence of water generation near the catalyst surface and an increase in the proton conductivity of the binder. However, for the powder cathodes where the Nafion:PVDF weight ratio was greater than 50:50 (i.e., 75:25, 80:20, and 83:17), there was an initial power drop followed by a slow rise in MEA power output with eventual stabilization after ca. 30 hours. This behavior will be discussed further in the following section.

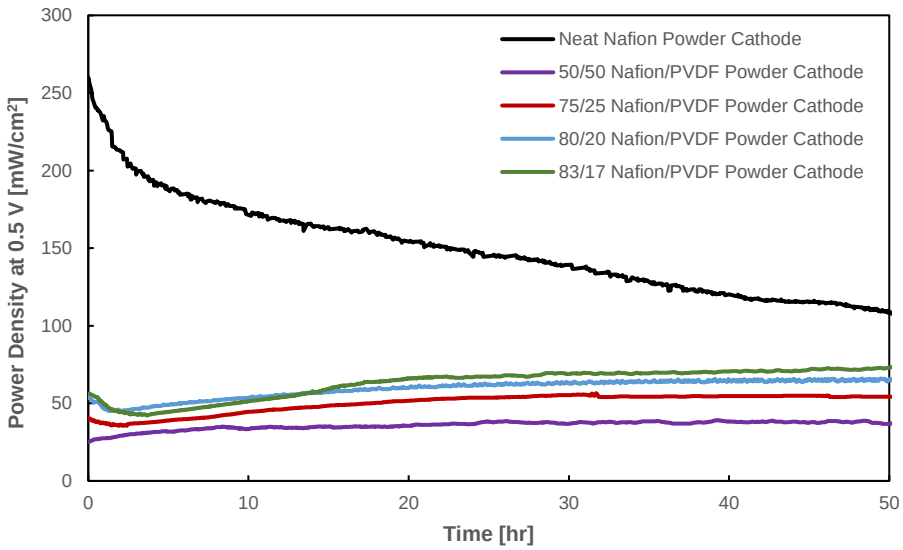

Figure 3.3. H_2/air fuel cell power density at 0.5 V vs. time of MOF catalyst powder cathode at cathode Nafion:PVDF binder weight ratio of 50:50, 75:25, 80:20, and 83:17, and a powder cathode MEA with a neat Nafion binder. For all the cathodes, total binder content was constant relative to the amount of catalyst at 50 wt% and a PGM-free catalyst cathode at a loading of 3.0 mg/cm^2. Fuel cell operating conditions: 80 °C, 100% relative humidity, 200 kPa_{abs}, and 0.125/0.5 SLPM H_2/air feed gas flow rate. All MEAs have a Nafion 211 membrane and a Pt/C catalyst powder anode at a loading of 0.1 mg_{Pt}/cm^2.

3.3.3 Effect of Nafion/PVDF Binder Ratio on Fuel Cell Performance of Fiber Cathode MEAs

This section presents and discusses the differences in performance of Nafion/PVDF fiber mat cathode MEAs at different cathode binder weight ratios (Nafion:PVDF weight ratio binders of 50:50, 67:33, 75:25, 80:20, and 83:17). For these MEAs, the cathode catalyst loading was fixed at 3.0 mg/cm^2, and the total binder content was constant relative to the amount of catalyst at 50 wt%. Well-formed fibers could not be electrospun with a binder containing less than 17 wt% PVDF, so the highest Nafion:PVDF weight ratio binder in this study was 83:17 (w:w). Also, binders with more than 50 wt% PVDF

were not examined because the proton conductivity of the binder would be too low, as was seen previously by Slack.[16] It should be noted that the lowest PVDF content of fiber mat cathodes with PMF catalyst was 20 wt% (see Chapter II). The difference in minimum PVDF content of inks for electrospinning PMF versus MOF catalysts was attributed to the smaller MOF catalyst size and the ability of the MOF catalyst to disperse more easily and completely in a Nafion/PVDF ink.

The H_2/air fuel cell V-i polarization curves for fiber cathode MEAs with Nafion/PVDF binder are shown in Figure 3.4a, and Figure 3.4b, along with a polarization curve for a powder cathode MEA with MOF catalyst and a neat Nafion binder (the same MEA as shown in Figure 3.2). As discussed in Chapter II, a fiber cathode MEA at a given Nafion/PVDF binder outperformed the corresponding powder cathode MEA over the entire fuel cell operating potential range. The power output improvement of the fiber cathode MEA was associated with the fiber mat morphology where there is lower gas transport resistance (a consequence of the high inter- and intra- fiber porosity of the fiber cathode with better mixing of catalyst and Nafion binder) and less agglomeration of catalyst particles, as was the case for PMF catalyst in Chapter II and Pt-based catalyst cathodes in reference [26].

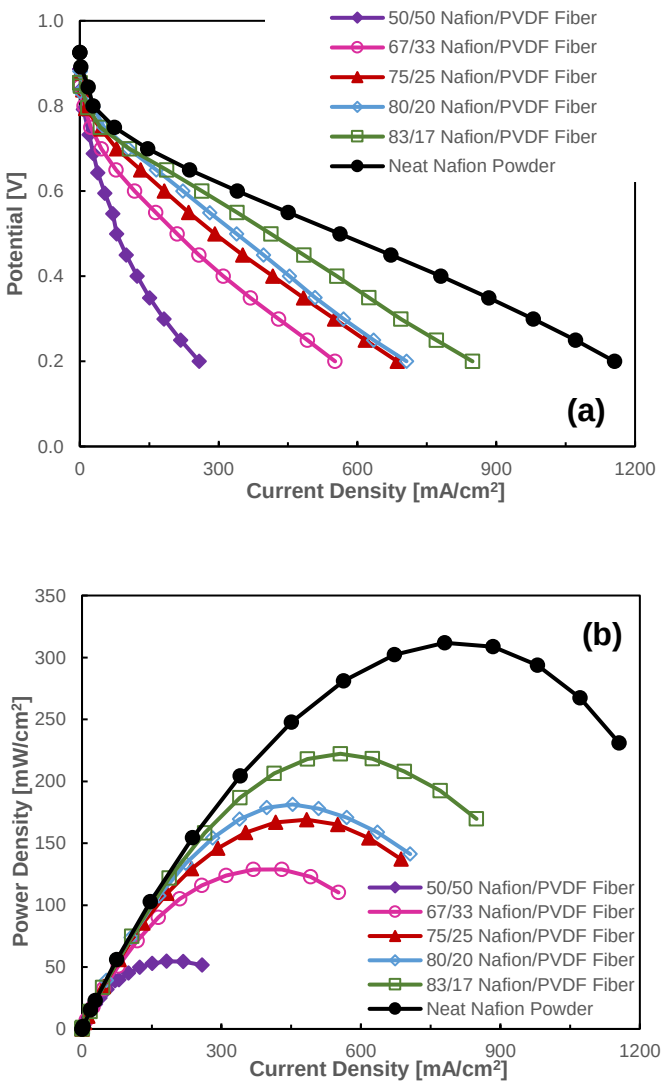

Figure 3.4. H_2/air fuel cell (a) polarization curves and (b) power density versus current density of MOF-catalyst fiber mat cathode MEA at cathode Nafion:PVDF binder weight ratio of 50:50, 67:33, 75:25, 80:20, and 83:17, and a powder cathode MEA with a neat Nafion binder. For all the cathodes, total binder content was constant relative to the amount of catalyst at 50 wt% and PGM-free catalyst cathode at a loading of 3.0 mg/cm^2. Fuel cell operating conditions: 80 °C, 100% relative humidity, 200 kPa_{abs}, and 0.125/0.5 SLPM H_2/air feed gas flow rate. All MEAs have a Nafion 211 membrane and a Pt/C catalyst powder anode at a loading of 0.1 mg_{Pt}/cm^2.

The effect of Nafion/PVDF weight ratio on MEA durability was determined in experiments where the MEA was held at a constant potential of 0.5 V. The results of

these experiments are shown in Figure 3.5. As can be seen, the MOF fiber cathode MEA behavior over time was much different from that of an MEA with a powder cathode. Taking the 83:17 Nafion:PVDF fiber cathode MEA as an example, there was a rise in power density for ca. one hour to a maximum of 206 mW/cm^2, followed by a rapid drop in power density for the next 15 hours to a low of 102 mW/cm^2, and then a slow rise in MEA power output with eventual power stabilization at 112 mW/cm^2 after ca. 50 hours. The complex transient behavior of the MOF cathode MEA before power stabilization was attributed to the activation and deactivation of different catalyst sites on MOF particles. In PGM-free catalysts, sites for the oxygen reduction reaction are Fe atoms coordinated with N atoms embedded into a carbon matrix,[27,28] with two proposed configurations: FeN_4C_{12} (S1 sites) and FeN_4C_{10} (S2 sites) [29]. Although both are active for the electrochemical reduction of oxygen, the S1 sites are more active but less stable than S2 sites [30–33]. The better stability of S2 sites (resistance to demetallation during the oxygen reduction reaction) is associated with stronger Fe-N bonds whose average bond distance is 1.9 Å versus 2.0 Å for S1 sites.[30,31] During a durability test, there is an initial activation phase for S1 sites, as evidenced by the significant but short-lived (one-hour) power rise. This activation was associated with water accumulation near the catalyst surface which improved the kinetics of the oxygen reduction reaction[20,21] and increased the proton conductivity of the cathode binder. After one hour, the S1 sites deactivated with a precipitous drop in power density for ca. 15 hours. Meanwhile, and in parallel with this occurrence, water was still being generated near the less active S2 sites, which required a longer time to be hydrated and activated. Eventually, after most (perhaps all) of the S1

sites were deactivated, the S2 sites became active and eventually dominated MEA performance with long-term stable power generation.

The dramatic up-and-down power swings during the first ca. 20 hours in Figure 3.5 were less severe as the PVDF content of the binder increased, with almost no short-time power density changes with a 50:50 Nafion:PVDF binder. These results suggest that: (i) as the PVDF content of the binder increases, more active sites (both S1 and S2 sites) are blocked, and (ii) PVDF preferentially blocks highly active but unstable S1 sites, which are primarily responsible for the short-time up and down power density swings.

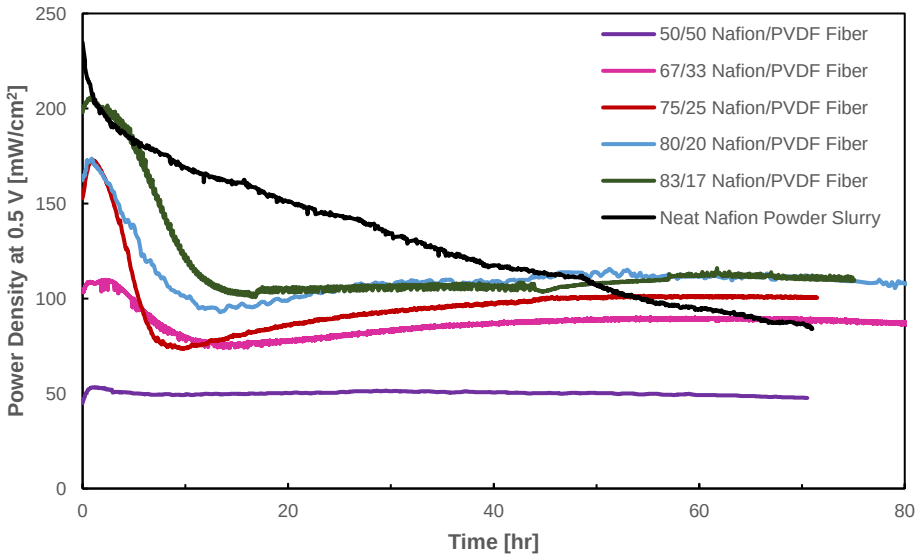

Figure 3.5. H_2/air fuel cell power density at 0.5 V vs. time of MOF-catalyst fiber mat cathode MEA at cathode Nafion:PVDF binder weight ratio of 50:50, 67:33, 75:25, 80:20, and 83:17, and a conventional powder cathode MEA with a neat Nafion binder. For all the cathodes, total binder content was constant relative to the amount of catalyst at 50 wt% and PGM-free catalyst cathode at a loading of 3.0 mg/cm^2. Fuel cell operating conditions: 80 °C, 100% relative humidity, 200 kPa_{abs}, and 0.125/0.5 SLPM H_2/air feed gas flow rate. All MEAs have a Nafion 211 membrane and a Pt/C catalyst powder anode at a loading of 0.1 mg_{Pt}/cm^2.

3.3.4 The Durability of Nafion/PVDF Fiber Cathode MEA under Potentiostatic Operation at Different Voltages

The long-term performances of MOF fiber cathode MEAs with a cathode binder of 83:17 (w:w) Nafion:PVDF and loading of 3.0 mg/cm^2 were examined when the MEA voltage was held constant at 0.3 V, 0.5 V, and 0.7 V (see Figure 3.6). The shape of the power density versus time plots (Figure 3.6a) differs for the three voltage hold experiments. At 0.3 V, there was an initial drop in power density for ca. 5 hours from 203 mW/cm^2 to 111 mW/cm^2, followed by a slow rise for ca. 50 hours, with a final power density stabilization at 158 mW/cm^2. The shape of the power density plot at 0.5 V was already explained when discussing the results in Figure 3.5. The power density at 0.7 V decreased continuously before stabilizing at ca. 40 hours, with an initial and final power density of 75 mW/cm^2 and 30 mW/cm^2, respectively. At a cell voltage of 0.3 V (where proton conduction and oxygen transport control the rate of oxygen reduction reaction), the rapid drop in power density for the first 5 hours is associated with the loss of S1 catalyst sites. The power loss at 0.3 V is faster than that at 0.5 V because more water and peroxide are generated at the lower voltage (the current is higher at 0.3 V than at 0.5 V, as shown in Figure 3.6b). The total current drives two reactions at the cathode,

$$4H^+ + 4e^- + O_2 \rightarrow H_2O \qquad (2)$$

$$2H^+ + 2e^- + O_2 \rightarrow H_2O_2 \qquad (3)$$

At time=0, the current generated at 0.3 V is 71% greater than that at 0.5 V, as shown in Figure 3.6b. Consequently, more water and peroxide are generated at 0.3 V. Thus, with more H_2O_2 present, there are more oxidative attacks on the carbon substrate of MOF catalyst particles, resulting in a fast power density decline. Also, more time was

required to flush peroxide out of the cathode (by electrogenerated water), resulting in a slower rise and a delayed stabilization in power density. The continuous power loss declines at 0.7 V (where the oxygen reduction reaction rate is kinetically controlled) due to the loss of active sites (mainly S1 sites). Since less water is generated at 0.7 V, most of the S2 sites were not activated, and consequently, the slow power rise and stabilization in power observed at 0.3 V and 0.5 V was not observed at 0.7 V.

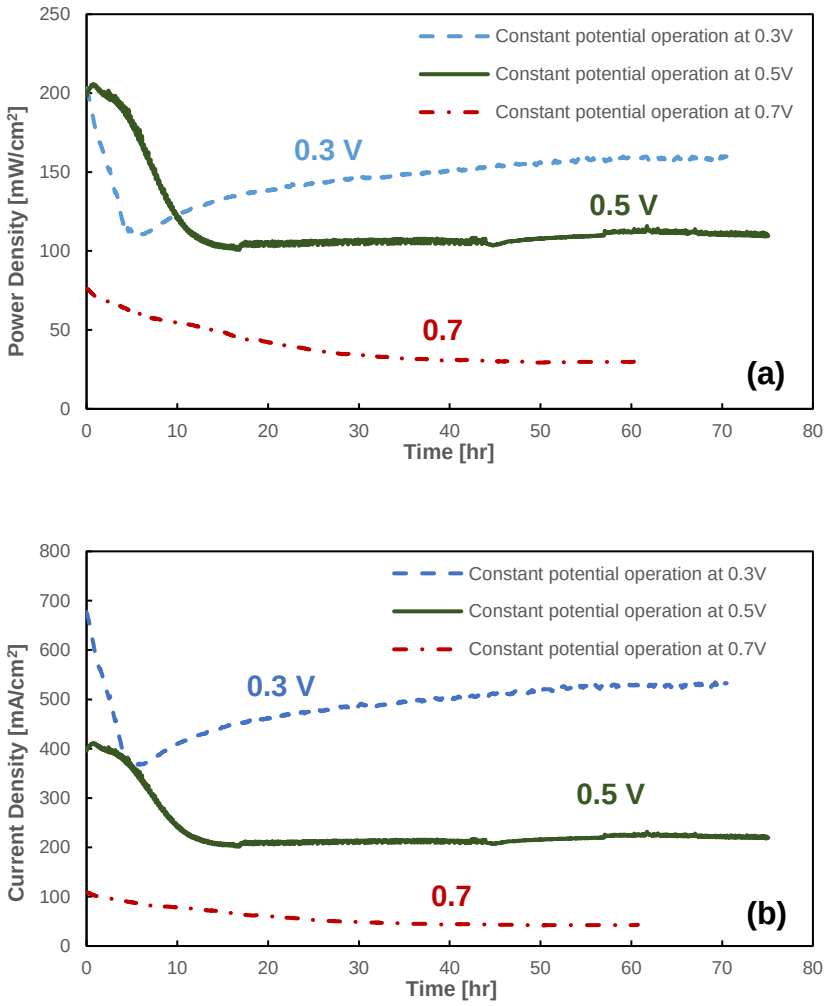

Figure 3.6. H_2/air fuel cell (a) power density versus time and (b) current density versus time of MOF catalyst fiber cathode MEAs at voltages of 0.3 V, 0.5 V, and 0.7 V. The fiber cathode biner was 83:17 (w:w) Nafion:PVDF, total binder content was relative to the amount of catalyst at 50 wt%, and the fiber cathode loading was 3.0 mg/cm^2. Fuel cell operating conditions: 80 °C, 100% relative humidity, 200 kPa_{abs}, and 0.125/0.5 SLPM H_2/air feed gas flow rate. All MEAs have a Nafion 211 membrane and a Pt/C catalyst powder anode at a loading of 0.1 mg_{Pt}/cm^2. The 0.5 V plot is from Figure 3.5.

3.3.5 Summary of All Nafion/PVDF Binders

Table 3.3 summarizes the stability of MEAs fabricated in Chapter II and Chapter III. It can be seen that: (i) long-term power density was stabilized when PVDF was added

to Nafion in the cathode binder, regardless of catalyst type (PMF or MOF catalyst), or cathode morphology (powder cathode or fiber mat cathode); (ii) at the same Nafion/PVDF weight ratio, a fiber cathode MEA generated more power than the powder cathode for both PMF and MOF cathode catalyst; (iii) at the same Nafion/PVDF weight ratio and the same cathode catalyst loading, the MEA with a MOF catalyst cathode generated more power than a PMF catalyst cathode, which was attributed to a higher density of ORR active sites on MOF catalyst particles[34]; (iv) at the same Nafion:PVDF weight ratio of 80:20, stable power generation was achieved in a MOF fiber cathode, whereas a PMF fiber cathode underwent long-term degradation, which may be due to the fact that the active sites in PMF catalysts are less stable than the S2 active sites on MOF particles[34] and thus require more PVDF (hydrophobicity) to achieve long-term stabilized power output.

For a fiber cathode composed of 50:50 Nafion/PVDF binder and MOF catalyst, the stabilized power density at 0.5 V was 47 mW/cm^2, while a power density of 85 mW/cm^2 was reported by Slack (also with MOF catalyst from Pajarito Powder)[16]. The different stable power levels are attributed to a difference in cathode catalyst/binder composition, 50:50 (w:w) catalyst:binder in the present study versus 70:30 (w:w) catalyst:binder in Slack's work. In the present study, the MOF catalyst could not be electrospun into fibers when the electrospinning solution contained 70 wt% catalysts and 30 wt% Nafion/PVDF binder (only electrospray droplets were produced). The obvious conclusion here is that the MOF catalyst used in the present study was different from that used by Slack (Pajarito Powder did not provide any data/information which could be used to differentiate the two catalysts).

Future work on PGM-free fiber mat cathodes should focus on the Nafion/PVDF binder weight ratio, the catalyst/binder weight ratio, the ion exchange capacity of the PFSA ionomer in the cathode binder, and the molecular weight of PVDF in the cathode binder. Methods/conditions for electrospinning fibers with less Nafion/PVDF binder should be identified. Core-shell fibers should be examined where the shell has a higher Nafion/PVDF ratio (for good proton conduction), and the core is more hydrophobic (to expel electro-generated peroxide quickly).

Table 3.3. (Stable) Power Density (0.5 V) after 50 hours of a 0.5 V constant voltage operation for PMF or MOF Catalyst Cathode MEAs (Chapter II and Chapter III).

Catalyst	Cathode	Binder	stable power density (0.5 V) after 50 hours of a 0.5 V constant voltage hold [mW/cm^2]
PMF Catalyst	Powder Cathode	Nafion	93 (power density is degrading at the rate of 1.0 mW/cm^2/hr)
		50:50 Nafion:PVDF	
	Fiber Cathode	Nafion (PEO extracted)	117 (power density is degrading at the rate of 0.7 mW/cm^2/hr)
		50:50 Nafion:PVDF	41
		67:33 Nafion:PVDF	65
		75:25 Nafion:PVDF	88
		80:20 Nafion:PVDF	96 (power density is degrading at the rate of 0.2 mW/cm^2/hr)
MOF Catalyst	Powder Cathode	Nafion	107 (power density is degrading at the rate of 1.2 mW/cm^2/hr)
		50:50 Nafion:PVDF	38
		75:25 Nafion:PVDF	55
		80:20 Nafion:PVDF	69
		83:17 Nafion:PVDF	71
	Fiber Cathode	50:50 Nafion:PVDF	47
		67:33 Nafion:PVDF	85
		75:25 Nafion:PVDF	100
		80:20 Nafion:PVDF	112
		83:17 Nafion:PVDF	112

3.4 Conclusions

This chapter presented and discussed the performance of powder and fiber cathode MEAs with a MOF-based PGM-free ORR catalyst synthesized and provided by Pajarito Powder, LLC. This catalyst is an alternative to supported precious metal catalysts. A conventional powder cathode MEA with a neat Nafion binder was prepared and evaluated in an H_2/air fuel cell. This MEA initially outperformed all cathodes with Nafion/PVDF binder, but it encountered severe degradation during a constant voltage hold durability test. In contrast, the cathode with a Nafion/PVDF binder achieved stable power output in both a powder and a fiber mat cathode MEA, where the addition of PVDF in the cathode binder increased the cathode's hydrophobicity. As was observed in Chapter II, PVDF addition also dramatically decreased the initial fuel cell power output since the addition of PVDF decreased the water concentration near the catalyst surface, and it lowered both the proton conductivity in the catalyst layer and the O_2 permeability of the binder. Transient plots of power density vs. time at 0.5 V for MOF catalyst cathode MEAs in this chapter differed from what was observed in Chapter II of PMF catalysts. We assumed MOF catalysts having two types of active sites, S1 and S2 sites (where S1 is more active than S2 and S2 is more stable than S1) a dramatic up-and-down swing in power density was observed due to the deactivation of S1 sites, and the slower activation and stabilization of S2 sites.

Additionally, a difference in power density vs. time was observed in constant voltage hold experiments (with an 83:17 (w:w) Nafion:PVDF MOF catalyst fiber mat cathode MEA) where the voltage was fixed at either 0.3 V, 0.5 V, or 0.7 V. At 0.3 V (high current

density operation), more water and H_2O_2 were generated, which resulted in the loss of S1 sites and the activation of S2 sites were faster than at 0.5 V. However, at 0.7 V (low current density operation), less water was produced, there was minimal activation of S2 sites, and thus there was no short-term rise in the power density. When evaluating the stability of MEA from Chapters II and III, the following conclusions were made: (1) the presence of PVDF in the cathode binder is key to stabilizing power output, (2) power output in a fiber cathode MEA is greater than that in a powder cathode MEA for the same binder composition, and (3) MOF-based PGM-free cathode catalysts are preferred over PMF catalysts since its long-term power output is stable and higher than PMF.

3.5 References

1. Wang, X. *et al.* Size-controlled large-diameter and few-walled carbon nanotube catalysts for oxygen reduction. *Nanoscale* **7**, 20290–20298 (2015).
2. Reshetenko, T. *et al.* The Effect of Proton Conductivity of Fe–N–C–Based Cathode on PEM Fuel cell Performance. *J Electrochem Soc* **167**, 084501 (2020).
3. Shao, Y., Dodelet, J., Wu, G. & Zelenay, P. PGM-Free Cathode Catalysts for PEM Fuel Cells: A Mini-Review on Stability Challenges. *Advanced Materials* **31**, 1807615 (2019).
4. Zhang, H. *et al.* High-performance fuel cell cathodes exclusively containing atomically dispersed iron active sites. *Energy Environ Sci* **12**, 2548–2558 (2019).
5. Martinez, U., Komini Babu, S., Holby, E. F. & Zelenay, P. Durability challenges and perspective in the development of PGM-free electrocatalysts for the oxygen reduction reaction. *Curr Opin Electrochem* **9**, 224–232 (2018).
6. Gopal, R. *et al.* Electrospun nanofibrous filtration membrane. *J Memb Sci* **281**, 581–586 (2006).
7. Padbury, R. & Zhang, X. Lithium-oxygen batteries - Limiting factors that affect performance. *J Power Sources* **196**, 4436–4444 (2011).

8. Ji, L., Lin, Z., Alcoutlabi, M. & Zhang, X. Recent developments in nanostructured anode materials for rechargeable lithium-ion batteries. *Energy Environ Sci* **4**, 2682–2689 (2011).

9. Waldrop, K., Wycisk, R. & Pintauro, P. N. Application of electrospinning for the fabrication of proton-exchange membrane fuel cell electrodes. *Curr Opin Electrochem* **21**, 257–264 (2020).

10. Brodt, M. *et al.* Fabrication, In-Situ Performance, and Durability of Nanofiber Fuel Cell Electrodes. *J Electrochem Soc* **162**, F84–F91 (2015).

11. Park, A. M. & Pintauro, P. N. Alkaline Fuel Cell Membranes from Electrospun Fiber Mats. *Electrochemical and Solid-State Letters* **15**, B27 (2012).

12. Ballengee, J. B. & Pintauro, P. N. Morphological Control of Electrospun Nafion Nanofiber Mats. *J Electrochem Soc* **158**, B568 (2011).

13. Li, J. *et al.* Designing the 3D Architecture of PGM-Free Cathodes for H 2 / Air Proton Exchange Membrane Fuel Cells To cite this version : HAL Id : hal-02352319 Designing the 3D architecture of PGM-free cathodes for H 2 / air proton exchange membrane fuel cells. (2020).

14. Shui, J., Chen, C., Grabstanowicz, L., Zhao, D. & Liu, D.-J. Highly efficient nonprecious metal catalyst prepared with metal–organic framework in a continuous carbon nanofibrous network. *Proceedings of the National Academy of Sciences* **112**, 10629–10634 (2015).

15. Kabir, S. *et al.* Improving the bulk gas transport of Fe-N-C platinum group metal-free nanofiber electrodes via electrospinning for fuel cell applications. *Nano Energy* **73**, 1–3 (2020).

16. Slack, J. *et al.* Electrospun Fiber Mat Cathode with Platinum-Group-Metal-Free Catalyst Powder and Nafion/PVDF Binder. *ChemElectroChem* **5**, 1537–1542 (2018).

17. Wenjing Zhang, P. N. P. High Performance Nanofiber Fuel Cell Electrodes_Supporting Information. *ChemSusChem* **2**, 1025–1027 (2000).

18. Brodt, M. *et al.* Fabrication, In-Situ Performance, and Durability of Nanofiber Fuel Cell Electrodes. *J Electrochem Soc* **162**, F84–F91 (2015).

19. Nawn, G. *et al.* Structural analyses of blended Nafion/PVDF electrospun nanofibers. *Physical Chemistry Chemical Physics* **21**, 10357–10369 (2019).

20. Ramaker, D. E., Korovina, A., Croze, V., Melke, J. & Roth, C. Following ORR intermediates adsorbed on a Pt cathode catalyst during break-in of a PEM fuel cell by in operando X-ray absorption spectroscopy. *Physical Chemistry Chemical Physics* **16**, 13645–13653 (2014).

21. Wang, J. X., Markovic, N. M. & Adzic, R. R. Kinetic Analysis of Oxygen Reduction on Pt(111) in Acid Solutions: Intrinsic Kinetic Parameters and Anion Adsorption Effects. *Journal of Physical Chemistry B* **108**, 4127–4133 (2004).

22. Woo Park, J. *et al.* Electrospun Nafion/PVDF single-fiber blended membranes for regenerative H2/Br2 fuel cells. *J Memb Sci* **541**, 85–92 (2017).

23. Oliveira, F. *et al.* Process influences on the structure, piezoelectric, and gas-barrier properties of PVDF-TrFE copolymer. *J Polym Sci B Polym Phys* **52**, 496–506 (2014).

24. Mohamed, H. F. M. *et al.* Free volume and permeabilities of O2 and H2 in Nafion membranes for polymer electrolyte fuel cells. *Polymer (Guildf)* **49**, 3091–3097 (2008).

25. Herranz, J. *et al.* Unveiling N-Protonation and Anion-Binding Effects on Fe / N / C Catalysts for O 2 Reduction in Proton-Exchange-Membrane Fuel Cells. *Journal of Physical Chemistry C* **115**, 16087–16097 (2011).

26. Slack, J. J. *et al.* Nanofiber Fuel Cell MEAs with a PtCo/C Cathode. *J Electrochem Soc* **166**, F3202–F3209 (2019).

27. Thompson, S. T. *et al.* ElectroCat: DOE's approach to PGM-free catalyst and electrode R&D. *Solid State Ion* **319**, 68–76 (2018).

28. Chung, H. T. *et al.* Direct atomic-level insight into the active sites of a high-performance PGM-free ORR catalyst. *Science (1979)* **357**, 479–484 (2017).

29. Liu, K., Wu, G. & Wang, G. Role of Local Carbon Structure Surrounding FeN4 Sites in Boosting the Catalytic Activity for Oxygen Reduction. *Journal of Physical Chemistry C* **121**, 11319–11324 (2017).

30. Ohyama, J. *et al.* High Durability of a 14-Membered Hexaaza Macrocyclic Fe Complex for an Acidic Oxygen Reduction Reaction Revealed by In Situ XAS Analysis. *JACS Au* **1**, 1798–1804 (2021).

31. Moriya, M. *et al.* Fourteen-membered macrocyclic Fe complexes inspired by Fen4-center-embedded graphene for oxygen reduction catalysis. *Journal of Physical Chemistry C* **124**, 20730–20735 (2020).

32. Li, J. *et al.* Identification of durable and non-durable FeNx sites in Fe–N–C materials for proton exchange membrane fuel cells. *Nat Catal* **4**, 10–19 (2021).

33. Liu, S. *et al.* Atomically dispersed iron sites with a nitrogen–carbon coating as highly active and durable oxygen reduction catalysts for fuel cells. *Nat Energy* **7**, 652–663 (2022).

34. Primbs, M. *et al.* Establishing reactivity descriptors for platinum group metal (PGM)-free Fe-N-C catalysts for PEM fuel cells. *Energy Environ Sci* **13**, 2480–2500 (2020).

CHAPTER IV

FABRICATION, MORPHOLOGY, AND PERFORMANCE OF PGM-FREE CATALYSTS CATHODE MEAS

4.1 Introduction

In this chapter, a new generation of PGM-free catalysts that differs from that described in Chapter II was utilized. Both are synthesized through a hard-templating-pore-former approach by Pajarito Powder. The catalyst from Chapter II will hereafter be labeled Gen-1 PMF, and the new catalyst in this chapter is Gen-2 PMF. Two generations of PMF catalysts were utilized to fabricate Nafion powder cathode, Nafion fiber cathode, and 75:25 (w:w) Nafion:PVDF fiber cathode. The PGM-free catalyst cathodes were incorporated into MEAs with Nafion 211 and a Pt/C powder anode (0.1 mg_{Pt}/cm^2) and evaluated in H_2/air fuel cell at 80 °C, 200 kPa_{abs} and 100% relative humidity (RH). Experiments focus on determining the effect of catalysts on cathode morphology, power output, and MEA durability.

4.2 Experimental

4.2.1 Catalyst Synthesis of PMF Catalysts

Two generations of PMF catalysts were synthesized in this chapter, and according to the data provided by Pajarito Powder[1], the difference between Gen-1 and Gen-2 PMF

catalysts are: (1) there was a 50% agglomerate reduction in Gen-2 PMF catalysts as measured by Dynamic Light Scattering (DLS); (2) during the Gen-2 PMF catalyst manufacturing, there was an extra procedure, where acid washing is followed by a mild thermal treatment to improve dispersion in inks.

4.2.2 Membrane-Electrode-Assembly (MEA) Preparation, Fuel Cell Tests, and Scanning Electron Microscope

The ink composition, ink preparation procedure, and MEA fabrication of the Nafion powder cathode were the same as illustrated in Chapter II.

The electrospinning solution of Nafion/PEO fiber mats or Nafion/PVDF fiber mats in this chapter was prepared following the same solution composition and procedure as illustrated in Chapter II. The electrospinning conditions (potential, relative humidity, flow rate, and needle tips to collector distances as listed in Table 2.1) are different for Nafion/PVDF fiber and Nafion/PEO fibers, as illustrated in Chapter II. The catalyst difference (Gen-1 or Gen-2 PMF catalysts) did not affect the electrospinning condition.

The Membrane-electro-assembly (MEA) fabrication of Nafion fiber cathode and Nafion/PVDF cathode has been described in detail in Chapter II.

Fuel cell data and scanning microscope images were collected following the same procedure as in Chapter II.

4.3 Results and Discussions

4.3.1 PMF Catalyst Cathode Morphology

Top-down SEM images of conventional powder cathodes with a neat Nafion binder and Gen-1 or Gen-2 PMF catalysts are shown in Figures 4.1a and 4.1b, respectively. Large catalyst powder aggregates were observed even after thoroughly mixing the catalyst/Nafion ink. The maximum particle/aggregate size for the Gen-1 PMF catalyst was ~4 μm, whereas that for the Gen-2 PMF powder was ~2.5 μm.

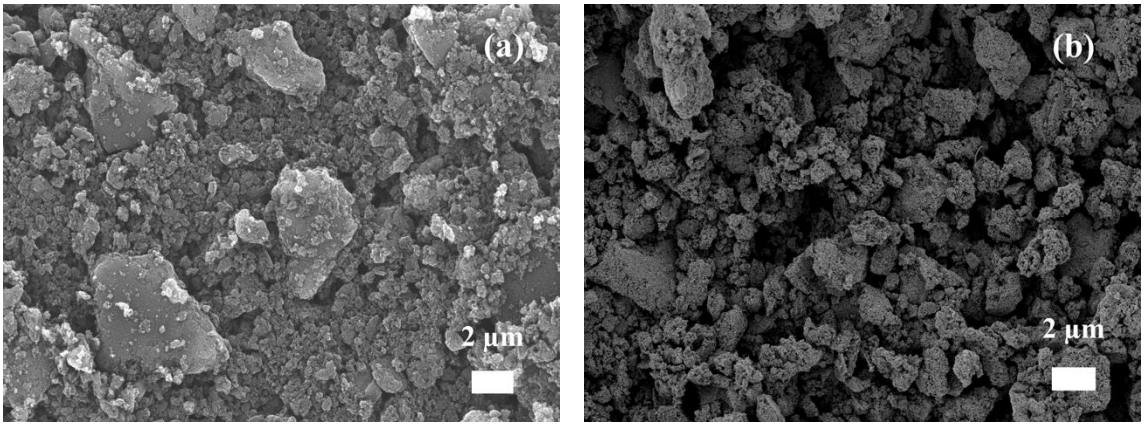

Figure 4.1. Top-down SEM images of powder cathode with a neat Nafion binder utilizing (a) Gen-1 PMF catalysts and (b) Gen-2 PMF catalysts.

SEM images of electrospun fiber mats with Gen-1 or Gen-2 PMF catalysts are shown in Figures 4.2a and 4.2b. With the Gen-2 PMF catalyst, bead-on-fiber defects were eliminated. With a more uniform catalyst distribution along a fiber length. The

better fiber morphology was associated with the smaller particle size for the Gen-2 PMF catalyst.

A Nafion/PEO fiber mat cathode (made by hot pressing fiber mats onto a Nafion membrane) after PEO extraction is shown in Figure 4.2c (for the Gen-1 PMF catalyst) and Figure 4.2d (for the Gen-2 PMF catalyst). PEO was removed from the fiber electrode half-CCM by soaking it in hot water (80 °C) for two hours. Waldrop et al.[2] previously confirmed that this hot water-soaking step would remove PEO from a Pt/C catalyst + Nafion/PEO fiber mat. Henceforth, such fiber mats are denoted as a Nafion fiber cathode since there is no PEO when the electrodes are evaluated in a fuel cell.

The hot-pressing compacted both the Gen-1 and Gen-2 PMF fiber cathodes, with a decrease in inter-fiber porosity. With the Gen-1 PMF catalyst, there was some loss in fiber integrity/quality after PEO extraction, whereas the Gen-2 PMF fibers were essentially unchanged after the water-soaking step.

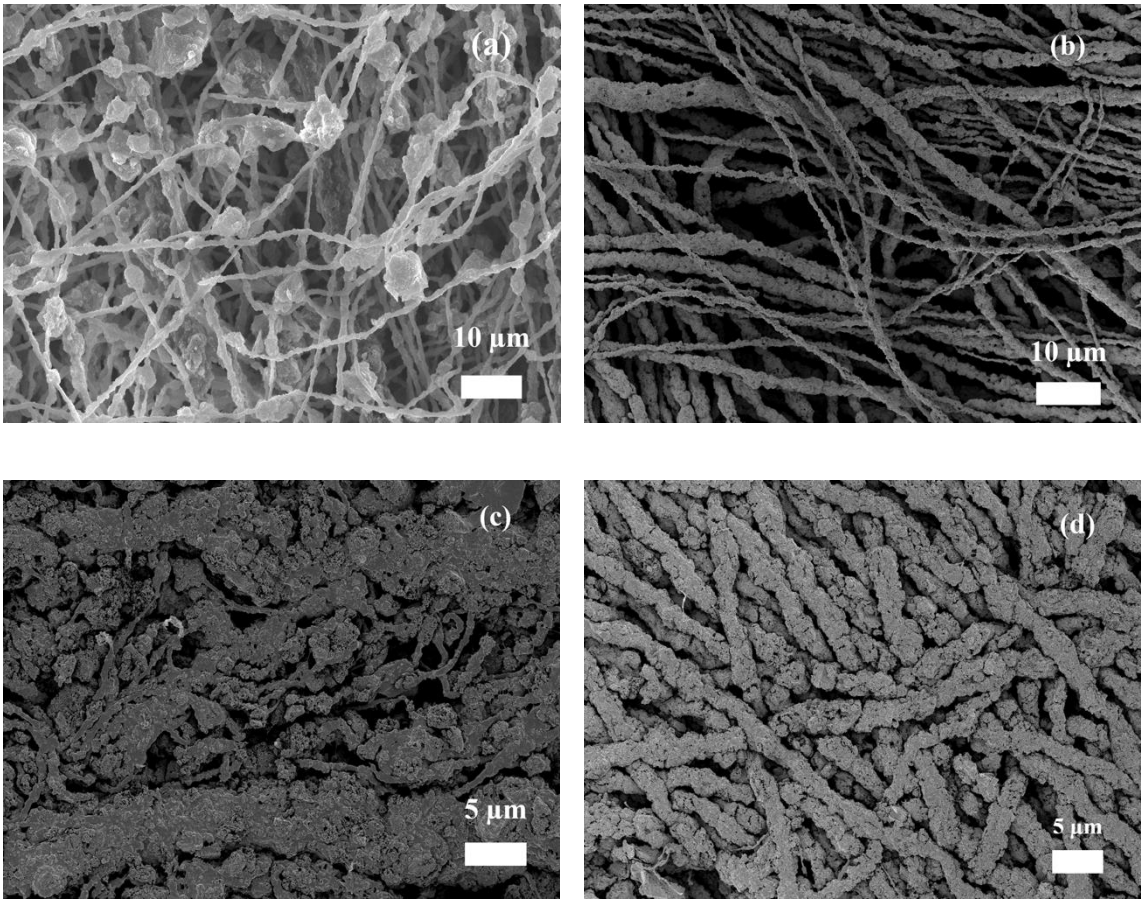

Figure 4.2. Top-down SEM images of fiber mats with Nafion/PEO binder (before PEO extraction) using (a) Gen-1 PMF catalysts, (b) Gen-2 PMF catalysts, and fiber mat cathode after hot-pressing (at the compaction pressure of 35 MPa) and water-soaking procedure (PEO extraction) of (c) Gen-1 PMF catalysts and (d) Gen-2 PMF catalysts.

SEM images of electrospun fiber mats with Gen-1 or Gen-2 PMF catalysts and 75:25 (w:w) Nafion:PVDF binder are shown in Figures 4.3a and 4.3b. With the Gen-2 PMF catalyst, there were fewer bead-on-fiber defects with a more uniform catalyst distribution along a fiber length. The better fiber morphology was also associated with the smaller particle size for the Gen-2 PMF catalyst.

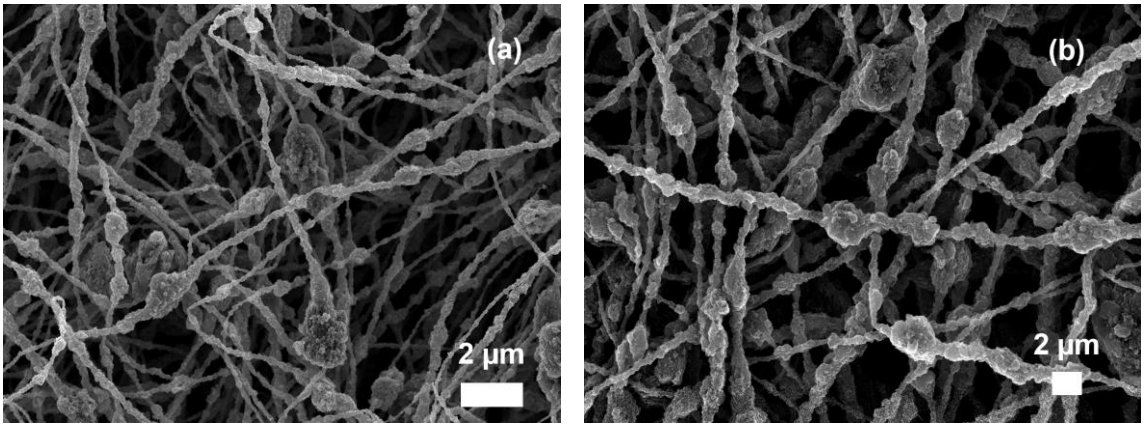

Figure 4.3. Top-down SEM images of fiber mats with a 75:25 (w:w) Nafion:PVDF binder using (a) Gen-1 PMF catalysts, (b) Gen-2 PMF catalysts.

4.3.2 Fuel Cell Performance of Gen-1 and Gen-2 PMF Catalyst Cathode MEAs

The fuel cell polarization curves of Gen-1 and Gen-2 PMF cathode MEAs in Nafion powder cathodes, Nafion fiber cathodes and 75:25 (w:w) Nafion:PVDF fiber cathodes are shown in Figure 4.4. Polarization data were collected at 100% RH, 80 °C, and 200 kPa_{abs}. The polarization data of Gen-1 cathode MEAs were from Chapter II. As can be seen in Figure 4.4, all MEAs with the Gen-2 PMF catalyst generated more power than MEAs with Gen-1 PMF catalysts. The superiority of the Gen-2 PMF catalyst powder cathode was attributed to the increased catalyst activity (Gen-2 is more active than Gen-1).

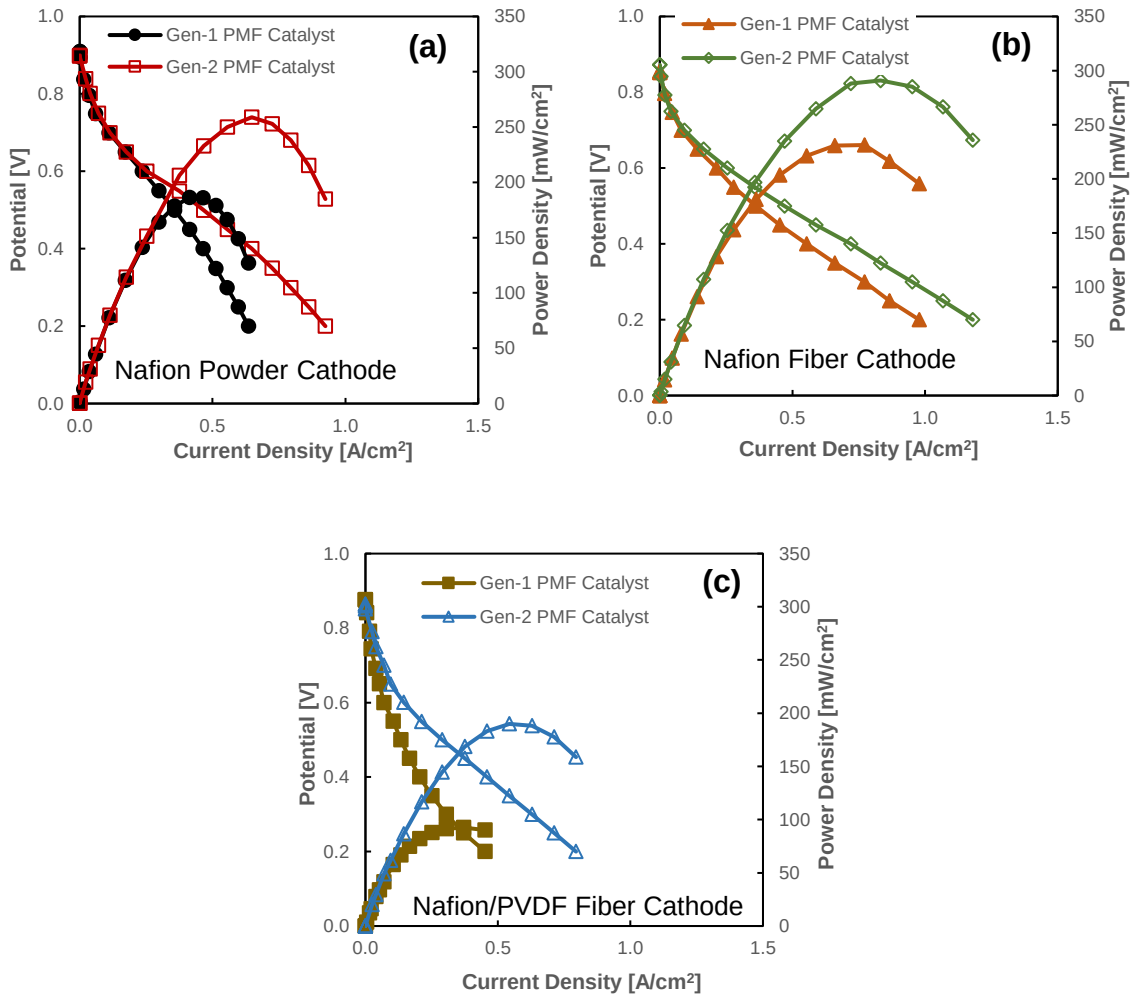

Figure 4.4. H_2/air fuel cell polarization curves for MEAs employed (a) Nafion powder cathode, (b) Nafion fiber (PEO extracted) cathode, and (c) 75:25 (w:w) Nafion:PVDF fiber cathode using Gen-1 (solid symbol) and Gen-2 (open symbol) PMF catalysts. In all the cathodes, the catalyst loading is 3.0 mg/cm^2. Fuel cell operating conditions: 80 °C, 100% relative humidity, 200 kPa_{abs}, and H_2/air 0.125/0.5 SLPM (standard liter per minute) feed gas flow rate. All MEAs have a Nafion 211 membrane and a Pt/C catalyst powder anode at a loading of 0.1 mg_{Pt}/cm^2.

4.3.3 Durability of Gen-1 and Gen-2 PMF Catalyst Cathode MEAs

The durability of MEAs in Figure 4.4 was shown in Figure 4.5 was evaluated by a potentiostatic hold experiment at 0.5 V with H_2/air gas feeds. Figure 4.5 shows the plot of power density vs. time at 0.5 V for a 50-hours test, where the data of Gen-1 cathode MEAs were from Chapter II.

Same as observed in Chapter II, the transient behavior for Nafion powder (Figure 4.5a) or Nafion fiber (Figure 4.5b) cathode MEA with Gen-1 or Gen-2 catalysts were comparable. The power drop was fast during the first 10 hours of the test, and then the degradation slowed with a near-line power loss versus time. The only difference was MEA with Gen-2 PMF catalyst cathodes generated 30% more power than Gen-1 catalyst cathode MEAs at 0.5 V. The parallel power density vs. time plots suggested that there were no durability differences between Gen-1 and Gen-2 PMF catalysts.

For the 75:25 (w:w) Nafion:PVDF fiber cathode MEA with Gen-1 catalysts, the power density at 0.5V increased after start-up and then stabilized at 88 mW/cm^2 after approximately 15 hours of operation. However, for the 75:25 (w:w) Nafion:PVDF fiber cathode MEA with Gen-2 catalysts, the power did not stabilize after the initial rise but instead reached a maximum power density of 150 mW/cm^2, and then slowly decreased for the remainder of the test at a decay rate of 0.37 mW/cm^2/hr. The slow decline was due to insufficient PVDF (hydrophobicity) in the cathode binder to stop catalyst degradation. The power loss in Gen-2 PMF catalysts with Nafion/PVDF binder is because more water and peroxide are generated (the current is higher in Gen-2 MEA than in Gen-1 MEA). Since more water and peroxide are generated, 25% PVDF in the cathode binder is not

enough to expel all water and peroxide out of the cell. Thus, there was a greater oxidative attack on Gen-2 catalysts, resulting in a power density decline.

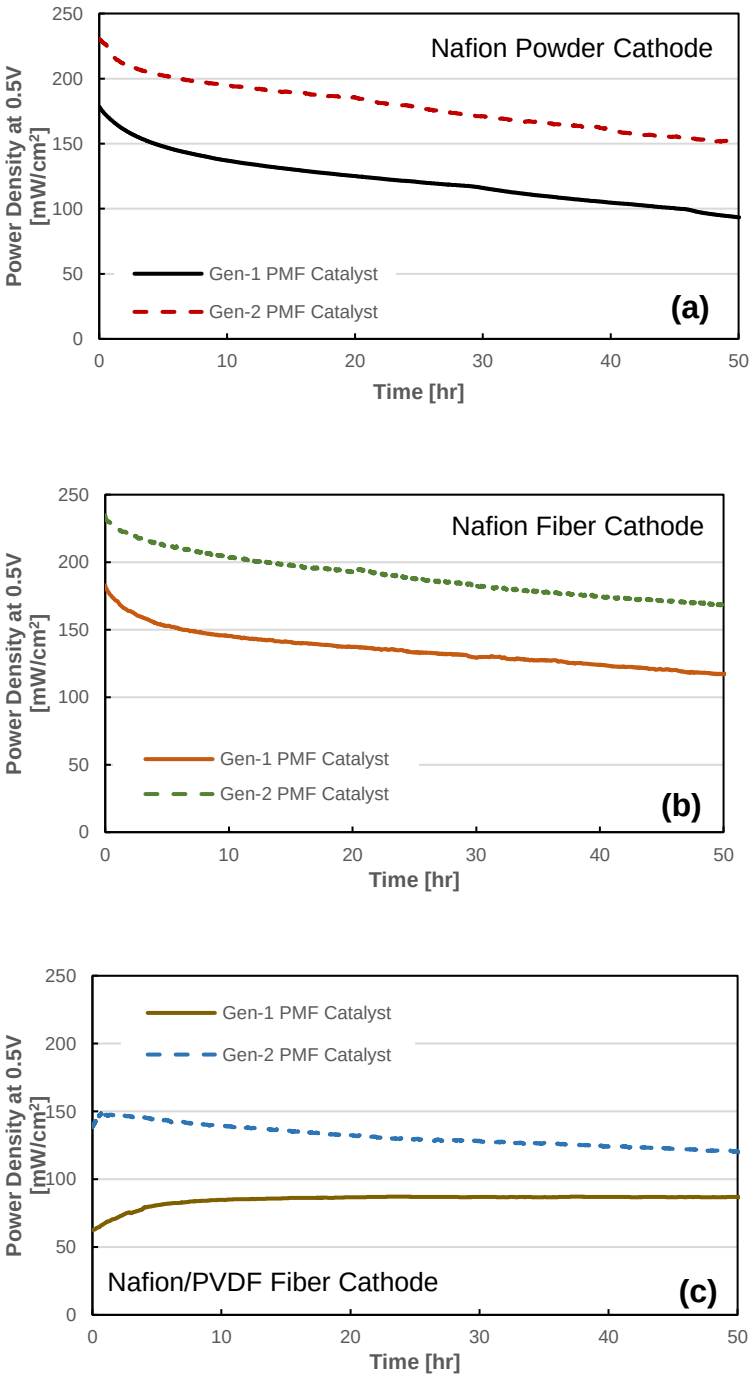

Figure 4.5. H_2/air power density at 0.5 V vs. time for MEAs employed (a) Nafion powder cathode, (b) Nafion fiber (PEO extracted) cathode, and (c) 75:25 (w:w) Nafion:PVDF fiber cathode using Gen-1 (solid line) and Gen-2 (dash line) PMF catalysts. In all the cathodes, the catalyst loading is 3.0 mg/cm^2. Fuel cell operating conditions: 80 °C, 100% relative humidity, 200 kPa_{abs}, and H_2/air 0.125/0.5 SLPM (standard liter per minute) feed gas flow rate. All MEAs have a Nafion 211 membrane and a Pt/C catalyst powder anode at a loading of 0.1 mg_{Pt}/cm^2.

4.4 Conclusion

A new generation PMF catalyst (Gen-2 PMF catalysts) from Pajarito Powder was fabricated and evaluated in this chapter. Nafion powder cathodes with the Gen-2 PMF catalysts showed a smaller particle/agglomeration size. Nafion/PEO or Nafion/PVDF fibers with the Gen-2 PMF material had a better morphology (a more uniform fiber diameter, with fewer agglomerates and bead-on-fiber defects), as compared to the Gen-1 PMF fibers described/discussed in Chapter II of this dissertation.

Fiber mat and powder cathode MEAs with this Gen-2 catalyst were prepared and tested in H_2/air fuel cells. The Gen-2 PMF catalysts MEAs with Nafion powder, Nafion fiber, or Nafion/PVDF fiber cathodes generated more power at the entire operating potential. The Nafion power and Nafion fiber cathode MEA with Gen-1 or Gen-2 PMF catalysts showed a similar degradation trend under 50-hour constant voltage operation at 0.5V, while Gen-2 MEAs generated approximately 30% more power. The 75:25 (w:w) Nafion:PVDF fiber cathode MEA with Gen-1 PMF catalysts generated stable power output of 88 mW/cm^2 at 0.5V for 50 hours, while the Nafion/PVDF fiber cathode MEA with Gen-2 PMF catalysts generated more power (highest power density at 0.5V of 150 mW/cm^2) but degraded at a rate of 0.37 mW/cm^2/hr due to insufficient PVDF (hydrophobicity).

4.5 Reference

1. Serov, A. *et al.* Varipore^{TM}: A Powerful Manufacturing Platform for Fuel Cell and Electrolyzer Applications. *ECS Meeting Abstracts* **MA2019-02**, 1734–1734 (2019).
2. Waldrop, K. *et al.* Electrospun Nanofiber Electrodes for High and Low Humidity PEMFC Operation. *J Electrochem Soc* **170**, 024507 (2023).

CHAPTER V

HYBRID CATHODE MEAS WITH PGM-FREE CATALYST FOR IMPROVED FUEL CELL PERFORMANCE AND MEA DURABILITY

5.1 Introduction

In this chapter, a new type of hybrid fiber/particle cathode with Gen-2 PMF catalyst is described. Membrane-electrode-assemblies (MEAs) were evaluated in terms of initial power output (power density at beginning-of-life (BOL)) and the power generated after a 30 K voltage cycling accelerated stress test (square-wave cycles between 0.6 V and 0.95 V, 3 seconds each step). Three types of hybrid cathodes (containing both catalyst particles and fiber) were designed, fabricated, and evaluated: (1) hybrid type I cathode in which catalyst particles are interspersed between catalyst/binder fibers; (2) hybrid type II cathode in which catalyst particles and Nafion are interspersed between catalyst/binder fibers; and (3) hybrid type III cathode in which catalyst particles, Nafion, and Fluorinated Ethylene Propylene (FEP) are interspersed with electrospun catalyst/binder fibers. For all hybrid cathodes, redispersed fibers were used in which the binder for PMF catalyst particles was Nafion (i.e., fibers were electrospun with a mixture of Nafion and polyethylene oxide (PEO), in which the PEO was removed after fiber electrospinning). The hybrid cathode MEAs were compared to (1) an MEA with a conventional powder cathode with Nafion binder; (2) an MEA where the cathode was composed of only redispersed fibers; (3) a fiber mat cathode MEA with neat Nafion binder, where the fibers mat is used directly in a MEA; (4) the best fiber mat cathode MEA with a cathode

composed of Nafion/PVDF binder and Gen-1 PMF catalyst; and (5) the best fiber mat cathode MEA with Nafion/PVDF binder and a MOF-based PGM-free catalyst.

5.2 Experiment

5.2.1 Electrospinning PGM-free Catalyst Fiber Mat with Nafion and PEO Binder and Nafion Powder Cathode Preparation

The Nafion fiber cathodes and Nafion powder cathodes were prepared with the Gen-2 PMF catalyst (described in Chapter IV), using the same general procedures as described in Chapter II. The fiber cathodes were prepared by electrospinning an ink composed of PMF catalyst powder, Nafion perfluorosulfonic acid, and polyethylene oxide (PEO) as the electrospinning carrier polymer (PEO was leached out of the fiber mats after electrospinning by a hot water soaking step). The only difference between electrospinning inks and inks for powder cathodes in this study was the ink mixing procedure. In Chapter II, 60 minutes of ultrasonication (VibraCell Ultrasonicator, Sonic & Materials Inc.) was followed by 30 minutes of bath sonication (FS20D Ultrasonic Cleaner, Fisher Scientific Inc.). For the inks used in this chapter, 90 minutes of bath sonication were employed. In addition, in this chapter, powder cathodes were prepared by coating gas diffusion layers (Sigracet 22 BB) with ink using a manually drawn Meyer rod. The rod coating was repeated multiple times (with intermittent drying for 10 minutes) until the cathode catalyst loading achieved 3.0 mg/cm^2.

5.2.2 Redispersed Fiber Cathode and Hybrid Cathode Preparation

In this chapter, MEAs were prepared with cathodes composed of fibers that were deposited on gas diffusion layers. In contrast to all the fiber cathodes discussed previously in Chapters II–IV, pre-formed electrospun fibers were first dispersed in a solvent, and the resulting ink was coated on a gas diffusion layer to produce a cathode (rather than directly attaching fiber mats to gas diffusion layers or a Nafion membrane). A type of FEP Teflon dispersion (Chemours (formerly DuPont) Teflon^{TM} FEPD 121 dispersion (55 wt%)) was added into some cathode inks to provide some hydrophobicity to the cathode and to assist in fiber dispersing. Seven types of inks with pre-formed fibers were prepared as listed in Table 5.1: (1) fibers dispersed in an alcohol and water solvent (ink #1); (2) fibers dispersed in an alcohol and water solvent with added FEP Teflon dispersion (ink #2); (3) inks containing pre-formed fibers and catalyst powder (ink #3); (4) inks containing pre-formed fibers, Nafion, and catalyst powder (ink #4); and (5) inks containing pre-formed fibers, Nafion, FEP, and catalyst powder (inks #5–7).

Prior to the preparation of any of the seven inks, electrospun fibers, made with a Nafion and PEO binder, were annealed at 140 °C for 40 minutes, and then the fibers were crushed and broken into small segments. For inks #1 and #2, 158 mg of annealed fibers were mixed with 1065 mg water and sonicated for 5 minutes using an FS20D Ultrasonic Cleaner (Fisher Scientific Inc.). For ink #1, 531 mg of isopropanol was added to the fiber or water mixture, followed by 30 additional minutes of sonication bath mixing. For ink #2, 723 mg at 5 wt% FEP dispersion (Chemours Teflon^{TM} FEPD 121 dispersion (55 wt%), diluted with water to solid weight of 5 wt%), was added to the fiber dispersing

mixture, followed by the addition of 531 mg of isopropanol and 30 minutes of mixing in the sonication bath.

For ink #3, catalyst particles (Gen-2 PMF catalyst, Pajarito Powder LLC) were dispersed with water and isopropanol and sonicated for 60 minutes. The annealed fibers were added to the mixture, followed by 30 additional minutes of sonication bath mixing. For ink #4–7, catalyst particles were dispersed with water, isopropanol, and Nafion (1100 EW Nafion dispersion, 20 wt% in an alcohol-based solvent as received from Ion Power) and sonicated for 60 minutes. For ink #4, fibers were added to the mixture, followed by 30 additional minutes of sonication bath mixing. For ink #5–7, fibers and different amounts of 5 wt% FEP dispersion were added to the mixture and sonicated for 30 minutes.

After the bath-sonication, the pre-formed fiber cathodes were made using Mayer rod coating, which was drawn manually to create catalyst layers on carbon paper gas diffusion layers (GDL, 22BB from Sigracet). The rod coating was repeated multiple times (with intermittent drying for 10 minutes) until the cathode catalyst loading achieved 3.0 mg/cm^2, which then became the gas-diffusion-electrode (GDE) for MEA fabrication.

Table 5.1. Composition for Inks with Pre-formed Fibers

Cathode	Ink Composition
1	158 mg fiber, 1065 mg water, 531 mg IPA
2	159 mg fiber, 1065 mg water, 531 mg IPA, 723 mg stock solution B[2]
3	33 mg catalyst, 79 mg fiber, 755 mg water, 377 mg IPA
4	33 mg catalyst, 79 mg fiber, 819 mg water, 352 mg IPA, 198 mg stock solution A[1]
5	33 mg catalyst, 79 mg fiber, 782 mg water, 400 mg IPA, 198 mg stock solution A, 336 mg stock solution B
6	33 mg catalyst, 79 mg fiber, 528 mg water, 470 mg IPA, 198 mg stock solution A, 753 mg stock solution B
7	33 mg catalyst, 79 mg fiber, 195 mg water, 561 mg IPA, 198 mg stock solution A, 1295 mg stock solution B

[1]Stock Solution A: 20 wt% Nafion in water/alcohol 43/58 (w/w)

[2]Stock Solution B: 5 wt% FEP in water

5.2.3 Pt/C Anode Preparation

All PGM-free catalyst cathode MEAs employed a Pt/C powder anode that was made with ink (2.5 wt% solid), composed of 65 wt% Pt/C catalyst (Tanaka Kikinzoku Kogyo TEC10E50E 46.1% platinum on carbon) and 35 wt% Nafion dispersion (20 wt% 1100 EW Nafion ionomer in an alcohol-based solvent as received from Ion Power) in a 1/2 (w/w) water/isopropanol mixed solvent. The ink was prepared using the following procedure: (i) wetting Pt/C catalyst powder with water, (ii) mixing wet catalyst with isopropanol and Nafion dispersion (1100 EW Nafion ionomer in an alcohol-based solvent as received from Ion Power), (iii) bath-sonicating the mixture for 30 minutes, and (iv) mechanically stirring the ink for 12 hours. The ink was then manually airbrush sprayed onto a Sigracet 22BB GDL at a Pt loading of 0.1 mg_{Pt}/cm^2.

5.2.4 Membrane-Electrode-Assembly Preparation

Membrane-electrode-assemblies (MEAs) with a Nafion fiber cathode, Nafion powder cathode, a cathode made with inks with pre-formed fibers, and a hybrid cathode were prepared using the same general procedures described in Chapter IV.

The Nafion fiber cathode was prepared by cutting the Nafion/PEO fiber mats into 5 cm^2 squares and stacking three mats to achieve a catalyst loading of 3.0 mg/cm^2 (each mat provided 1.0 mg/cm^2 of catalysts). The stacked fiber mats were first hot-pressed onto a Nafion 211 membrane at 140 °C and 35 MPa for 5 minutes. The resulting half-CCM was soaked in hot water (80 °C) for two hours and then dried in a vacuum overnight. The dried half-CMM was then hot-pressed with Pt/C powder anode (0.1 mg_{Pt}/cm^2) and carbon paper GDLs (22BB from Sigracet) at 140 °C for 5 minutes.

The powder cathode was hot pressed with a Pt/C powder anode, a Nafion 211 membrane, and 22BB GDLs (Sigracet) at 35 MPa and 140 °C for 5 minutes.

The cathodes with pre-formed fibers (cathodes listed in Table 5.1) were first soaked in hot water at 80 °C for 2 hours and then dried in a vacuum overnight. After that, the cathodes were hot-pressed with a Nafion 211 membrane, a Pt/C powder anode, and 22BB GDLs (Sigracet) at 140 °C and 35 MPa for 5 minutes.

5.2.5 Fuel Cell Tests

Fuel cell tests were performed using a commercial test station (Scribner Series 850e test station) with temperature, relative humidity, backpressure, and mass flow under control. The fuel cell test fixture accommodated a 5-cm^2-membrane-electrode-assembly and contained single anode and cathode serpentine flow channels. After loading the MEA

into the fuel cell test station, the cell was heated to 80 °C with 0.1 SLPM (standard liter per minute) of H_2 in the anode and 0.1 SLPM of N_2 in the cathode for 2 hours to hydrate the membrane and electrodes. Polarization curves at BOL were collected with 0.7/1.7 SLPM of H_2/air (corresponding to stoichiometries of 10/10) in the anode and cathode. The fuel cell operating conditions were 80 °C, 100% RH, and 200 kPa_{abs}.

Accelerated stress tests (AST) were conducted with 30,000 (30K) cycles, which consisted of square-wave potential cycling between 0.60 V and 0.95 V, with a step duration of 3 seconds. The AST operated with a gas flow rate of H_2/air 0.5/0.5 SLPM at 80 °C, 100% RH, and 200 kPa_{abs}. After the 30K cycles of AST, end-of-life (EOL) polarization was collected at the same operating condition as in BOL.

5.2.6 Scanning Electron Microscope Methods

The present study used a Zeiss MERLIN scanning electron microscope to collect top-down scanning electron microscope (SEM) images. The SEM images were gathered to evaluate the overall quality of the fiber mats, powder cathodes, redispersed fiber cathodes, and hybrid cathodes. Before imaging, samples (fiber mats, powder cathodes, redispersed fibers, or hybrid cathodes) were pressed slightly onto a double-sided conductive tape. Then, they were sputter coated with a thin layer of gold deposition to improve imaging contrast.

5.3 Results and Discussion

5.3.1 Redispersed Fiber Cathode

The Nafion/PEO fiber mat with Gen-2 PMF catalyst has been discussed and shown in Chapter IV. The cathode as a directly attached fiber mat to a gas diffusion layer is hereafter labeled in this chapter a Nafion fiber cathode (to be distinguished from a cathode made with pre-formed fibers dispersed in an ink). For all the cathodes with fiber mats or pre-formed fiber mats, the PEO was removed before the fuel cell tests by a water-soaking process, which was achieved by hot-pressing the fiber mats onto a Nafion 211 membrane followed by soaking in water (80 °C) for 2 hours.[1]

Figure 5.1 shows cathode #1 from ink #1, which was made by dispersing the fiber mats into the water and alcohol solvent and then coating the ink onto carbon paper. In cathode #1, the fibers became shorter, and most of the fiber morphology was maintained with a few catalyst particles aggregated.

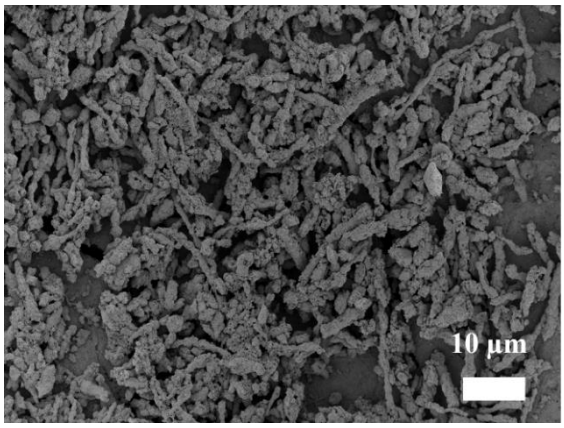

Figure 5.1. Top-down SEM images of cathode #1 from ink #1.

Polarization curves and power density plots at BOL and EOL (at the end of 30K voltage cycles) of the Nafion fiber cathode MEA and MEA #1 (with cathode ink #1) are plotted in Figures 5.2a and 5.2b. Figure 5.2c shows the EOL and BOL power density ratio. At both BOL and EOL, the polarization plots overlapped (6% differences at most), so there was no clear superiority of one cathode.

As discussed in Chapter II–IV, degradation occurred in MEA whose cathode had Nafion as the only binder component (i.e., the EOL:BOL power density ratio was below 1.0 in Figure 5.2c) due to peroxide attack (oxidation) on the carbon-based cathode catalyst active sites[2,3] where H_2O_2 was generated via a 2-electron reduction of O_2 with H^{+4}:

$$2H^+ + 2e^- + O_2 \rightarrow H_2O_2 \quad (1)$$

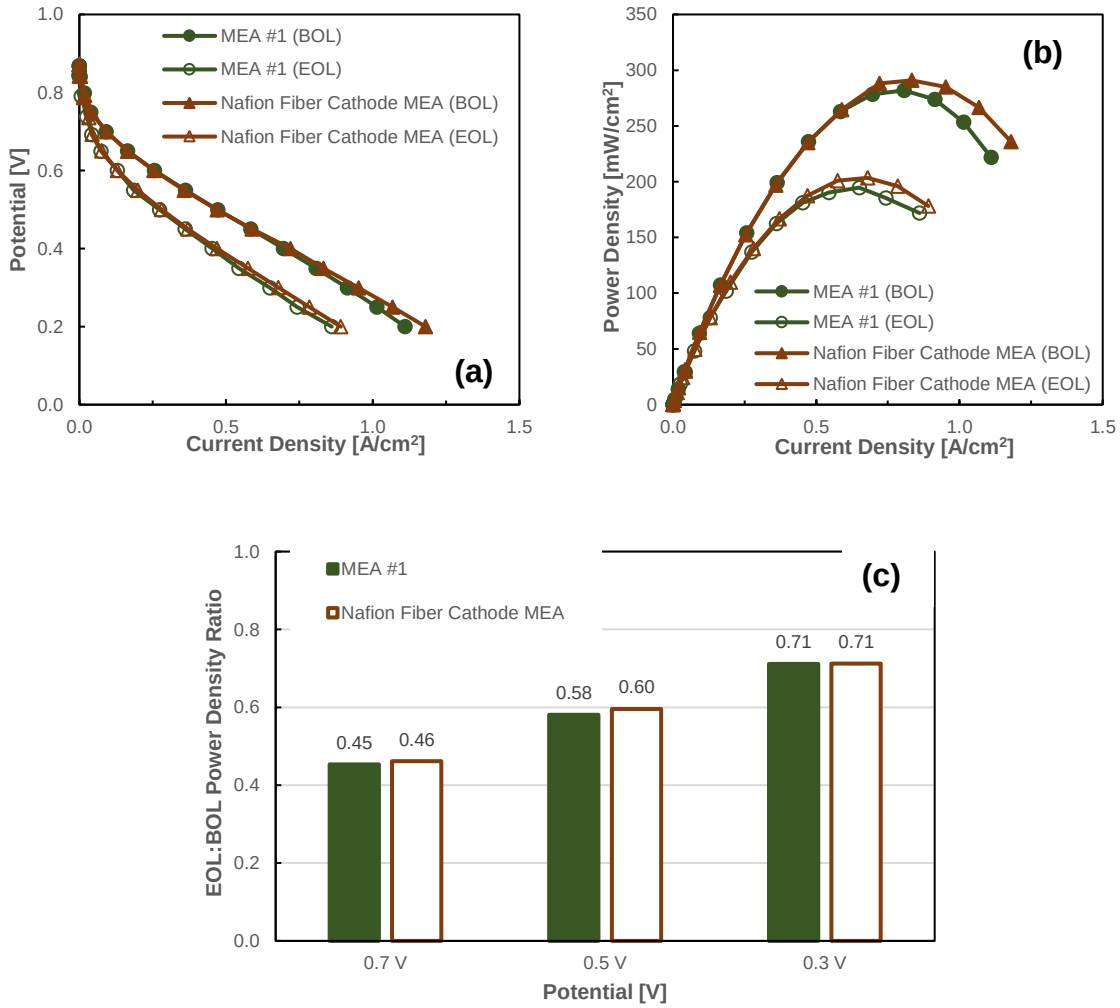

Figure 5.2. BOL (solid symbol) and EOL (open symbol) (a) polarization curves, (b) power density versus current density, and (c) the EOL:BOL power density ratio at 0.7 V, 0.5 V, and 0.3 V for Nafion fiber cathode MEA and MEA #1. Both cathodes were made with the same Nafion/PEO fiber mats and were soaked in water (80 °C) for 2 hours to remove PEO before MEA fabrication. The PGM-free catalyst cathode loading was 3.0 mg/cm^2. Fuel cell operating conditions: 80 °C, 100% relative humidity, 200 kPa$_{abs}$, and H_2/air 0.7/1.7 SLPM feed gas flow rate. All MEAs contain a Nafion 211 membrane and a Pt/C catalyst powder anode at a loading of 0.1 mg$_{Pt}$/cm^2.

5.3.2 Hybrid Cathodes

The new hybrid cathodes comprise electrospun particle/binder fibers and catalyst particles. Figure 5.3 is a schematic picture of a hybrid cathode. In the hybrid cathode, the

fiber mats were Gen-2 PMF catalysts electrospun with Nafion and PEO binder, and the catalyst particles were also Gen-2 PMF catalysts. In all hybrid cathodes prepared in the present study, the catalyst loading was 3.0 mg/cm^2, with 50 wt% of the catalyst in fiber mats and 50 wt% of the catalyst interspersing between fibers.

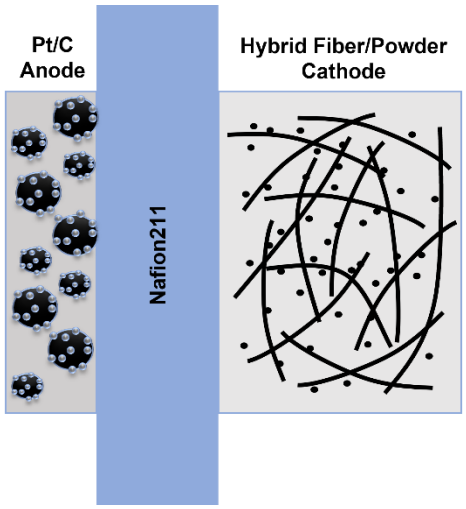

Figure 5.3. Schematic picture of the hybrid cathode.

Figure 5.4 shows the hybrid type I cathode (cathode #3 with ink #3), in which catalyst particles are interspersing between fibers. Nafion dispersion helps to minimize catalyst agglomerates in electrode inks.[5,6] Since cathode #3 had no Nafion outside of the fibers, catalyst agglomeration was not unexpected.

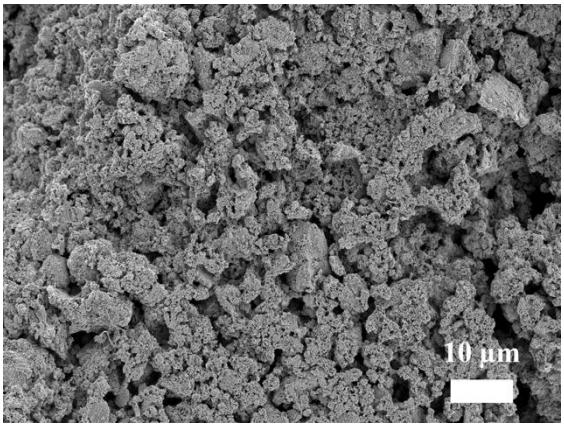

Figure 5.4. Top-down SEM images of hybrid type I cathode (cathode #3).

Polarization curves at BOL and EOL (after 30K cycles of an AST) of the hybrid type I cathode MEA (MEA #3 using cathode #3) were also collected. Figure 5.5a shows these polarization curves, Figure 5.5b shows power density versus current density plots, and Figure 5.5c is a bar chart of EOL:BOL power density ratio at 0.7 V, 0.5 V, and 0.3 V. As a comparison, Figure 5.5 also shows the data from a Nafion fiber cathode MEA.

At BOL, 20% less power was generated in MEA #3 in the entire potential region as compared to a Nafion fiber cathode MEA, which can be ascribed to poor proton transport to catalyst particles outside of the fibers. In cathode #3, all Nafion was located in the fiber, with no Nafion near catalyst particles between fibers. Thus, the Nafion-to-catalyst weight ratio in the cathode was only 0.6, while the weight ratio in the Nafion fiber cathode was 1.2.

At EOL, less power was generated in the entire potential region for MEA #3. However, the EOL:BOL power density ratio at 0.7 V and 0.5 V for MEA #3 was higher than that for the Nafion fiber cathode MEA, which was also related to the poor proton transport in cathode #3. As illustrated in Equation 1, hydrogen peroxide was generated

through the 2-electron reduction reaction. The lack of protons produced less peroxide, with less degradation of catalytic sites in cathode #3. Such an inverse correlation between catalyst activity and MEA durability was observed and reported in previous studies.[7–9]

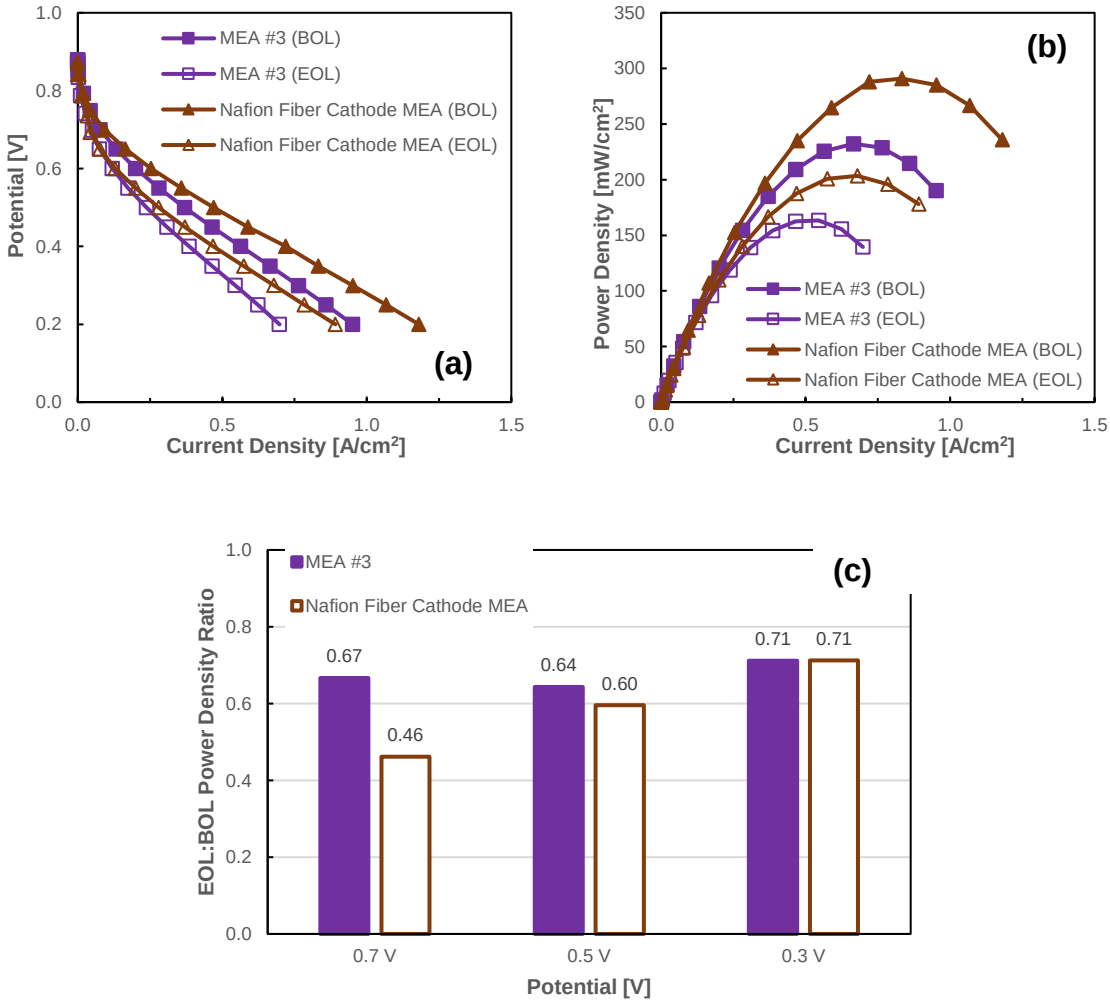

Figure 5.5. BOL (solid symbol) and EOL (open symbol) (a) polarization curves, (b) power density vs. current density, and (c) the EOL:BOL power density ratio at 0.7 V, 0.5 V, and 0.3 V for the Nafion fiber cathode MEA and MEA #3. Both cathodes were made with the same Nafion/PEO fiber mats with PEO extracted prior to MEA fabrication. The PGM-free catalyst cathode loading was 3.0 mg/cm^2. The fuel cell operating conditions were 80 °C, 100% relative humidity, 200 kPa$_{abs}$, and H_2/air 0.7/1.7 SLPM feed gas flow rate. All MEAs contained a Pt/C catalyst powder anode at the loading of 0.1 mg$_{Pt}$/cm^2 and a Nafion 211 membrane.

Figure 5.6 shows an SEM image of the hybrid type II cathode (cathode #4 from ink #4), in which catalyst particles and Nafion were interspersed between pre-formed fibers. The overall Nafion-to-catalyst ratio for this cathode was 1.2, the same as in the Nafion fiber mats cathode MEAs. The fiber morphology in cathode #4 was not as evident as in cathode #1 (Figure 5.1), possibly because the fiber morphology was blocked or covered by catalyst particles and dispersed Nafion ionomer micelles. Compared with cathode #3 (Figure 5.4), fewer large aggregates formed in cathode #4 as well, since Nafion dispersion between fibers helps to disperse catalyst particles and minimize catalyst agglomerates in electrode inks.

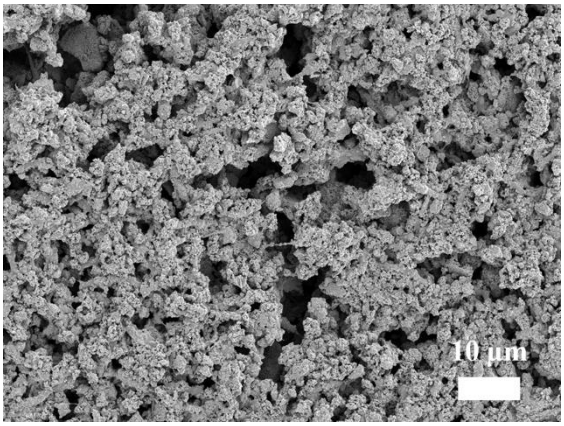

Figure 5.6. Top-down SEM images of hybrid type II cathode (cathode #4 from ink #4).

The durability of MEA #4 (with cathode #4) was then assessed by a 30K cycle AST. Figures 5.7a and b show the polarization curves and power densities at BOL and EOL; Figure 5.7c is a bar chart of the EOL:BOL power density ratios at 0.7 V, 0.5 V, and 0.3 V.

Compared with a Nafion fiber cathode MEA at BOL, MEA #4 generated approximately 15% more power, which could be attributed to the following combined effects. First, adding extra Nafion helped the catalyst particles to disperse instead of agglomerate, as shown by the SEM image (Figure 5.6). Second, the cathode thickness of cathode #4 was 80 μm (vs. 95 μm for Nafion fiber cathode) at 3.0 mg/cm^2 loading. A thinner cathode would facilitate proton transport from the membrane to catalyst active sites at the back of the electrode (i.e., lowering the IR drop in the cathode).[10] Third, Nafion between the fibers provided pathways to transport protons to catalyst particles outside of the fibers. Last, catalyst particles between fibers increased active site accessibility to the O_2 reactant. At EOL, MEA #4 also generated approximately 15% more power than the MEA with the fiber cathode. The durability of the two cathodes was comparable, i.e., the EOL:BOL power density ratio was the same.

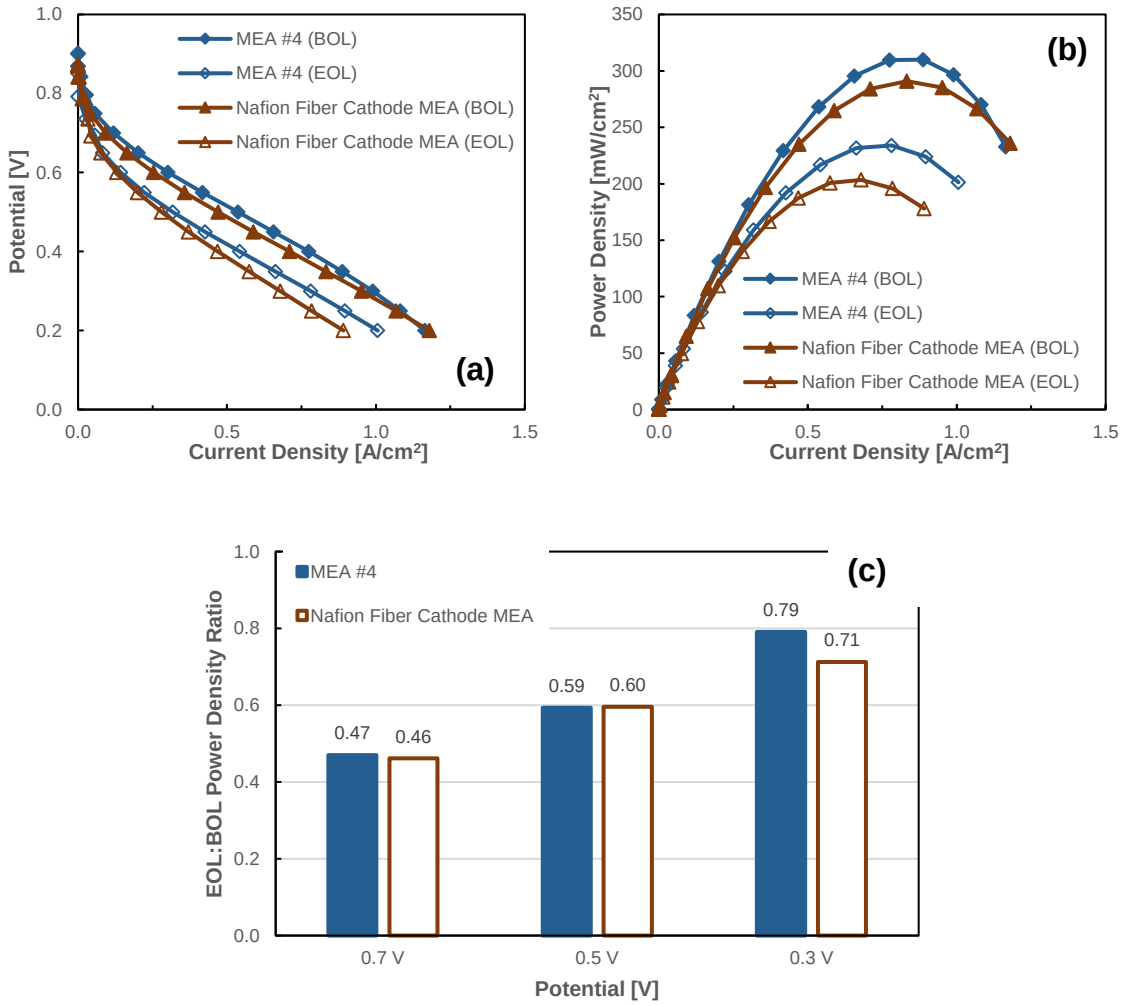

Figure 5.7. BOL (solid symbol) and EOL (open symbol) (a) polarization curves, (b) power density vs. current density, and (c) the EOL:BOL power density ratio at 0.7 V, 0.5 V, and 0.3 V for the Nafion fiber cathode MEA and MEA #4. The Nafion-to-catalyst weight ratio in the cathode was 1.2 inside and between fibers, and the PGM-free catalyst cathode loading was 3.0 mg/cm^2. The fuel cell operating conditions were 80 °C, 100% relative humidity, 200 kPa$_{abs}$, and H_2/air 0.7/1.7 SLPM feed gas flow rate. All the MEAs contained a Nafion 211 membrane and a Pt/C catalyst powder anode at a loading of 0.1 mg$_{Pt}$/cm^2.

5.3.3 Effect of Adding Fluorinated Ethylene Propylene (FEP) to Hybrid Cathodes

Figure 5.8 shows hybrid type III cathodes (cathodes #5, #6, and #7 using inks #5, #6, and #7), where catalyst particles, Nafion, and FEP (a hydrophobic additive) were

interspersing between fibers. The overall Nafion-to-catalyst ratio for this cathode was 1.2. Three types of hybrid type III cathodes were prepared, with FEP content of 10 wt% (cathode #5, Figure 5.8a), 20 wt% (cathode #6, Figure 5.8b), and 30 wt% (cathode #7, Figure 5.8c). Figure 5.8d shows cathode #7 at high magnification, in which FEP particles (the oval particles) were uniformly distributed above fiber surfaces. Adding 10 wt% of FEP had no apparent effect on dispersing the catalyst or breaking up the fibers. However, upon further increasing the FEP content, the void space between fibers became less.

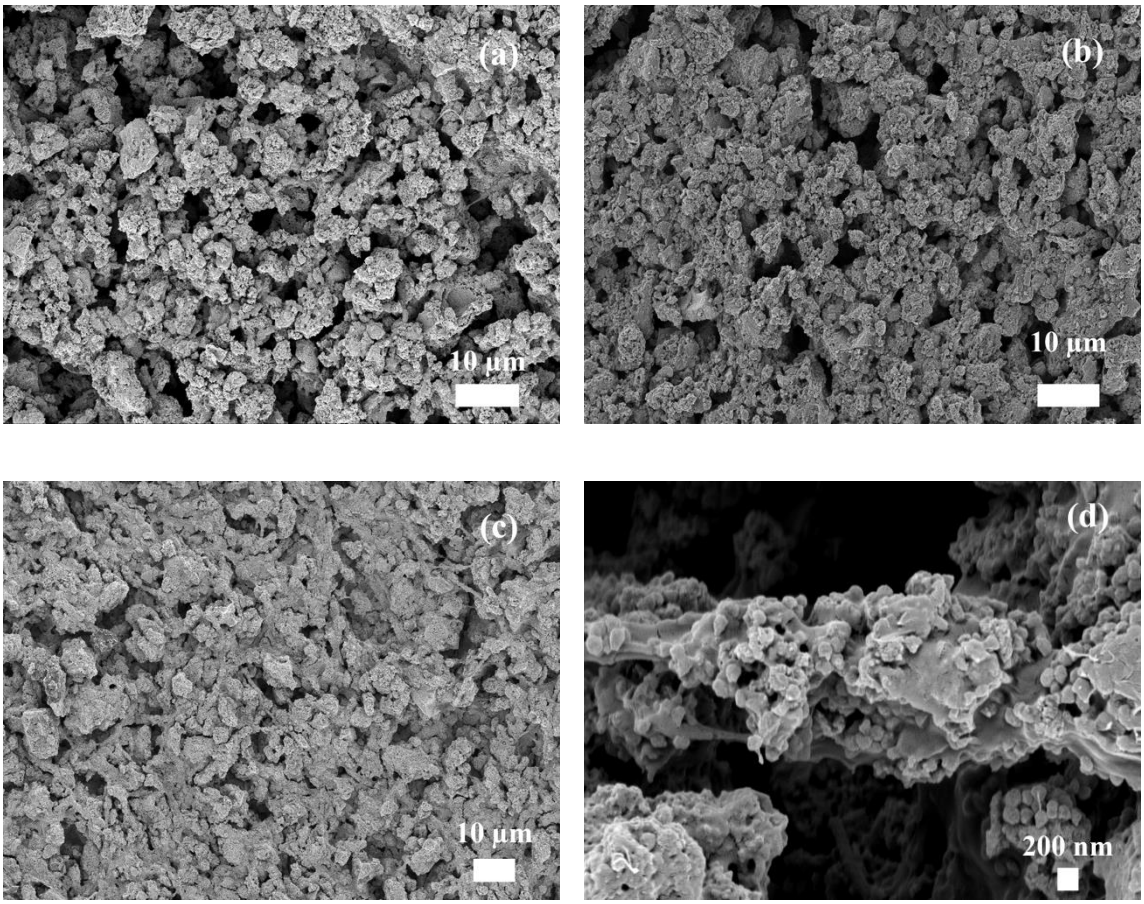

Figure 5.8. Top-down SEM images of hybrid type III cathode with FEP content of (a) 10 wt% (cathode #5), (b) 20 wt% (cathode #6), and (c, d) 30 wt% (cathode #7). Images (a–c) were collected at 3,000x magnification, and image (d) at 30,000x magnification.

When the FEP content in the hybrid type III cathode increased from 10 wt% to 30 wt%, less power was generated for the potential region 0.2–1.0 V. Increased FEP content led to a decrease in power generation due to: (1) the hydrophobicity of the FEP quickly expels electrogenerated water away from catalyst sites and slowed the oxygen reduction reaction rate since water is needed for fast oxygen reduction reaction (ORR) kinetics;[11,12] (2) FEP diluted Nafion binder outside the fibers and lowered proton.[13]

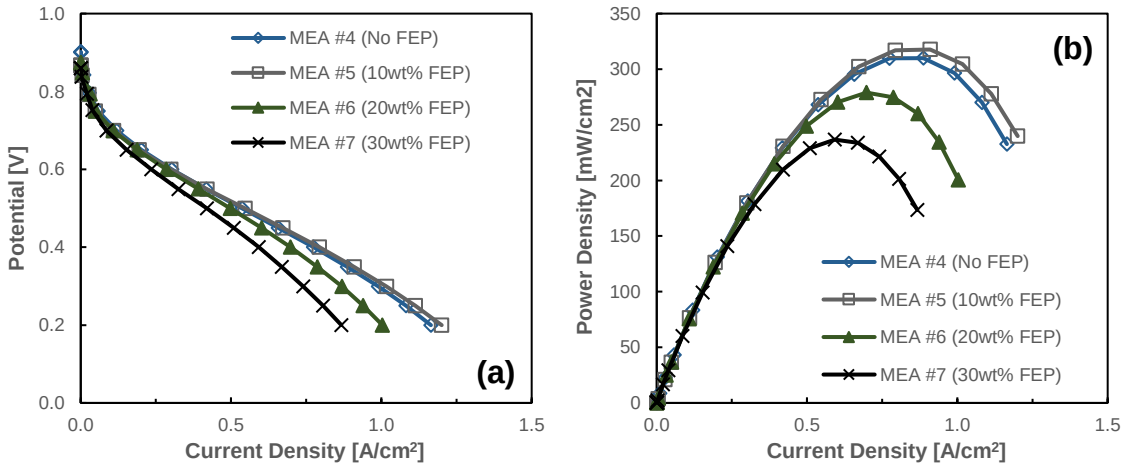

Figure 5.9. H_2/air (a) polarization curves, (b) power density vs. current density at the BOL for the hybrid cathode MEAs (no FEP, 10 wt%, 20 wt%, and 30 wt% FEP). All the cathodes were made with the same Nafion and PEO binder fiber mats, the Nafion-to-catalyst weight ratio was 1.2 inside and between fibers, and the PGM-free catalyst cathode loading was 3.0 mg/cm^2. The fuel cell operating conditions were 80 °C, 100% relative humidity, 200 kPa_{abs}, and H_2/air 0.7/1.7 SLPM feed gas flow rate. All the MEAs contained a Nafion 211 membrane and a Pt/C catalyst powder anode at a loading of 0.1 mg_{Pt}/cm^2.

At EOL (Figure 5.10), when the FEP content in the cathode was 30 wt% (MEA #7), the polarization curves at BOL and EOL overlap. As shown in Appendix A of this dissertation, MEA #7 has been made and evaluated three times. The differences of power output and durability (i.e., EOL:BOL power density ratio) are within 10%.

The improved durability in the hybrid type III cathode was attributed to the FEP hydrophobicity. Increased cathode hydrophobicity helped to expel water and electrogenerated peroxide away from catalyst particles. A similar durability improvement was achieved by adding PVDF into the PGM-free catalyst cathode, as discussed in Chapters II and III and in the research paper by Slack et al.[14]

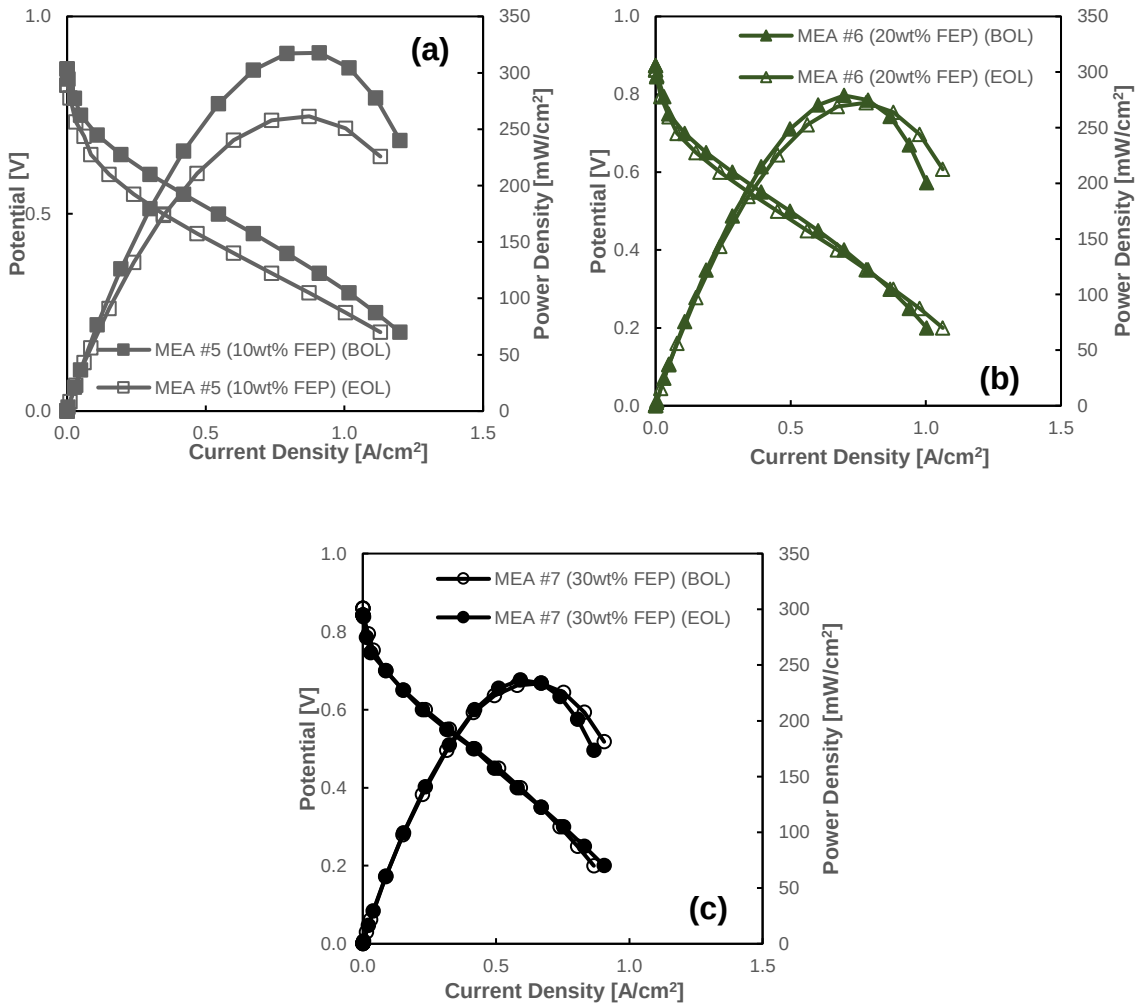

Figure 5.10. BOL (solid symbol) and EOL (open symbol) H_2/air polarization curves and power density vs. current density for hybrid type III cathode MEAs: (a) MEA #5 (10 wt% FEP), (b) MEA #6 (20 wt% FEP), and (c) MEA #7 (30 wt% FEP). All the cathodes were made with the same fiber mats with PEO extracted. The Nafion-to-catalyst weight ratio was 1.2 inside and between fibers, and PGM-free catalyst cathode loading was 3.0 mg/cm^2. The fuel cell operating conditions were 80 °C, 100% relative humidity, 200 kPa_{abs}, and H_2/air 0.7/1.7 SLPM feed gas flow rate. All the MEAs contained a Nafion 211 membrane and a Pt/C catalyst powder anode at a loading of 0.1 mg_{Pt}/cm^2.

Figures 5.11a and b show polarization curves and power densities plots at EOL for MEAs #4, #5, #6, and #7 (no FEP, 10 wt%, 20 wt%, and 30 wt% FEP), and Figure 5.11c is a bar chart of EOL:BOL power density ratios at 0.7 V, 0.5 V, and 0.3 V. The

results in Figure 5.11c show the durability improvement (i.e., the EOL:BOL power density ratio increased) as the FEP content in the hybrid cathode increased. In the present study, MEA #7 was the most durable (no degradation after 30K voltage cycles of an accelerated stress test). However, the EOL polarization curves indicate that MEA #6 (20 wt% FEP) generated more power than MEA #7. (i.e., the power density for MEA #7 changed less after the durability test, but the initial and final powder densities were less than the corresponding power densities for MEA #7. Consequently, the best compromise after the 30K-cycle accelerated stress test in terms of power output and durability was achieved by MEA #6 (20 wt% FEP in hybrid cathode).

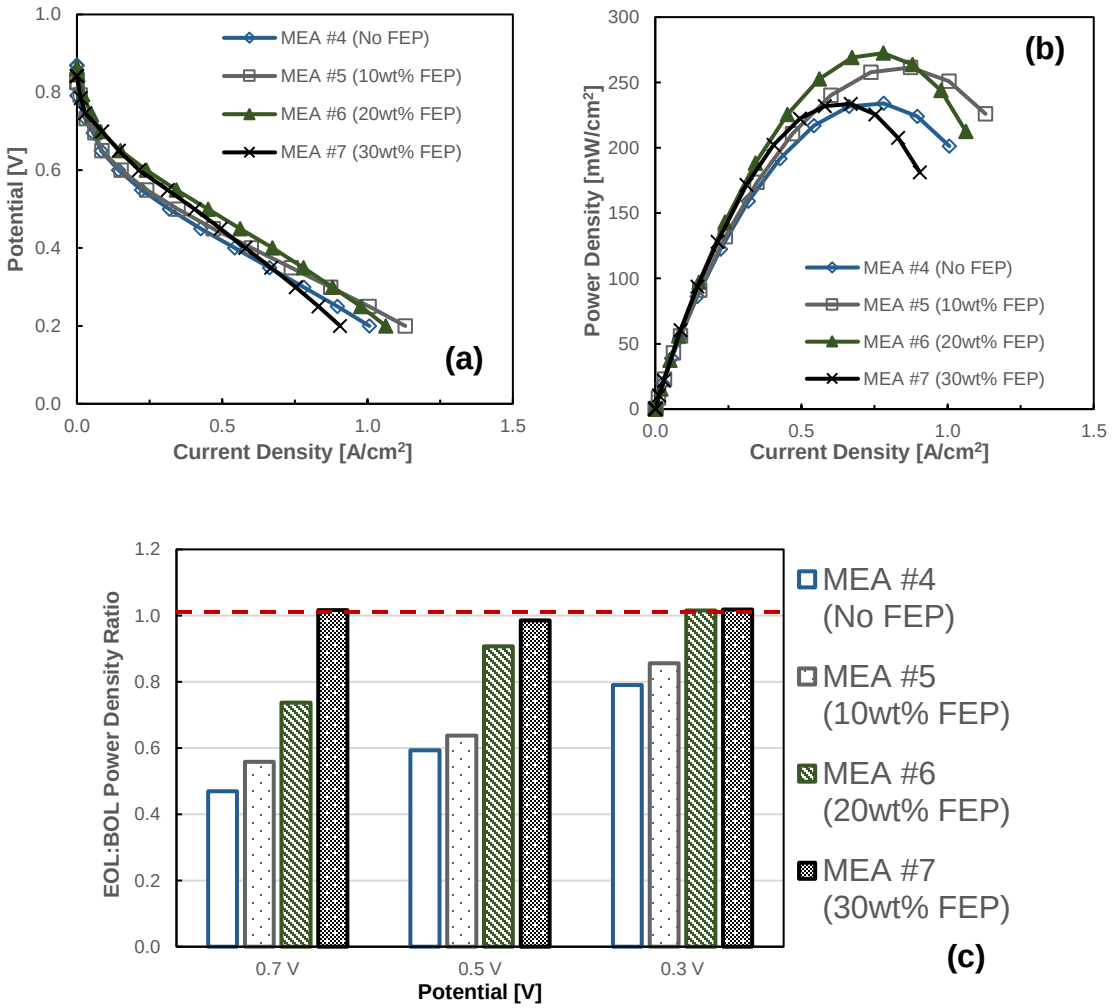

Figure 5.11. The H_2/air (a) polarization curves, (b) power density vs current density at the EOL, and (c) the EOL:BOL power density ratio at 0.7 V, 0.5 V, and 0.3 V MEAs #4–7 (no FEP, 10 wt%, 20 wt%, and 30 wt% FEP). The Nafion-to-catalyst weight ratio was 1.2 inside and between fibers and the PGM-free catalyst cathode loading of 3.0 mg/cm^2. The fuel cell operating conditions were 80 °C, 100% relative humidity, 200 kPa$_{abs}$, and H_2/air 0.7/1.7 SLPM feed gas flow rate. All the MEAs contained a Nafion 211 membrane and a Pt/C catalyst powder anode at a loading of 0.1 mg$_{Pt}$/cm^2.

5.3.4 Effect of Adding Fluorinated Ethylene Propylene (FEP) into Powder or Pre-Formed Fiber Cathodes

This section focuses on the effect of adding 20 wt% FEP to cathode #1 (redispersed fibers) or to a conventional powder cathode on fuel cell power output and MEA durability. The powder cathode with a neat Nafion binder has already been shown in Chapter IV. Figure 5.12a shows the powder cathode with a Nafion/FEP binder (20 wt% FEP), where FEP addition decreased the cathode porosity. Figure 5.12b shows cathode #2, prepared by adding 20 wt% FEP into the electrode ink solution for cathode #1. The FEP addition did not affect catalyst particle agglomeration or break up the fiber morphology.

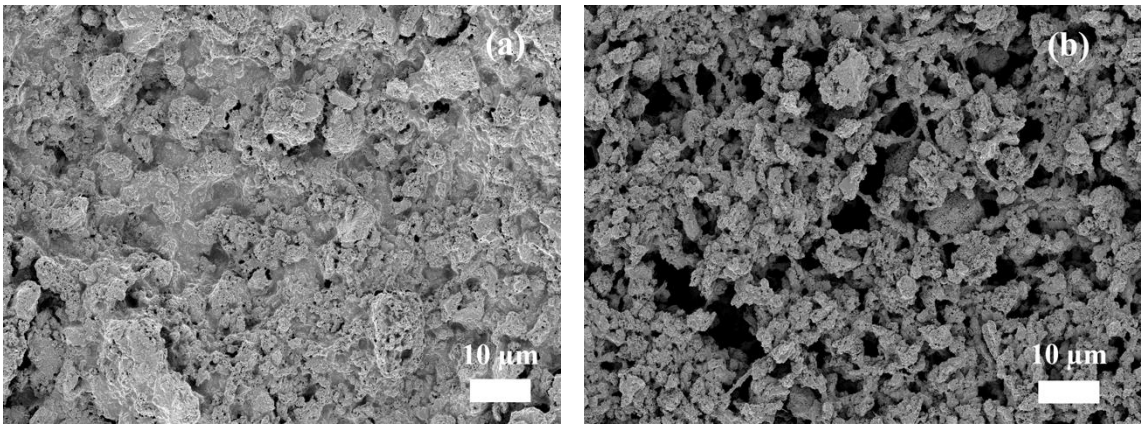

Figure 5.12. Top-down SEM images of (a) the powder cathode with a Nafion/FEP binder (20 wt% FEP) and (b) cathode #2 (20 wt% FEP in the redispersed fiber cathode).

Figures 5.13a and b show fuel cell polarization curves and power densities of the powder cathode MEAs with either a neat Nafion binder or a Nafion/FEP binder at the BOL and EOL. Figures 5.14 a and b show polarization curves and power densities of

MEAs #1 and #2 at the BOL and EOL. Figures 5.14c and 5.15c show the EOL:BOL power density ratios at 0.7 V, 0.5 V, and 0.3 V.

As shown in Figure 5.13, at BOL, the MEA of the powder cathode with a Nafion/FEP binder generated a similar current density in the high-potential region as the powder MEA with a neat Nafion binder. However, the powder cathode MEA with a Nafion/FEP binder encountered more severe water flooding (more rapid power density drop at high current densities) than the power cathode MEA with a neat Nafion binder (maximum power density of the Nafion binder 259 mW/cm^2 vs. Nafion/FEP binder 214 mW/cm^2). This water flooding issue could be attributed to the polymer film that blocked or restricted reactant gas and water transport (in and out of the cathode) during fuel cell operation. A substantial power drop (ca. 40% less power) in the MEA with the Nafion/FEP redispersed fiber cathode was observed, possibly due to the FEP particles between fibers that blocked proton transport between fibers.

Adding 20 wt% FEP to the powder cathode only moderately affected MEA durability (no change in the EOL and BOL power density ratio). In contrast, by adding FEP into a redispersed fiber cathode, the EOL:BOL power density ratio increased substantially (Figure 5.14c). A possible explanation is that in the powder cathode, FEP did not uniformly mix throughout the cathode, and thus only protected some catalyst particles, while its presence decreased the effective conductivity of the cathode binder. In contrast, the fibers in a redispersed ink provided sites for FEP deposition, which resulted in a more uniform distribution of FEP. Thus, during the oxygen reduction and water generation, cathode catalyst sites were in close proximity to FEP particles, which protected such sites from H_2O_2 attack.

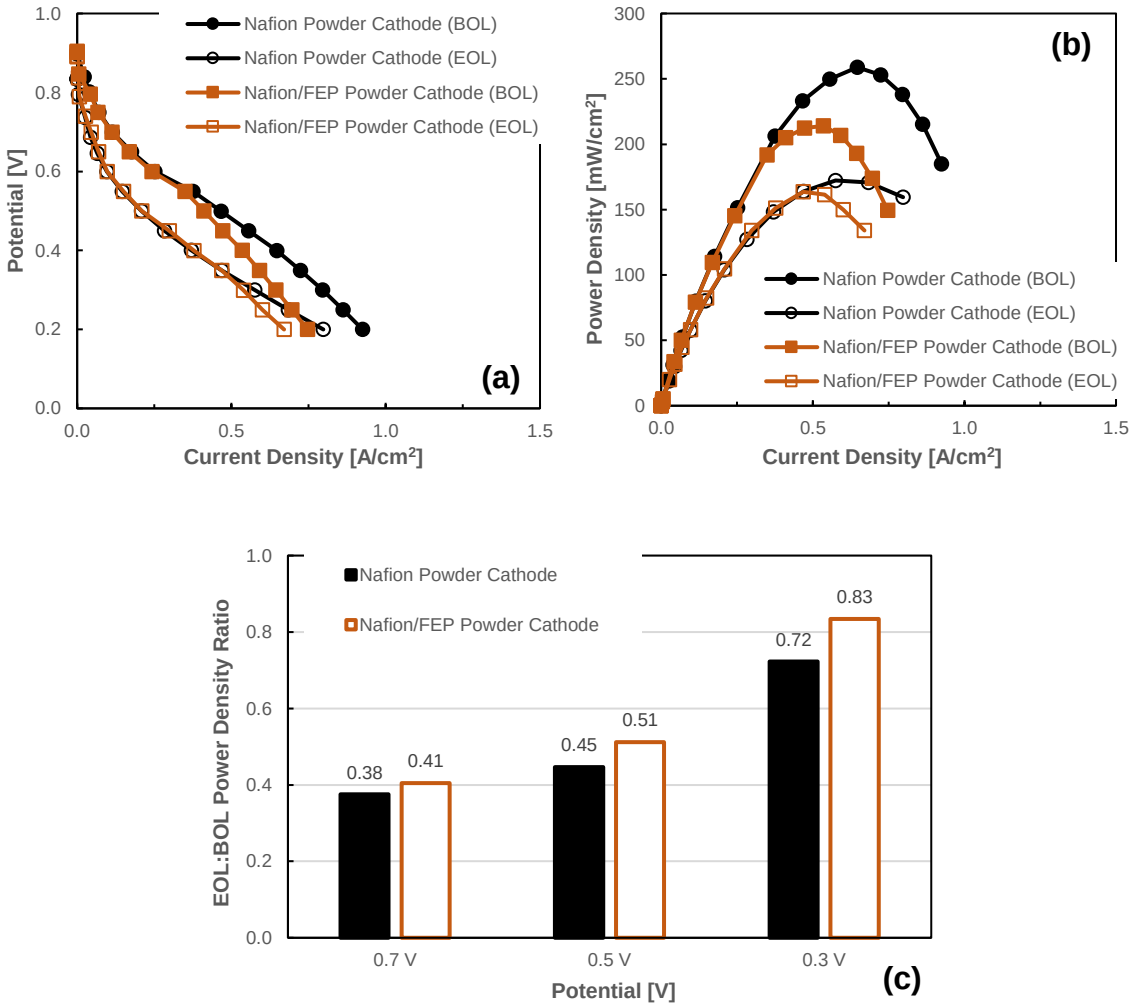

Figure 5.13. BOL (solid symbol) and EOL (open symbol) (a) polarization curves, (b) power density vs. current density, and (c) the EOL:BOL power density ratio at 0.7 V, 0.5 V, and 0.3 V for the powder cathode MEA with the Nafion binder and the powder cathode MEA with Nafion/FEP (20 wt% FEP) binder. The fuel cell operating conditions were 80 °C, 100% relative humidity, 200 kPa_{abs}, and H_2/air 0.7/1.7 SLPM feed gas flow rate. All the MEAs contained a Nafion 211 membrane and a Pt/C catalyst powder anode at a loading of 0.1 mg_{Pt}/cm^2. The PGM-free catalyst cathode loading was 3.0 mg/cm^2.

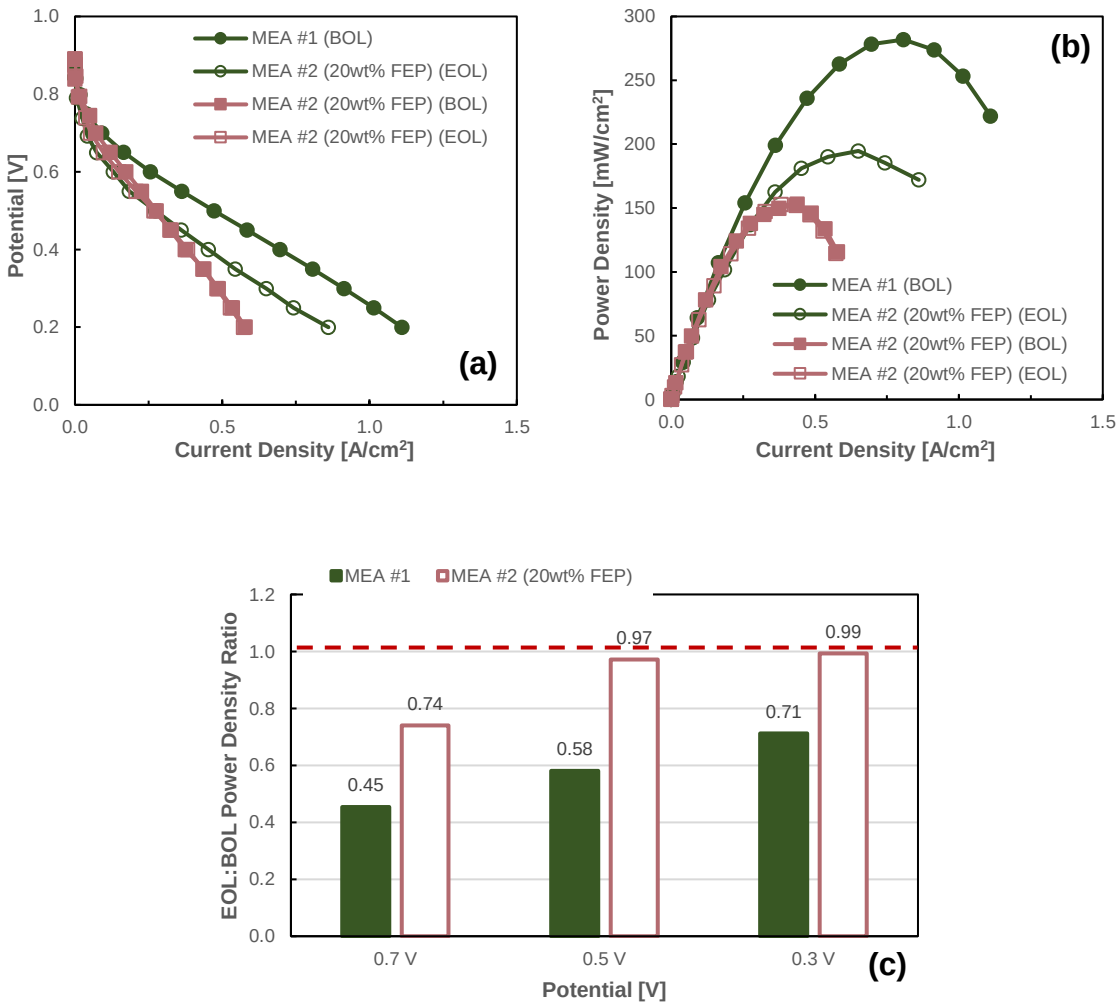

Figure 5.14. BOL (solid symbol) and EOL (open symbol) (a) polarization curves, (b) power density versus current density, and (c) the EOL:BOL power density ratio at 0.7 V, 0.5 V, and 0.3 V for the Nafion redispersed fiber cathode MEA and the Nafion/FEP redispersed fiber (20 wt% FEP) cathode MEA. Both cathodes were made with the same Nafion/PEO fiber mats and soaked in water (80 °C) for 2 hours to remove the PEO. The PGM-free catalyst cathode loading was 3.0 mg/cm^2. The fuel cell operating conditions were 80 °C, 100% relative humidity, 200 kPa$_{abs}$, and H_2/air 0.7/1.7 SLPM feed gas flow rate. All the MEAs contained a Nafion 211 membrane and a Pt/C catalyst powder anode at a loading of 0.1 mg$_{Pt}$/cm^2. The Nafion redispersed fiber cathode plots were the same as shown in Figure 5.2.

Table 5.2 summarizes the EOL:BOL power density ratios at 0.5 V and power densities at 0.5 V at EOL (after a 30K-cycle AST) for all of the MEAs in the present study. This table reveals the superiority of MEAs #6 and #7 (a hybrid cathode with 20 wt% or 30 wt% FEP). It should be noted that in Chapter II, the highest stable power output at 0.5 V was 88 mW/cm^2, for the 75:25 (w:w) Nafion:PVDF fiber cathode MEA with Gen-1 PMF catalysts. In Chapter II, the highest stable power output at 0.5 V was 110 mW/cm^2, for the 80:20 or 83:17 (w:w) Nafion:PVDF fiber cathode MEA with MOF-based catalysts. Both of those MEAs did not work as well as hybrid cathode MEAs #6 and #7, which generated 226 and 202 mW/cm^2 at 0.5 V, with steady power output for extended periods of time (an EOL:BOL power density ratio > 0.9).

Table 5.2. EOL:BOL Power Density Ratio and EOL Power Density at 0.5V for MEAs with Different Cathodes after 30K-cycle ASTs.

MEA	EOL:BOL Power Density Ratio at 0.5V	Power Density at 0.5V at EOL [mW/cm^2]
Powder cathode MEA with Nafion binder	0.45	104
Powder cathode MEA with Nafion/FEP binder	0.51	105
Nafion fiber cathode MEA	0.59	140
MEA #1	0.59	137
MEA #2 (20wt% FEP)	0.97	134
MEA #3	0.65	119
MEA #4	0.59	159
MEA #5 (10wt% FEP)	0.65	174
MEA #6 (20wt% FEP)	0.91	226
MEA #7 (30wt% FEP)	0.97	202

5.4 Conclusion

In this study, Fe-N-C-based PGM-free catalysts provided by Pajarito Powder, synthesized through a new hard-templating-pore-former approach, and designated as Gen-2 PMF catalysts, were incorporated into hybrid fuel cell cathodes. The cathodes were used to make MEAs with a Nafion 211 membrane and a Pt/C powder anode (0.1 mg_{Pt}/cm^2) and the MEAs were assessed in H_2/air fuel cells in terms of initial power and durability. The catalyst durability was evaluated by a 30K-cycle AST, and polarization curves were collected at BOL and EOL.

Fiber mats were electrospun with Gen-2 PMF catalysts, Nafion, and PEO, and were used to fabricate MEAs (the same methods and materials as in Chapter IV). The fiber mats were then used to fabricate a redispersed fiber cathode (cathode #1), which performed the same as a conventional Nafion fiber cathode MEA.

The Nafion/PEO/Gen-2 PMF fiber mats were also used to fabricate three hybrid cathodes: The hybrid type I in which PMF catalyst particles are interspersed between fibers; an MEA with this cathode generated 20% less power than a Nafion fiber cathode MEA with a 10% durability improvement (i.e., 10% higher EOL:BOL power density ratio at 0.5 V). The hybrid type II cathode where catalyst and Nafion were interspersed between fibers; an MEA with this cathode generated 15% more power than the Nafion fiber cathode, with similar durability. The hybrid type III cathode where PMF catalyst, Nafion, and FEP Teflon (a hydrophobic polymer) were interspersed between fibers, where the FEP content was either 10 wt%, 20 wt% or 30 wt%. As the FEP content increased, the power output at BOL decreased (due to the addition of uncharged FEP,

which lowered the ORR kinetics and proton transport), and the MEA durability increased (due to an increase in cathode hydrophobicity). While the power output was low with 30 wt% FEP, there was no apparent cathode degradation during the durability experiment and the BOL and EOL polarization plots overlapped. The highest power output at EOL (after a 30K-cycle AST) was generated by an MEA with a hybrid cathode containing 20 wt% FEP. The effect of adding FEP directly to Nafion/catalyst powder cathode at a concentration of 20 wt%, was much different from adding FEP outside of the fibers. When FEP was inside the powder cathode, there was no change in BOL power densities versus a Nafion powder cathode at high potentials, a loss in power at moderate and low potentials (moderate/high current densities), and no improvement in MEA durability versus a Nafon powder cathode MEA. When FEP was outside the fibers, there was a 40% loss in BOL power densities versus a fiber (or redispersed fiber) cathode, and an improvement in MEA durability versus fiber cathode MEA.

5.5 References

1. Waldrop, K. *et al.* Electrospun Nanofiber Electrodes for High and Low Humidity PEMFC Operation. *J Electrochem Soc* **170**, 024507 (2023).
2. Goellner, V., Armel, V., Zitolo, A., Fonda, E. & Jaouen, F. Degradation by Hydrogen Peroxide of Metal-Nitrogen-Carbon Catalysts for Oxygen Reduction. *J Electrochem Soc* **162**, H403–H414 (2015).
3. Choi, C. H. *et al.* Unraveling the Nature of Sites Active toward Hydrogen Peroxide Reduction in Fe-N-C Catalysts. *Angewandte Chemie - International Edition* **56**, 8809–8812 (2017).

4. Lefèvre, M. & Dodelet, J. P. Fe-based catalysts for the reduction of oxygen in polymer electrolyte membrane fuel cell conditions: Determination of the amount of peroxide released during electroreduction and its influence on the stability of the catalysts. *Electrochim Acta* **48**, 2749–2760 (2003).

5. Yang, D. *et al.* Influence of the dispersion state of ionomer on the dispersion of catalyst ink and the construction of catalyst layer. *Int J Hydrogen Energy* **46**, 33300–33313 (2021).

6. So, M. *et al.* The effect of solvent and ionomer on agglomeration in fuel cell catalyst inks: Simulation by the Discrete Element Method. *Int J Hydrogen Energy* **44**, 28984–28995 (2019).

7. Osmieri, L. *et al.* Status and challenges for the application of platinum group metal-free catalysts in proton-exchange membrane fuel cells. *Curr Opin Electrochem* **25**, 100627 (2021).

8. Larouche, N., Chenitz, R., Lefèvre, M., Proietti, E. & Dodelet, J. P. Activity and stability in proton exchange membrane fuel cells of iron-based cathode catalysts synthesized with addition of carbon fibers. *Electrochim Acta* **115**, 170–182 (2014).

9. Yang, L. *et al.* Activity, Performance, and Durability for the Reduction of Oxygen in PEM Fuel Cells, of Fe/N/C Electrocatalysts Obtained from the Pyrolysis of Metal-Organic-Framework and Iron Porphyrin Precursors. *Electrochim Acta* **159**, 184–197 (2015).

10. Osmieri, L., Wang, H. & Neyerlin, K. C. Impact of Fabrication and Testing Parameters on the Performance of a Polymer Electrolyte Fuel Cell with Platinum Group Metal (PGM)-Free Cathode Catalyst. *J Electrochem Soc* **168**, 014503 (2021).

11. Ramaker, D. E., Korovina, A., Croze, V., Melke, J. & Roth, C. Following ORR intermediates adsorbed on a Pt cathode catalyst during break-in of a PEM fuel cell by in operando X-ray absorption spectroscopy. *Physical Chemistry Chemical Physics* **16**, 13645–13653 (2014).

12. Wang, J. X., Markovic, N. M. & Adzic, R. R. Kinetic Analysis of Oxygen Reduction on Pt(111) in Acid Solutions: Intrinsic Kinetic Parameters and Anion Adsorption Effects. *Journal of Physical Chemistry B* **108**, 4127–4133 (2004).

13. Tsai, J. C. & Lin, C. K. Effect of PTFE content in gas diffusion layer based on Nafion®/PTFE membrane for low humidity proton exchange membrane fuel cell. *J Taiwan Inst Chem Eng* **42**, 945–951 (2011).

14. Slack, J. *et al.* Electrospun Fiber Mat Cathode with Platinum-Group-Metal-Free Catalyst Powder and Nafion/PVDF Binder. *ChemElectroChem* **5**, 1537–1542 (2018).

Chapter VI

CONCLUSION

1. Gen-1 PMF catalysts (synthesized through a hard-templating pore-former approach by Pajarito Powder) were used to form cathodes in which the catalyst:binder weight ratio was fixed at 50:50. MEAs were fabricated with a Nafion 211 membrane, a Pt/C powder anode (with a loading of 0.1 mg_{Pt}/cm^2), and one of the following cathodes:
    a. neat Nafion powder cathode
    b. powder cathode with a 50:50 (w:w) Nafion:PVDF binder
    c. fiber cathode with a Nafion binder (with the PEO carrier polymer extracted before the fuel cell test)
    d. fiber cathodes with 50:50, 67:33, 75:25, and 80:20 (w:w) Nafion:PVDF binder
2. Top-down SEM images showed large catalyst particles and agglomerates of multiple particles in the powder cathodes (with or without PVDF). All the electrospun fiber mats appeared to be porous, with a very rough surface. The average fiber diameters for each of the Gen-1 PMF catalyst fiber mats ranged from 0.9 to 1.7 μm, and there were smaller catalyst particle agglomerations in the fiber mats than in the powder cathodes.
3. Each Gen-1 PMF catalyst cathode MEA was tested at BOL and was subjected to a constant voltage operation at 0.5 V with the fuel cell operating at 80 °C, 100% RH, 200 kPa_{abs}, and 0.125/0.5 SLPM (standard liters per minute) hydrogen/air

feed gas flow rate. The Nafion powder cathode MEA and the Nafion fiber cathode MEA (with PEO extracted) generated the same polarization curves at a high potential region (>0.55 V). However, due to water flooding, a rapid power drop occurred in the powder cathode at a voltage below 0.55 V. During the 50 hours of constant voltage operation, both MEAs degraded immediately after the operation started and showed a similar trend: a rapid power drop during the first 10 hours of the test, after which the degradation slowed, with a nearly linear power loss over time (degradation decay rate of fiber vs. powder cathode: 0.7 mW/cm^2/hr vs. 1.0 mW/cm^2/h, respectively).

4. The BOL polarization curves of MEAs with a 50:50 (w:w) Nafion:PVDF cathode binder exhibited dramatically less power generation than those of cathodes with a Nafion binder due to the addition of PVDF.
5. Stable power density at 0.5V is achieved in 50:50 (w:w) Nafion:PVDF cathode MEAs regardless of cathode morphology. The transient power density vs. time plots of both MEAs showed a rise in power after start-up and stabilized at 25 mW/cm^2 (powder) and 41 mW/cm^2 (fiber) after 50 hours of constant voltage operation at 0.5V.
6. The BOL polarization curves of Nafion/PVDF fiber cathode MEAs exhibited less power generation over the entire operating potential region (0.2 V to OCV) when the PVDF content in the fiber cathode binder was increased from 20 wt% to 50 wt%. Stable power density at 0.5 V was achieved with Nafion:PVDF binder weight ratios of 50:50 (41 mW/cm^2), 67:33 (65 mW/cm^2), and 75:25 (88 mW/cm^2).

7. The power density at 0.5 V of 80:20 Nafion:PVDF fiber cathode MEAs increased after the constant voltage operation started, achieved a high point (103 mW/cm^2), and degraded at a rate of 0.2 mW/cm^2/hr. Subsequently, an MEA with a 75:25 (w:w) Nafion:PVDF fiber cathode binder achieved the highest stable power of 88 mW/cm^2 at 0.5 V, indicating that there was a balance between the necessary hydrophobicity to expel peroxide and the required Nafion binder content to ensure good proton conductivity and oxygen transport.
8. Gen-1 PMF catalyst fiber cathodes with 75:25 (w:w) Nafion:PVDF binders at loadings of 0.75, 1.5, and 3.0 mg/cm^2 were fabricated into MEAs and tested. They exhibited an increase in power with increasing cathode loading up to 3.0 mg/cm^2, but the impact of loading on power was more pronounced with lower catalyst contents. Stable power output at 0.5 V was achieved at all three cathode catalyst loadings.
9. MOF-based catalysts (synthesized by Pajarito Powder) were used to form cathodes in which the catalyst:binder weight ratio was fixed at 50:50. The MEAs were fabricated with a Nafion 211 membrane, a Pt/C powder anode (with a loading of 0.1 mg_{Pt}/cm^2), and one of the following cathodes:
    a. neat Nafion powder cathode
    b. powder cathodes with 50:50, 75:25, 80:20, and 83:17 (w:w) Nafion:PVDF binders
    c. fiber mat cathodes with 50:50, 67:33, 75:25, 80:20, and 83:17 (w:w) Nafion:PVDF binders

10. The MOF catalyst cathode MEAs were all tested at BOL and subjected to a potentiostatic operation at 0.5 V, with the fuel cell operating at 80 °C, 100% RH, 200 kPa_{abs}, and 0.125/0.5 SLPM hydrogen/air feed gas flow rate. The MOF-based catalyst powder cathode with a neat Nafion binder outperformed all the cathodes with Nafion/PVDF binders at BOL. However, it exhibited severe degradation after the durability test started.
11. At the same Nafion:PVDF weight ratios (50:50, 75:25, 80:20, and 83:17), the MOF-based catalyst fiber cathode MEAs generated more power than the corresponding MOF catalyst powder cathode MEAs. All the MOF catalyst cathodes with a Nafion/PVDF binder achieved long-term stable power density at 0.5 V regardless of cathode morphology (powder or fiber mat cathode). Furthermore, more power was generated at all potentials as the PVDF content in the powder or fiber cathode binder decreased from 50 wt% to 17 wt%.
12. The transient plots of power density over time at 0.5 V for MOF-based catalysts with a fiber cathode exhibited a dramatic up-and-down power swing. As an example, the 83:17 Nafion:PVDF fiber cathode MEA showed a rise in power density for ca. 1 hour to a maximum of 206 mW/cm^2, followed by a rapid drop in power density for the next 15 hours to a low of 102 mW/cm^2 and then a slow rise in MEA power output that eventually stabilized at 112 mW/cm^2 after ca. 50 hours. In MOF catalysts, we assumed that there were two active sites, S1 and S2 (with S1 being more active and S2 more stable), which resulted in the dramatic up-and-down power swings (through a process of S1 site deactivation and S2 site activation) before stabilization was achieved.

13. The dramatic up-and-down power swings during the first ca. 20 hours of constant voltage operation at 0.5 V were less severe as the PVDF content in the fiber cathode binder increased, with almost no short-term power density changes with the 50:50 (w:w) Nafion:PVDF binder.
14. The highest stable power output of MOF-based catalysts at 0.5 V (112 mW/cm^2) was achieved with 80:20 and 83:17 (w:w) Nafion:PVDF fiber cathode binders.
15. The MOF-based catalyst 83:17 (w:w) Nafion:PVDF fiber cathode MEA's durability was evaluated by constant voltage operation at 0.7 V, 0.5 V, and 0.3 V. The transient power density vs. time plots differed because different amounts of water or H_2O_2 were generated. At 0.3 V, because more water and H_2O_2 were produced, the loss of S1 sites and activation of S2 sites happened faster than at 0.5 V. However, at 0.7 V, because less water was generated, there were few (or even no) activations of S2 sites, and thus there was no rise in the power density at 0.7 V over time.
16. At the same Nafion:PVDF weight ratio and cathode catalyst loading, an MEA with a MOF-based catalyst cathode generated more power than an MEA with a Gen-1 PMF catalyst cathode, which is attributable to a higher density of active ORR sites on the MOF catalyst particles.
17. Powder and fiber mat cathode MEAs with a Gen-2 PMF catalyst from Pajarito Powder were fabricated and evaluated. The powder cathodes with the Gen-2 PMF powder showed a smaller particle/agglomeration size. Fibers with the Gen-2 PMF material had a better morphology (a more uniform fiber diameter, with fewer

agglomerates and bead-on-fiber defects) than the Gen-1 PMF powder cathodes described in Chapter II.

18. Fiber mat and powder cathode MEAs with Gen-2 PMF catalysts were prepared and tested using a Nafion 211 membrane and a Pt/C powder anode (with a loading of 0.1 mg_{Pt}/cm^2). Initial fuel cell tests of the powder/fiber cathode MEAs were performed at 80 °C, 100% RH, and 200 kPa_{abs} pressure with H_2 and air feed streams. The MEAs with the Gen-2 PMF catalysts generated more power than those with the Gen-1 PMF catalysts.
19. The Nafion powder and Nafion fiber cathode MEA with Gen-1 or Gen-2 PMF catalysts showed a similar degradation trend under 50-hour constant voltage operation at 0.5V, while Gen-2 MEAs generated approximately 30% more power.
20. The 75:25 (w:w) Nafion:PVDF fiber cathode MEA with Gen-1 PMF catalysts generated stable power output of 88 mW/cm^2 at 0.5V for 50 hours, while the 75:25 (w:w) Nafion:PVDF fiber cathode MEA with Gen-2 PMF catalysts generated more power (highest power density at 0.5V of 150 mW/cm^2) but degraded at a rate of 0.37 mW/cm^2/hr due to insufficient PVDF (hydrophobicity).
21. A redispersed fiber cathode was prepared by redispersing the Nafion/PEO fiber mats into solvent and then coating the GDL with it. The redispersed fiber cathode was soaked in water (80 °C) for two hours to remove the PEO before MEA fabrication. The redispersed fiber cathode MEA exhibited the same catalytic activity and durability as the Nafion fiber cathode MEA (directly attaching fiber mats onto GDL, to be distinguished from a cathode made with pre-formed fibers dispersed in an ink).

22. Nafion/PEO fiber mats with Gen-2 PMF catalysts were used to fabricate three different types of hybrid cathodes, which were composed of catalyst particles and fiber mats. The loading of the hybrid cathodes remained 3.0 mg/cm^2, with a 50:50 weight ratio of catalyst from fibers and catalyst between fibers. All the hybrid cathodes were soaked in hot water (80 °C) for two hours to extract the PEO before fabrication into MEAs. The three types of hybrid cathodes are described below.
    a. hybrid type I cathode, in which catalyst particles are interspersed between catalyst/binder fibers
    b. hybrid type II cathode, in which catalyst particles and Nafion are interspersed between catalyst/binder fibers
    c. hybrid type III cathodes, in which catalyst particles, Nafion, and Fluorinated Ethylene Propylene (FEP) are interspersed with electrospun catalyst/binder fibers
23. The hybrid type I cathode MEA generated 20% less power than the fiber cathode MEA due to the formation of large catalyst aggregates or agglomerations.
24. The hybrid type II cathode MEA generated 15% more power and exhibited similar durability (i.e., EOL:BOL power density ratio) to the fiber cathode.
25. In the hybrid type III cathode MEAs, the power output at BOL decreased (due to the addition of FEP, which reduced the ORR kinetics and proton transport) and the MEA durability increased (due to increased cathode hydrophobicity) as the FEP content increased.

26. The BOL and EOL plots generated by the hybrid type III (30 wt% FEP) cathode MEAs overlapped (showing no degradation).
27. The hybrid type III (20 wt% FEP) cathode MEA represented a compromise between catalyst activity and durability, as it generated the highest power output at EOL (after 30K cycles of AST).
28. When FEP was inside the powder cathode, there was no change in BOL power densities versus a Nafion powder cathode at high potentials, a loss in power at moderate and low potentials (moderate/high current densities), and no improvement in MEA durability versus a Nafon powder cathode MEA.
29. For the redispersed fiber cathode with 20% FEP outside, there was a 40% loss in BOL power densities versus a redispersed fiber cathode at the entire operating potential region. The MEA with redispersed fiber cathode with 20% FEP outside showed no degradation after 30K cycles of AST.

Chapter VII

SUGGESTIONS FOR FUTURE WORK

1. Although the present work successfully electrospun PGM-free catalysts with Nafion and PVDF binder, bead-on-fiber defects were observed in all the cathode binder combinations. PGM-free catalysts with Nafion and higher molecular weight PVDF should be electrospun to reduce or eliminate the bead-on-fiber defects.
2. The addition of PVDF to the fiber cathode binder decreased the MEA power output, as it decreased the proton conductivity in the cathode binder. PFSA with a lower equivalent weight, such as 830 or 720, should be examined to increase the fiber cathode's proton conductivity.
3. The difference in long-term power output between the result of Slack et al.[1] (with a catalyst:binder [Nafion+PVDF] weight ratio of 70:30) and that observed in the present study (with a catalyst:binder weight ratio of 50:50) requires further investigation. Methods or conditions for electrospinning fibers with less Nafion/PVDF binder should be identified.
4. Future work should examine both the Nafion:PVDF binder weight ratio and the catalyst:binder weight ratio.
5. In the PGM-free catalyst fiber cathode with Nafion/PVDF binder, an increase in power with increasing cathode loading up to 3.0 mg/cm^2, but the power increase was limited due to the increased cathode thickness. More work should be done to

decrease the fiber cathode thickness such as increasing the compaction pressure or redispersing the fiber mats.

6. As a trade-off between durability and power output was observed in the Nafion/PVDF fiber cathode MEA, a dual-fiber electrospinning approach should be explored to optimize the balance of durability and power output.[2] Dual-fiber electrospinning provides many potential advantages to improve cathode design, for example, by (i) making layered electrode mats by electrospinning more hydrophilic fibers near the membrane and more hydrophobic fibers near the GDL or (ii) electrospinning fibers with the highest power output and simultaneously electrospinning fibers with good durability.
7. A core-shell fiber should be examined in which the shell has a higher Nafion:PVDF ratio (for good proton conduction) and the core is more hydrophobic (to quickly expel electro-generated peroxide).
8. The MOF catalyst MEAs had dramatic up-and-down power swings during the first approximately 20 hours and eventually stabilized when S2 sites dominated. The addition of PVDF (which increased cathode hydrophobicity) stopped the degradation of S2 sites, but not the degradation of S1 sites. Future work should be done on preventing loss at S1 sites.
9. The durability of the MOF catalyst cathode MEA was evaluated by potentiostatic tests at 0.7 V, 0.5 V, and 0.3 V, and the transient behaviors (power density over time) differed. This may indicate that degradation occurred differently at different voltages, so other durability tests, such as ASTs or carbon corrosion tests, should also be conducted on Nafion/PVDF PGM-free catalyst cathode MEAs.

10. A comparison of Gen-1 and Gen-2 PMF catalysts in regard to morphology and fuel cell performance showed the superiority of smaller catalyst particles in electrospinning. Future work should fabricate electrospun fiber mats with even smaller PGM-free catalysts.
11. The AST in this work comprised 30K cycles between 0.6 V and 0.95 V. It is necessary to conduct more cycles on PGM-free catalyst cathodes to measure the MEA's durability.
12. The hybrid type III cathode showed superior fuel cell performance and MEA durability. Future work should:
    a. Use a MOF-based catalyst to fabricate a hybrid cathode, as the work described in Chapters II and III has shown the superiority of the MOF-based catalyst cathode MEA.
    b. Change the weight ratio of catalyst from fibers to catalyst between fibers (to other than 50:50).
    c. Use a lower equivalent weight PFSA ionomer to fabricate fiber mats or add it between fibers to increase the cathode's proton transportation,
    d. Use different fiber mats (e.g., Nafion/PVDF or Nafion/PAA fiber mats) to make hybrid cathodes.
    e. Replace FEP with other hydrophobic polymers (e.g., PVDF or Teflon).
    f. Add more than one type of fiber mat (e.g., Nafion/PEO and Nafion/PVDF or Nafion/PVDF at two different weight ratios) to make hybrid cathodes.

APPENDIX A

DATA REPRODUCIBILITY

In Figure 2.7, the polarization curve of a 75:25 (w:w) Nafion:PVDF fiber cathode MEA was collected at 80 °C with air and hydrogen at 200 kPa_{abs} and 100% relative humidity (RH). This Nafion/PVDF blended fiber cathode MEA was reproduced three times as shown in Figure A.1. The polarization curve shown in Figure 2.7 is MEA 1 in Figure A.1. As shown in Figure A.1, differences between three MEAs are within 10%, which is within the expectation. The variations are attributed to small errors in measuring the cathode catalyst weight when making MEAs and small differences in the morphology quality of the fiber electrodes because the MEAs were made with different fiber mats.

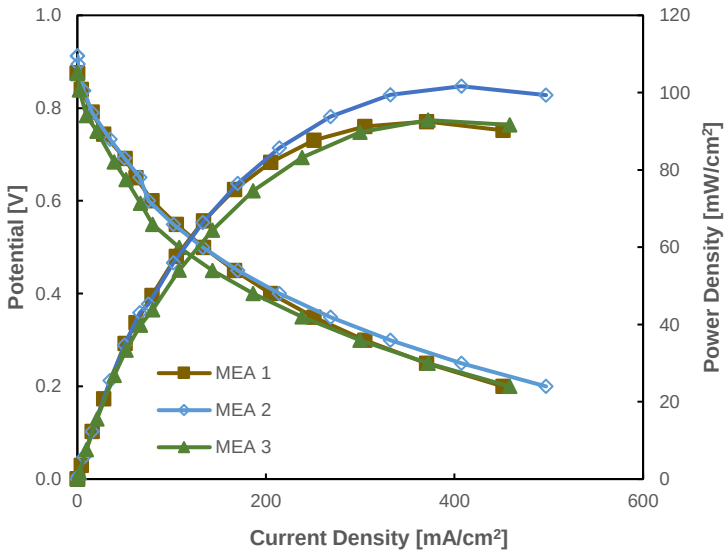

Figure A.1. H_2/air polarization curves and power density vs. current density of three PMF-catalyst fiber cathode MEAs at cathode Nafion:PVDF binder weight ratio of 75:25. For all the cathodes, the total binder content was constant relative to the amount of catalyst at 50 wt%, and the PGM-free catalyst cathode loading was 3.0 mg/cm^2. Fuel cell operating conditions: 80 °C, 100% relative humidity, 200 kPa_{abs} pressure, and 0.125/0.5 SLPM (standard liters per minute) H_2/air feed gas flow rate. All MEAs have a Nafion 211 membrane and a Pt/C catalyst powder anode at a loading of 0.1 mg_{Pt}/cm^2.

In Figure 5.10, the polarization curve of MEA #7 was collected. MEA #7 contained a hybrid cathode, in which catalyst powders, Nafion and FEP were interspersing fiber mats (the MEA A shown in Figure A.2a). Polarization curves at beginning-of-life (BOL) and end-of-life (EOL, after 30K cycle AST) were collected. Two more MEAs with the same composition were made and evaluated as shown in Figure A.2 b and c, and Figure A.3 showed the power density ratio of EOL to BOL of the three MEAs. Polarization curves (V-i data) in Figure A.2 a-c indicated that the high-power output was reproducible within 10%. Additionally, the loss in power after a 30K cycle AST was also reproducible across MEAs, as shown in Figure A.3. Here, the EOL:BOL ratio at 0.7 V, 0.5 V, and 0.3 V was reproducible within 10%

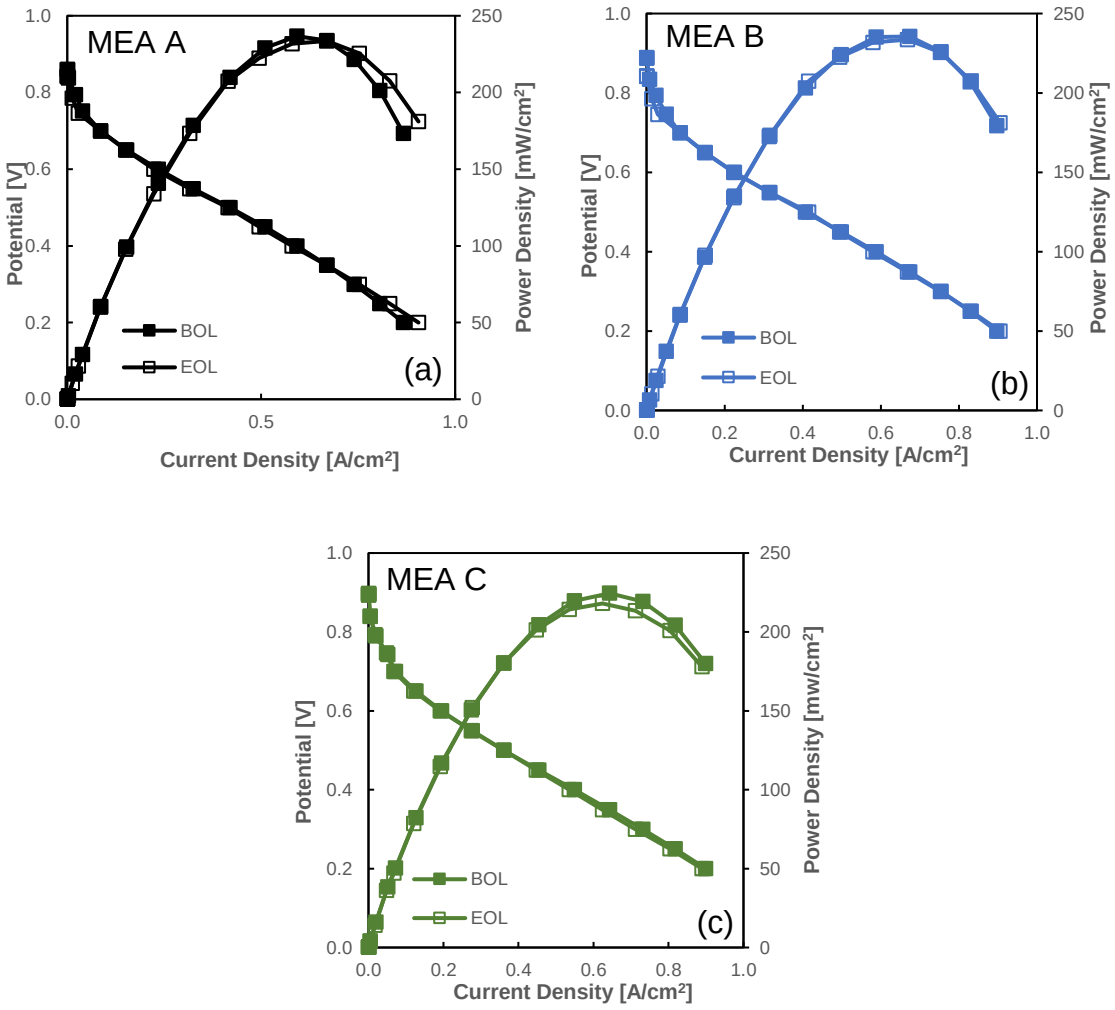

Figure A.2. BOL (solid symbol) and EOL (open symbol) H_2/air polarization curves and power density vs. current density for hybrid type III cathode MEAs with 30 wt% FEP. Three MEAs with the same composition are made and labeled as (a) MEA A, (b) MEA B, and (c) MEA C. All the cathodes were made with the same fiber mats with PEO extracted. The Nafion-to-catalyst weight ratio was 1.2 inside and between fibers, and PGM-free catalyst cathode loading was 3.0 mg/cm^2. The fuel cell operating conditions were 80 °C, 100% relative humidity, 200 kPa_{abs}, and H_2/air 0.7/1.7 SLPM feed gas flow rate. All the MEAs contained a Nafion 211 membrane and a Pt/C catalyst powder anode at a loading of 0.1 mg_{Pt}/cm^2.

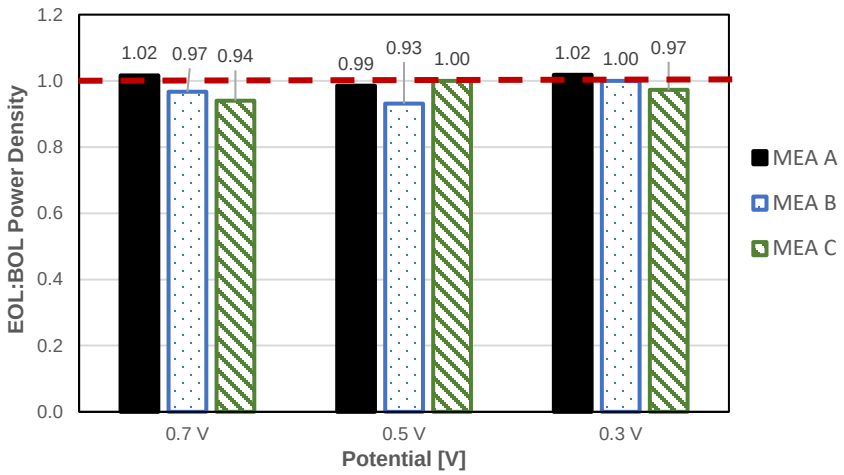

Figure A.3. The EOL:BOL power density ratio at 0.7 V, 0.5 V, and 0.3 V of the three hybrid type III cathode MEAs with 30 wt% FEP in Figure A.2.